Cyprus University of Technology

Faculty of Geotechnical Sciences and Environmental Management

Doctoral Dissertation

WATER-SALT-ORGANIC INTERACTIONS WITHIN ATMOSPHERIC AEROSOL: A MOLECULAR DYNAMICS STUDY

Anastasia Salameh

Limassol, March 2021

CYPRUS UNIVERSITY OF TECHNOLOGY

FACULTY OF GEOTECHNICAL SCIENCES AND
ENVIRONMENTAL MANAGEMENT

DEPARTMENT OF CHEMICAL ENGINEERING

Doctoral Dissertation

WATER-SALT-ORGANIC INTERACTIONS WITHIN ATMOSPHERIC AEROSOL: A MOLECULAR DYNAMICS STUDY

Anastasia Salameh

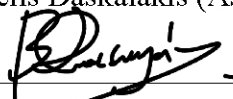Limassol, March 2021

Approval Form

Doctoral Dissertation

WATER-SALT-ORGANIC INTERACTIONS WITHIN ATMOSPHERIC AEROSOL: A MOLECULAR DYNAMICS STUDY

Presented by

Anastasia Salameh
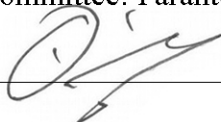
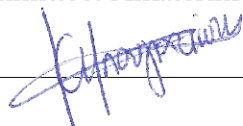Supervisor: Vangelis Daskalakis (Assistant Professor)

Signature _____

Member of the committee: Farantos Stavros (Professor Emeritus)

Signature _____

Member of the committee: Aikaterini Bougiatioti (Senior Researcher)

Signature _____

Cyprus University of Technology

Limassol, March 2021

Copyrights

"To my father, in loving memory"

ACKNOWLEDGMENTS

This work would not have been possible without the help and support of many people, to whom I must express my deepest gratitude.

My profound gratitude goes out to my supervisor, Assistant Professor Vangelis Daskalakis. For introducing me to the computational science research field and enabling me to work on exciting projects. His profound knowledge and insightful thoughts on scientific research have taught me a lot. I am grateful for his guidance, confidence, support, and motivation, without which this thesis would not have been possible.

I wish to express my deepest gratitude to my mother and brother for their constant love and encouragement. Mom, I do not know how to repay what I have received from you for the rest of my life. The devotion, patience, and responsibility that you have shown in your life have been and will be the source of my strength—Elias for being with me, supporting me, and giving me so much joy over these years.

To Dimitris Nikolaidis. Your love and support gave me the encouragement to follow my dreams, no matter how difficult the path was. I know that there will be many twists and turns ahead. Still, I'm confident that your continuous support and advice will be invaluable.

Finally, I'd like to express my appreciation to my friends Niko, Maria, and Antonis for their continuous encouragement and support. For your companion, support and help through the most challenging time of mine.

PUBLICATIONS

This thesis is based in part on the following articles prepared during the research project:

   I.   Correlation between Surface Tension and the Bulk Dynamics in Salty Atmospheric Aquatic Droplets

       Authors: Anastasia Salameh, Flora Vorka, Vangelis Daskalakis

       Publication: The Journal of Physical Chemistry C

       Publisher: American Chemical Society

       Date: Jun 1, 2016

       Copyright © 2016, American Chemical Society

   II.   Atmospheric Ice Nucleation by Glassy Organic Compounds: A Review

       Authors: Anastasia Salameh, Vangelis Daskalakis

       Publication: Chemistry of Compounds Journal

       Publisher: Verizona Open Access (CCJ-Journal)

       Date: Feb 6, 2017

       Copyright © 2017, Verizona Open Access

ABSTRACT

This thesis's focal point is to advance our knowledge regarding the interactions between water, salt, and organics in the atmosphere, with applications in ice nucleation and cloud condensation nuclei (CCN) formation. This knowledge can be employed in the future for atmospheric modeling. High in the clouds, water molecules transition into ice crystals within particles composed of a mix of sea salt and organic materials. These crystals are significant players in the generation of rain and snow, controlling the balance between heating and cooling the planet by scattering the sunlight. The particles that seed ice crystals are swirled into the atmosphere from both land and sea. But only a few particles can act as a nucleus for forming ice crystals or condensation nuclei, making them more effective ice/ cloud nucleators. This suggests that the few particles that do seed or nucleate ice crystals have specific physical or chemical properties. Ice nucleation is a crucial step in cloud formation and precipitation and plays an important role in the Earth's hydrological cycle, energy balance, and radiative balance. Given its significance, atmospheric ice/cloud nucleation on organic and salt aerosol particles is one of the microscopic processes that are still poorly understood. Significant uncertainties exist in the representation of nucleation processes in climate models. Therefore, probing aqueous organic and salt aerosol particles is a challenge. This opens the door for computer simulations and modeling of these intricate structures. The work presented herein probes these processes by employing molecular dynamic simulations to understand the impacts of aerosol-cloud interactions and atmospheric chemistry.

Keywords: water, atmospheric ice nucleation, salts, organics, molecular dynamics, simulations

TABLE OF CONTENTS

LIST OF TABLES

LIST OF FIGURES

LIST OF ABBREVIATIONS

The following abbreviations are used in this thesis:

ACF	Autocorrelation Function
ASFE	Absolute Solvation Free Energies
BCC	Body Centered Cubic
CCN	Cloud Condensation Nuclei
CNT	Classical Nucleation Theory
D	Diffusion Coefficient
DMS	Dimethyl Sulfide
FCC	Face Centered Cubic
FF	Force Field
FFT	Fast Fourier Transform
HPC	High-Performance Computing
IN	Ice Nuclei
INP	Ice Nucleating Particle
IPCC	Intergovernmental Panel on Climate Change
LJP	Lennard-Jones Potential
LTS	The Local Stress Tensor Code
LVOCs	Low-Volatile Organic Compounds
MD	Molecular Dynamics
MSD	Mean Square Displacement
NPF	New Particle Formation
NVOCs	Non-Volatile Organic Compounds
OA	Organic Aerosols
OM	Organic Matter

1   Introduction

Atmospheric cloud and ice nucleation of organic and salt aerosol particles are still one of the least understood atmospheric processes at the microscopic level. Significant uncertainties exist in the representation and incorporation of the latter in climate models. This research focuses on studying ice nucleation mechanisms of organic/ salt compounds and water to understand the impacts of nucleation on aerosol-cloud interactions. The main question is how ice nucleation or droplet formation is initiated in different temperatures (conditions), which we explore by employing molecular dynamic simulations.

In recent years, there has been a major increase in interest in understanding the factors that influence the Earth's climate. Aerosol particles are active components of the Earth's atmosphere, consisting of small liquid and solid particles suspended in air (Seinfeld and Pandis, 2016). They can be produced directly from anthropogenic and natural sources such as dust, sea salt, soot, and biological particles or condensation of low-volatility compounds (e.g., oxidized organic compounds) (Andreae and Rosenfeld, 2008; Tröstl *et al.*, 2016). Aerosols play vital roles in scattering and absorbing solar and infrared radiation, impacting Earth's radiative energy budget.

Atmospheric aerosols are at the center of both droplet and ice crystal formation as they can alter the droplet and ice crystal distributions in clouds (Lohmann, 2002). There is a large collection of literature in the field of atmospheric science that demonstrates the importance of cloud and ice-active aerosols in understanding cloud microphysical properties, formation, and life cycles (Jacobson *et al.*, 2000; McMurry, 2000; Pöschl, 2005; Kanakidou *et al.*, 2005; Lohmann and Feichter, 2005; Sun and Ariya, 2006; Prather, Hatch and Grassian, 2008; Knopf and Lopez, 2009; Hoose and Möhler, 2012; Kärcher and Seifert, 2016; Salameh and Daskalakis, 2017; Tomasi *et al.*, 2017; Kanji *et al.*, 2017; McNeill, 2017; Kreidenweis, Petters and Lohmann, 2018).

On the one hand, atmospheric aerosols can act as cloud condensation nuclei (CCN) and serve as a foundation for water vapor condensation to form cloud droplets (Pöschl, 2005; Andreae and Rosenfeld, 2008; De Mott *et al.*, 2011). On the other hand, they will act as ice nuclei (IN) to form cloud droplets and ice crystals (Boucher *et al.*, 2013). As a result, they have a big effect on the microphysical properties of water and ice clouds, which affect atmospheric processes that lead to rain, snow, hail, and other precipitation. Cloud

microstructure changes have an effect on how they deal with radiation. These potential impacts have led to aerosols' consideration as a significant modulator of global climate as described by the Intergovernmental Panel on Climate Change (IPCC) (Reay *et al.*, 2007). Therefore, understanding the processes that cause precipitation is critical for weather forecasting and predicting precipitation's evolution on a global scale in a changing environment (Sillmann *et al.*, 2017).

This thesis focuses on two types of aerosols: sea salt aerosol (SSA), which comes from sea spray and is one of the most widely distributed natural aerosols, and organic aerosol (OA), which accounts for a huge percentage of the global tropospheric aerosol (Boucher *et al.*, 2013). Despite the significant progress in understanding the chemical composition of salty and organic aerosols, there are many uncertainties in representing nucleation processes in climate models. Nucleation is a complicated process; thus, it needs to be studied both experimentally and computationally (at the atomic scale) (Sosso, Chen, *et al.*, 2016). This necessity opens the door for computer simulations and modelling of these intricate processes.

1.1 Thesis Objective

This thesis's main objective is to advance scientific knowledge on the interpretations of atmospheric aerosol-related processes in the atmosphere, focusing on the issues that still stand as open questions in atmospheric and climate studies. For this purpose, the research was approached from different aspects. The first is linked to the formation of new particles in the atmosphere. Molecular Dynamics (MD) simulations on salty aquatic droplets are used to show the relationship between surface tension and a bulk property like the static dielectric constant, which is closely related to water behavior in Köhler theory of droplet formation and growth (Salameh, Vorka and Daskalakis, 2016). The particles probed consist of water, salt (ammonium bisulfate), and surface-active organic matter (Salameh, Vorka and Daskalakis, 2016). This study's important finding is that surface-active organic matter on the surface of a salty droplet can change water orientation/activity's solvent properties in terms of water orientation/activity as measured by the static dielectric constant in bulk (Salameh, Vorka and Daskalakis, 2016).

The second one considers the ability of atmospheric particles, which consist of a plethora of organic compounds and water, to form glassy phases and initiate ice nucleation in low

temperatures. We employed supercooling dynamics (from 220K to 96K) and managed to identify a pattern of behavior in different organics related to the enhancement or inhibition of Ice Nucleation. In these studies, we employ the TIP4P/2005 water potential (Abascal and Vega, 2005) to describe water interactions. To monitor the formation of Ice/ glassy structures within the clusters, we used the Steinhardt local Q3, Q4, and Q6 order parameters (Steinhardt, Nelson and Ronchetti, 1983). We show that organic components do not partition evenly between the ice and aqueous phases. Organic-rich particles tend to stay unfrozen and can have an effect on aerosol-cold cloud interactions and the environment. We also show that compounds containing oxygen and nitrogen facilitate ice nucleation, whereas hydrocarbons (alkynes and cycloalkanes) do not.

1.2 Why Molecular Dynamics simulations?

Experiments have delivered much of our current knowledge of atmospheric molecules' molecular properties and processes, reinforced by models that reflect a simplified representation of the observable being measured. The model must trade off precision for simplicity to provide a comprehensive understanding of these processes. A simple model would not provide us with precise knowledge about the complex system's molecular properties. The more difficult and complex our problems are, the more detailed and reliable data about our system is desired. Here's where computer simulations come into play. When connected to powerful computers, models may generate a large number of data, allowing any property to be calculated in theory. Whereas the subtle details about molecular motions, and the fast timescale over which they occur, are challenging to probe experimentally, they represent no obstacle to a simulation. The simulation establishes a connection between the system's microscopic information and experimentally observed macroscopic properties. If the simulation model is good, the results can be compared to experiments and give the experimentalist insights, making the (often difficult) analysis of experimental data easier. This bridging role serves as a link between models and experimental results. Simulation methods are appropriately referred to as "*computer experiments*" (Feig *et al.*, 2018).

This thesis's work considers the rapid advancement of computer hardware, which has increased the popularity of computationally intensive simulations in atmospheric science. This is essentially due to the increase in the computational power available that has

allowed researchers to shift from systems of a few atoms to large complexes in a solvated environment. Molecular dynamics has become a critical research methodology when one wants to probe systems at the atomic scale with an increasing number of degrees of freedom. MD simulations employ classical and statistical mechanics based on the Newtonian Equations of motion from microscopic properties to the macroscopic picture of a system, providing a microscopic insight into its physical properties (Coveney and Wan, 2016). Documenting and analyzing the changing coordinates, velocities, and forces on a system of particles allows dynamic processes and statistical properties to be monitored and analyzed in microscopic detail. Atoms are expressed by mass points with partial charges in MD simulations using classical force fields (Schlick, 2010; Hospital *et al.*, 2015; Perilla *et al.*, 2015). The inter-atomic interactions are modeled by potential functions that produce satisfactory results at a reduced computational cost compared to *ab initio* methods. However, when combined with quantum chemistry-based ab initio methods, the MD technique has allowed for the accurate representation of the abundant liquid water in atmospheric particles.

1.3 Thesis Outline

This work is organized into six chapters: First, an extensive background theory of aerosol-cloud interactions is given in Chapter 2. This chapter presents a theoretical overview of atmospheric aerosols, cloud condensation nuclei, and ice nucleation. The main concepts that define them, their properties and their characteristics, and their impacts, are portrayed in detail. Chapter 3 is devoted to the basic concepts of Molecular Dynamics simulations.

The rest of the manuscript is devoted to answering the objectives. In Chapter 4, the correlation between the surface tension and the static dielectric constant is presented. In this chapter, the computational methods, results, and conclusions are portrayed. In Chapter 5, MD simulations are employed to investigate organic atmospheric particles' ability to form glassy phases and initiate ice nucleation in low temperatures.

Finally, in Chapter 6, a summary of this thesis's main conclusions and the future outlook are presented.

2   Theory of Aerosol - Cloud Interactions

Recognizing and quantifying aerosol and clouds' interactions are among the many significant challenges in evaluating and predicting human activities' impact on climate change. Clouds mainly regulate the Earth's radiation energy budget and precipitation distribution. Thereby they play a dominant role within the climate system. Currently, known interactions between aerosols and clouds consist of several facets. Firstly, by acting as CCN, a high concentration of aerosol particles can result in an increased number of liquid cloud droplets, and they can further lead to the formation of cloud droplets. Secondly, they act as IN, causing ice crystals to grow, impacting the radiative balance, which has become a significant climate concern. This chapter describes the properties of atmospheric aerosols and the physical theory behind cloud condensation and ice nucleation.

2.1   Atmospheric Aerosols

Atmospheric aerosol research started more than a century ago. After the mid-twentieth century, substantial advances were made inspired by environmental protection issues. At that time, climate and aerosol scientists created climate models that took aerosols and other chemical species into account. Aerosols have a deep impact on the Earth's atmosphere through their radiative effect and an indirect effect through their interactions with the cloud system. By definition, "*an atmospheric aerosol is a suspension of small airborne particles in the ambient atmosphere*" (Hinds, 1999). While the word particle is associated with solid material, atmospheric aerosols may be liquid or solid or have exotic morphologies such as two-phase liquid particles or organic glasses (McNeill, 2017).

Atmospheric aerosols have various sources, natural and anthropogenic (Jacobson *et al.*, 2000; Kanakidou *et al.*, 2005; Andreae and Rosenfeld, 2008; Sillmann *et al.*, 2017; Kreidenweis, Petters and Lohmann, 2018). Combustion sources can emit them directly into the atmosphere (*primary particles*) (Baltensperger and Prévôt, 2008) or form from photochemical reactions by gas-to-particle formation from gas-phase species (*secondary particles*) (Boucher *et al.*, 2013). As a result, aerosols have various chemical compositions, and their size can span from 1 nm to 100 µm in diameter. Particle size distribution, particle density, particle phase, particle shape, particle number, the total mass

of suspended particulate matter, and chemical composition are the fundamental properties needed for aerosol characterization (Seinfeld and Pandis, 2016).
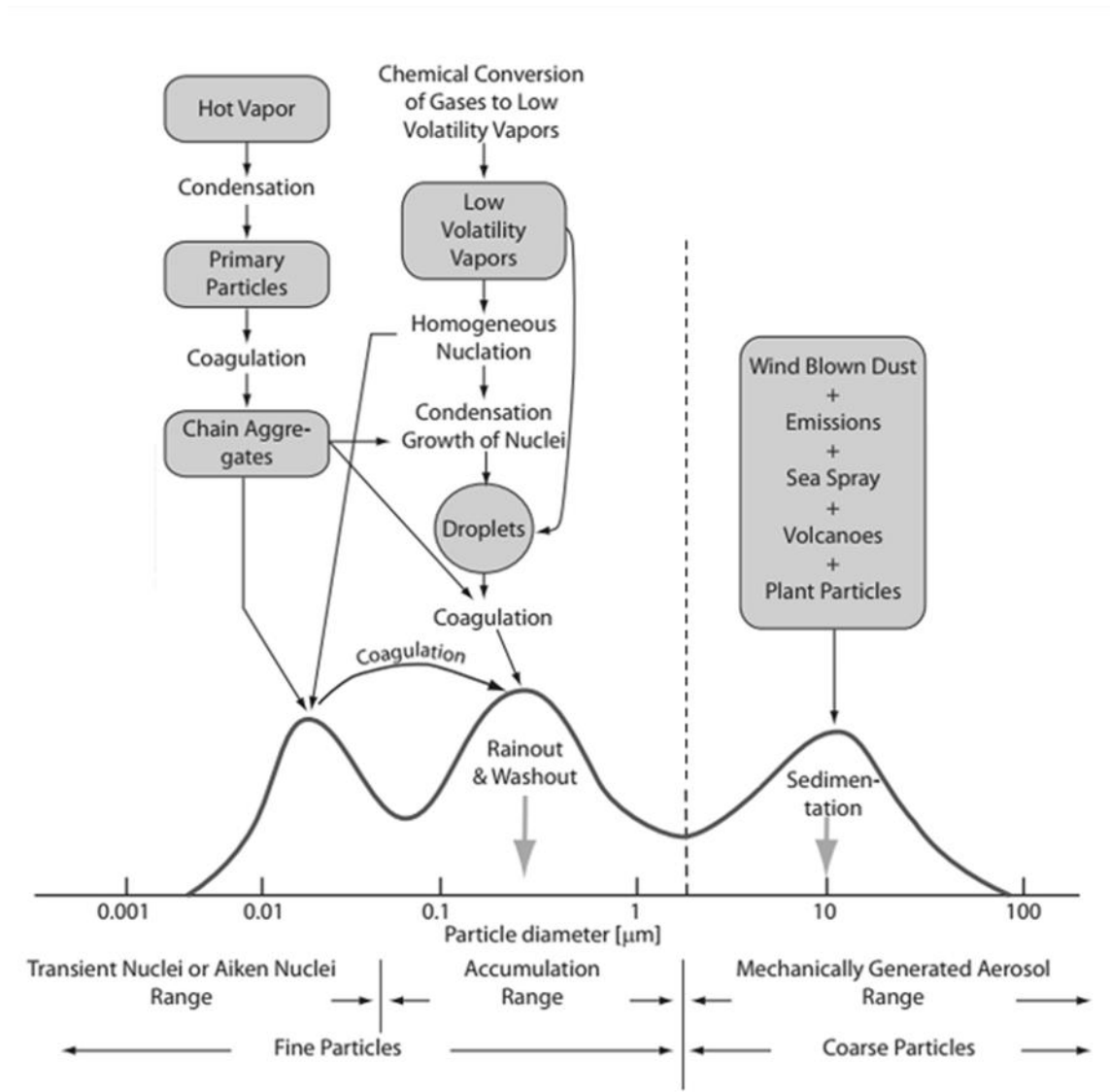
Figure 1: The distribution of particle surface area in an idealized diagram. The modes, sources, particle formation and removal mechanisms of atmospheric aerosols are depicted. Adapted from (Seinfeld and Pandis, 2016).

Particle size is one of the principal parameters for characterizing aerosols' behavior (Stephens, 2005). Phase, volatility, chemical reactivity, hygroscopicity, light absorption, scattering, and nucleation activity are all described by their size and composition (Salameh and Daskalakis, 2017). Chemical transport and lifetimes in the atmosphere, the hydrologic cycle, visibility, cloud formation, climate, environmental, and human health

are all affected by aerosol properties (Jacobson *et al.*, 2000; McMurry, 2000; Lohmann and Feichter, 2005; Pöschl, 2005; Sun and Ariya, 2006; Hoose and Möhler, 2012; Yakobi-Hancock, Ladino and Abbatt, 2014; McNeill, 2017; Salameh and Daskalakis, 2017; Kreidenweis, Petters and Lohmann, 2018).

Atmospheric aerosols span a wide range of sizes from a few nm to around 100 µm in diameter related to their sources, their different transformation and removal processes. The size distribution of aerosol particles is generally classified into two size modes: the fine mode (D < 2.5µm) and the coarse mode (D > 2.5µm). The modes result from numerous emissions and atmospheric processes. A schematic of the size modes distribution and their relevant processes is presented in Figure 1.

The coarse mode consists of dust, larger sea salt particles, and anthropogenic particles generated through physical or mechanical processes. The coarse particles have a very short lifespan in the atmosphere, just a few hours, due to their large size and mass, and contribute only a small fraction of the cloud-active particles (Andreae and Rosenfeld, 2008). A further separation of the fine mode is done by characterizing the nucleation mode (D < 10nm), the Aitken mode (10nm < D < 0.1µm) and the accumulation mode (0.1 < D < 2.5µm) (Seinfeld and Pandis, 2016).

Fine aerosols are emitted in the atmosphere by various natural and anthropogenic sources. Aitken mode particles and the smallest group particles described as nucleation mode are formed by a nucleation process in which gaseous molecules of low volatility condense to create solid, semisolid, or liquid matter. The nucleation mode contains particles emitted directly into the atmosphere and particles formed in the atmosphere by gas-to-particle conversion. Because of their high concentration, they coagulate very fast. Consequently, they have relatively short lifetimes in the atmosphere and end up in the accumulation mode. The accumulation mode includes combustion particles, smog particles, and coagulated nuclei-mode particles. They are generated in the atmosphere by photochemical reactions. Accumulation mode particles are small, and they coagulate too slowly to reach the coarse mode. Therefore, they have a long lifetime in the atmosphere, and they make for most of the visibility effects of atmospheric aerosols.

2.1.1   Sources of atmospheric aerosols

Aerosol chemical composition is a mixture of organic and inorganic compounds resulting from their diverse sources (Andreae and Crutzen, 1997). The inorganic mass fraction is mainly salts, with ammonium sulfate being the most abundant (Zhang *et al.*, 2007). Simultaneously, the contribution of organics to atmospheric particulate matter mass can be as high as 90% (Kanakidou *et al.*, 2005). There are two main classifications used to distinguish aerosol particles from the point of their source. The first classifies the particles according to their origin, *anthropogenic* or *natural*. In contrast, the second proposes to differentiate the particles by their mode of emission in the atmosphere, *primary aerosols* (emitted directly into the atmosphere) or *secondary aerosols* (formed via chemical and physical processing of gas-phase precursors). The two classifications may be combined for a complete description, the primary and secondary particles being of natural or anthropogenic origin, respectively.

2.1.1.1   Natural Aerosols

Sea Salt Aerosols: The main natural source of primary particles is sea salt, emitted from the oceans to the troposphere by evaporated sea spray, and are of the most widely distributed aerosols in the atmosphere (Ravishankara, 1997; Vignati *et al.*, 2010; Sun *et al.*, 2012). Sea-salt aerosols (SSA) are ejected into the atmosphere by bubble bursting through the sea surface microlayer. They consist mainly of sodium chloride and small amounts of other salts and dissolved organic matter present in seawater (Wilson *et al.*, 2015). SSA particles' chemical composition may vary with location and time and are mainly constituted of Na^+, K^+, Mg_2^+, Ca_2^+, and SO_4^{2-} ions common in seawater (Cavalli *et al.*, 2004; O'Dowd *et al.*, 2004). They are characterized as non-light-absorbing, highly hygroscopic, and having coarse particle sizes. Due to hygroscopicity, an SSA can serve as a very efficient CCN modifying cloud reflectivity, lifetime, and precipitation process (Zieger *et al.*, 2017). Sea salt particles are also the major chemical sinks for sulfur dioxide (SO_2) in the cloudy marine boundary layer (Sun *et al.*, 2012). SSA forms by two main mechanisms: evaporation of sea-spray droplets produced by bubble bursting within foamy whitecaps and wind tearing off the wave crests (Norris *et al.*, 2013). Mixtures of sea salt and organics have affected surface tension, increasing for low surfactant concentrations and decreasing for higher concentrations (Sun *et al.*, 2012). SSA particles

activate heterogeneous ice nucleation via immersion freezing below 220 K (Wagner *et al.*, 2018). It is known that halide salts increase the surface tension of aqueous solutions, such as cloud droplets, with increasing concentration, influencing the water vapour condensation and, therefore, the cloud droplet growth (Wang *et al.*, 2018). They affect, in this way, the optical properties of atmospheric aerosol particles and clouds and, in the end, even the precipitation mechanism (Ramanathan *et al.*, 1989; Li *et al.*, 2010). Although the surface tension of salty or pure water clusters has been studied previously (Zakharov, Brodskaya and Laaksonen, 1997), and the static dielectric constant for ionic solutions of various concentrations has been well-defined and characterized (Levy, Andelman and Orland, 2012), there is still debate about their connection.

Mineral Dust: Mineral dust, originating from arid and semi-arid regions of the world, is the second significant contributor of natural primary particles (Hoose *et al.*, 2010; Wheeler and Bertram, 2012). The primary chemical constituents of mineral dust aerosol are earth crust elements: Si, Ca, Fe, Al, Mg, K, O (Zeb *et al.*, 2018). Dust can be created as strong winds whip small mineral dust from deserts into the atmosphere. Mineral dust is a well-established class of ice-nucleating particles (INPs) and plays a vital role in atmospheric IN as documented for the last 50 years.

Volcanic dust and biogenic particles: Volcanic dust and biogenic particles are other natural primary particles that are emitted. Volcanoes inject enormous amounts of ash, sulfur dioxide, dimethyl sulfide (DMS), and other gases into the stratosphere yielding sulfate aerosols upon oxidation (Tomasi and Lupi, 2016; Genareau *et al.*, 2018). The biosphere can also emit volatile organic compounds (VOC) that can be oxidized and form new particles. While there, these aerosols will remain for around two years in the stratosphere, minimizing the amount of solar energy that enters the lower atmosphere and the Earth's surface by partially reflecting sunlight into space. Aerosols can also be produced naturally through biological processes – pollens, spores, and plant waxes are examples of biological aerosols (Andreae and Crutzen, 1997; Wilson, 2012; O'Sullivan *et al.*, 2015). All these natural primary particles are mainly found in the coarse mode of the aerosol size distribution.

2.1.1.2 Anthropogenic Aerosols

Human activities produce anthropogenic aerosols, which are mostly found in urban and industrial settings. They can also be subject to long-range transport. Industrial dust, black carbon, and organic material are examples of primary particle emissions that can remain in the atmosphere for up to 3-5 days (Fuzzi *et al.*, 2015). Secondary aerosol sources of anthropogenic origin include sulfates from SO_2 emissions, biomass burning, organics from anthropogenic VOCs, ammonia emissions, and nitrates from nitrogen oxides (Bond *et al.*, 2007). These can be emitted through domestic heating using coal or wood, from industrial plants, vehicle emissions, agricultural and land activities, or large forest fires. After the industrial revolution, the amount of man-made sulfate aerosols in the atmosphere has risen dramatically, outweighing naturally occurring aerosols. Secondary aerosols such as nitrate and sulfate are generated when nitrogen oxide and sulfur dioxide are oxidized to nitric and sulfuric acids. They condense on preexisting aerosols and react with ammonia to form their corresponding ammonium salts in the particle phase (George and Abbatt, 2010). A substantial fraction of fine aerosols is composed of secondary organic aerosols (SOA) formed from oxidation of volatile organic gases emitted from natural sources such as vegetation and forests and vehicular exhaust (Andreae and Crutzen, 1997). Sulfuric acid can also nucleate to create new particles, some of which may be lost due to coagulation with larger particles. Simultaneously, the rest may grow to larger sizes via condensation of various secondary trace gases. Oceanic phytoplankton emits trace gases such as dimethyl sulfide, which upon oxidation can lead to the formation of secondary sulfate and methanesulfonic acid aerosols in the marine atmosphere. Sulfate aerosols absorb and reflect sunlight, reducing the amount of light reaching the Earth's surface; they often penetrate clouds, increasing the number of cloud droplets while decreasing their size. While natural sources account for most global emissions, which are primarily coarse mode contributions, anthropogenic sources account for most fine mode contributions (Seinfeld and Pandis, 2016).

2.2 Cloud Condensation Nuclei

Clouds are observable clusters, suspended in the atmosphere of small particles of water or ice, or both. They are one of the most visible and influential elements of the Earth's climate system, essential to weather but difficult to reliably forecast. Clouds appear in

various sizes and forms determined by atmospheric motions, composition and temperature. For decades, the inherent variety and variability of clouds have fascinated and challenged researchers. Three elements are required for the formation of clouds: water vapor, aerosols, and cooling. A cloud will not develop if any of these are missing. Water vapor or gaseous water is transferred mainly through evaporation from the surface to the atmosphere.

Aerosol particles affect clouds' microphysical properties through their role as CCN, which controls cloud water droplets' concentration and size (Li *et al.*, 2019). However, because of the considerable variation in the mixing of components in the atmosphere, an improved understanding of aerosol-cloud interactions is necessary to overcome uncertainties in this field and make better estimates of the emitted compounds' impact. Studying the processes and parameters that determine how an aerosol particle turns into a CCN and cloud droplet or ice crystals is essential.

Generally, CCN is aerosol particles capable of forming (activate) cloud droplets under atmospheric water supersaturations, specifically when relative humidity (RH) exceeds the saturation level. Air becomes commonly supersaturated through the uplift of moist air accompanied by adiabatic expansion and cooling. It usually occurs for a local turbulent convention in frontal systems, in large cyclonic areas, or along the mountain's slopes. CCN activation takes place via the uptake of water vapor primarily by the hydrophilic part of atmospheric particles. This hygroscopic growth of aerosols leads to aerosol particles' activation into CCN, initiating cloud formation (Seinfeld and Pandis, 2016). An aerosol particle's potential to become a cloud droplet depends on the particle's chemical composition and physical characteristics (Salameh and Daskalakis, 2017). Water solubility and surface tension are among the physical properties affecting the CCN activity of atmospheric aerosol particles.

Atmospheric aerosol particles act as surfaces for water vapor to condense on. The growth of aerosol particles by taking up water vapor is referred to as hygroscopic growth, and it takes place by water vapor condensing at a given RH. RH is expressed as the ratio of water pressure and saturation vapor pressure at the same ambient temperature, and it is expressed in %:

$$RH = \frac{P_w}{P_{ws}} \times 100 \%$$ **Eq. 1**

, where, P_w is the water vapor partial pressure at a given ambient temperature and P_{ws} is the water temperature saturation pressure at the same temperature.

The hygroscopic growth is defined as the ratio of the diameter of an aerosol particle at a specific RH to its dry diameter (D_{dry}) and can be described by the term growth factor (GF) as follows:

$$GF_D = \frac{RH}{D_{dry}}$$ **Eq. 2**

Hygroscopic growth refers to subsaturated conditions, where the RH is below 100%. When RH exceeds 100 %, the air becomes supersaturated, and the humidity is high enough for the particle to reach a critical size and act as CCN forming a cloud droplet (*see* Figure 2) (McFiggans *et al.*, 2006). For a given particle composition and size, the ambient water concentration above which the particle starts to grow without a limit and activates to make a cloud droplet is described by Köhler theory (Köhler, 1936). The Köhler theory's formulation shows that water solubility and surface tension are the main properties required to explain their CCN potential along with the physical dimensions of the aerosol particles (Seinfeld and Pandis, 2016).
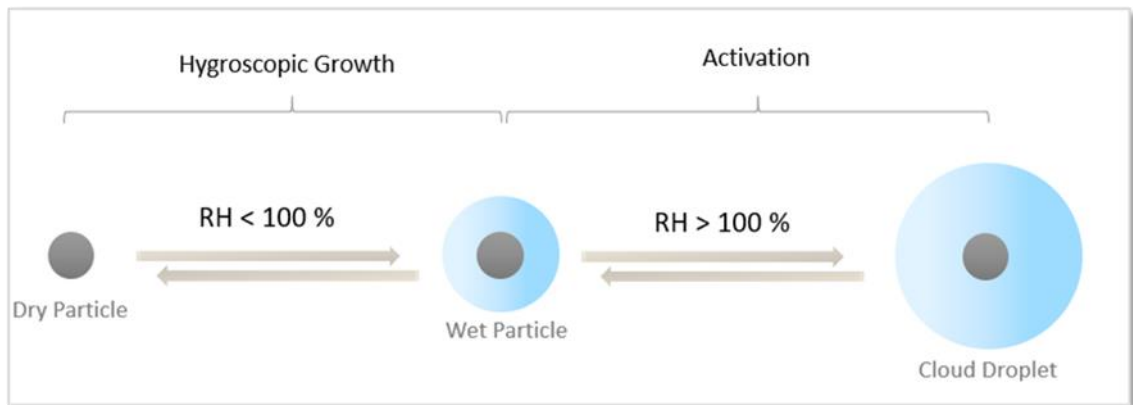
Figure 2: Schematic of aerosol particle growth and CCN activation

2.2.1 Köhler Theory

Köhler theory was developed in 1936 by the Swedish meteorologist Hilding Köhler, a Professor of Meteorology at Uppsala University. In the field of cloud physics, it is a well-known model that describes the condensational growth and activation of cloud droplets to form clouds employing equilibrium thermodynamics. It is commonly used as a parametric and predictive tool to determine water condensation conditions and cloud droplet activation and growth. This theory combines the Kelvin effect, which describes the change in saturation vapor pressure due to a curved surface, and Raoult's Law, which relates the saturation vapor pressure to the solute (Pruppacher, Klett and Wang, 1998).

According to the Kelvin effect, higher ambient water pressure must maintain equilibrium over a curved droplet surface compared to a planar surface due to the additional Gibbs free energy required to form the curvature. The liquid's curvature reduces the liquid phase's net inward attractive force, making it easier for water molecules to leave the droplet surface and migrate to the vapor phase. Kelvin equation (Eq. 3) gives the relationship between a curved droplet's equilibrium saturation pressure and the droplet diameter. It is derived from the difference between Gibbs free energy of flat and curved surface water at equilibrium with their respective vapor:

$$S_k = \frac{p_w(D_p)}{p_0} = exp\left(\frac{4\sigma_w M_w}{RT\rho_w D_p}\right) \qquad \textbf{Eq. 3}$$

where S_k is the Kelvin saturation ratio, p_w is the droplet water vapor pressure, p_0 is the corresponding saturation vapor pressure over a flat surface, σ_w is the droplet surface tension, M_w is the molecular weight of water, ρ_w is the density of pure water, and D_p, is the cloud droplet diameter, T is the absolute temperature of the droplet, R is the universal gas constant.

The Raoult effect is the second competing effect in Köhler theory. It describes how lower ambient vapor pressure is required to maintain equilibrium over water solution than pure water. When CCN particles dissolve in the atmosphere to form a liquid droplet, they lower vapor pressure over the droplet and allow the droplet to grow into a cloud droplet at relatively low supersaturation.

For highly diluted solutions, $\gamma_w \to 1$, Raoult's law is given by:

$$S_R = \frac{p_w(D_p)}{p_0} = a_w = x_w \gamma_w = \frac{n_w}{n_w + n_s} \gamma_w \qquad \text{Eq. 4}$$

where S_R is the is Raoult saturation ratio, a_w is the water activity, x_w is the mole fraction of water, γ_w is the activity coefficient of water, n_w is the number of moles of water, and n_s are the moles of the solute.

By combining the Kelvin effect and Raoult law, the Köhler equation provides the saturation ratio S at a given radius of water droplet formulated as follows:

$$ln\left(\frac{p_w(D_p)}{p_0}\right) = \frac{4\sigma_w M_w}{RT\rho_w D_p} - \frac{6n_s M_w}{\pi\rho_w D_p{}^3} \qquad \text{Eq. 5}$$

The first term of the equation represents the Kelvin effect, while the second term is the Raoult effect.

Figure 3 illustrates the combined effect from these two terms on the equilibrium supersaturation of water over solution droplets. The maximum point of the Köhler curve represents the critical supersaturation (S_c) point and it occurs at the critical radius (r_c), for activation. Droplets that reach this radius can activate and grow into a cloud droplet. Until the atmospheric supersaturation, S, reaches S_c, the particle cannot activate and expand into a cloud droplet.
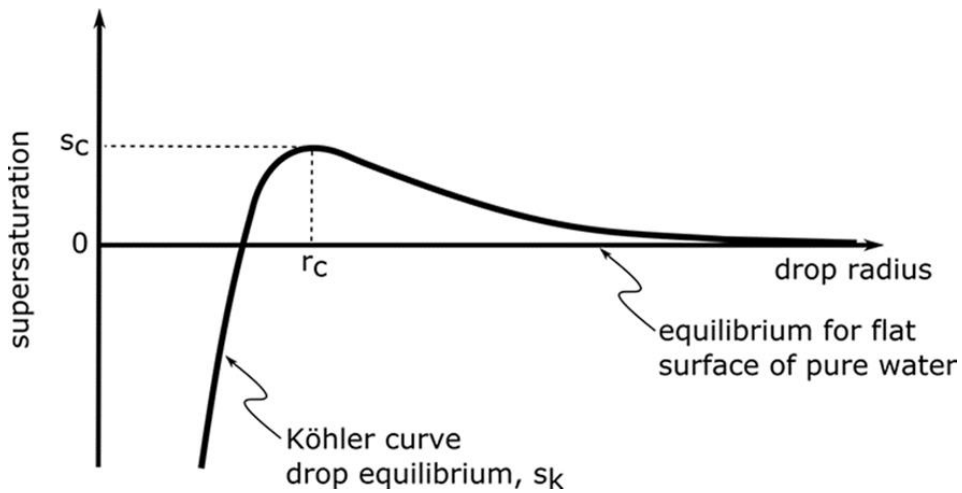
Figure 3: Schematic of Köhler curve. S_c and r_c are critical supersaturation and droplet radius at the critical point.

In detail, following the Köhler curve (*see* Figure 3), we need to compare the Köhler curve for each droplet to the environment's ambient supersaturation to see what happens to the droplet. The Köhler curve is the equilibrium supersaturation for each droplet, and it varies as a function of size. The amount of vapor available in the atmosphere is known as ambient supersaturation (S). When S is equal to S_c the droplet is in equilibrium with the environment. The droplet will always try to achieve this equilibrium condition by growing (condensing ambient water vapor) or shrinking (evaporating water). If $S_c < S$, then net condensation will occur, and the droplet will grow. If $S_c > S$, then net evaporation will occur, and the droplet will shrink. As long as the ambient is supersaturated (RH is above 100%), growth beyond r_c will rapidly transform the particle into a cloud droplet, and this process is called cloud droplet activation (Seinfeld and Pandis, 2016).

2.2.2 Surface Tension

Among the physical properties affecting the CCN activity of atmospheric aerosol particles is surface tension. Since atmospheric aerosols usually contain components composed of organic and inorganic molecules with different water solubilities, improved knowledge of these substances' effect on the surface tension and cloud droplets activation of atmospheric aerosols is of particular importance.

Surface tension is a macroscopic property quantifying microscopic molecular interactions, and it is an essential parameter for many biological or industrial processes. It can be defined as the force that the liquid molecules perform to minimize the liquid's surface area (Werner *et al.*, 2014). For a system at constant volume, temperature, and composition

$$\gamma = \left(\frac{\partial A}{\partial \mathcal{A}} \right)_{N,V,T} \qquad \textbf{Eq. 6}$$

where A is the Helmholtz free energy and $\mathcal{A}$ is the surface area. The corresponding expression at constant pressure involves the Gibbs free energy G

$$\gamma = \left(\frac{\partial G}{\partial \mathcal{A}} \right)_{N,P,T} \qquad \textbf{Eq. 7}$$

The surface tension results from an imbalance of intermolecular attractive forces (cohesive forces) between molecules. A molecule at the surface of a liquid experiences only net inward cohesive forces because it has a small number of neighbors. Hence, fewer attractive interactions than a molecule in bulk, while a molecule in the bulk of the liquid experiences cohesive forces with other molecules in all directions (*see* Figure 4).

For the water's vapor-liquid interface, the surface tension is $0.0728\,N/m$ at $20\,°C$, reflecting the strong hydrogen bonding between water molecules (Petersen and Saykally, 2006; Ghoufi, Malfreyt and Tildesley, 2016). One usually attributes the high surface tension of pure water to missing hydrogen bonds at the surface. Still, it has become challenging to calculate or simulate their contribution to the surface tension in both theory and simulations (Hauner *et al.*, 2017).
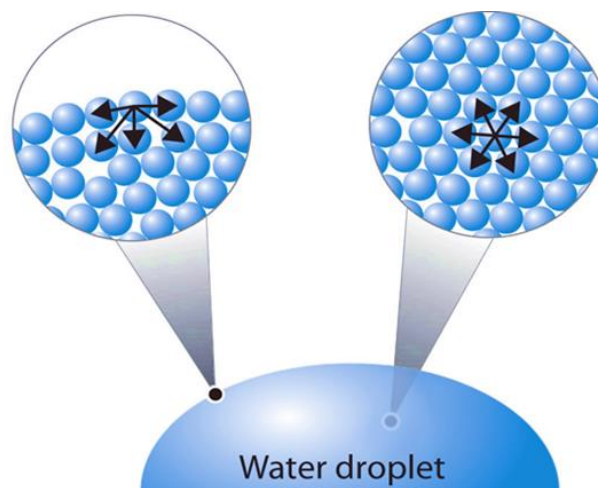
Figure 4: Schematic representation of the surface tension of a liquid

2.3 Ice Nucleation

Ice nucleation (IN) is a crucial atmospheric mechanism for cirrus and mixed-phase clouds' formation and properties. As previously mentioned, clouds form when water molecules condense into CCN, and liquid water in clouds warmer than -37°C can be supercooled, causing droplets to freeze. The ice formation rates in supercooled water are formulated in the so-called classical nucleation theory (Pruppacher, Klett and Wang, 1998). Ice nucleation can occur by two different mechanisms: homogeneous freezing of water and solution droplets at temperatures below -35°C, or heterogeneous ice nucleation caused by

insoluble aerosol particles. The heterogeneous IN aerosol particles nucleate into ice under supercooling conditions for temperatures between 0 and -35 ° C. While homogeneous freezing is needed for cirrus cloud formation, despite decades of research on ice nucleation processes, the primary process through which mixed-phase clouds shape (heterogeneous freezing) remains poorly understood. Various approaches have been established to compare the homogeneous and heterogeneous freezing rates of solution droplets to those of the pure water process (Thijssen, Vorstman and Roels, 1968; Franks, Mathias and Trafford, 1984; Sassen and Dodd, 1988; Richardson and Snyder, 1994; Koop *et al.*, 2000; Koop, 2004; Zobrist, Marcolli, Peter, *et al.*, 2008; Chukin, Pavlenko and Platonova, 2010). Given the importance and ubiquity of the water-ice phase transition, a greater understanding of the process is of both practical and fundamental interest.

2.3.1 Classical Nucleation Theory

The most accepted theoretical model used to explain the nucleation of a new thermodynamic process is classical nucleation theory (CNT). It's an approximate theory that reasonably predicts nucleation rates (Pruppacher, Klett and Wang, 1998). CNT was developed in the 1930s, and it stems from the work of Volmer and Weber, Becker and Döring, and Frenkel (Volmer, M.; Weber, 1926; Becker and Döring, 1935; Frenkel, 1946). CNT uses a classical method, the capillarity approximation, in which a small droplet initiating nucleation of the bulk liquid from vapor is considered a macroscopic entity. Within the capillarity approximation, thermodynamic arguments may be used to calculate the surface and bulk energy impacts to the free energy of critical particle formation (Laaksonen and Napari, 2001; Weinberg, Poisl and Granasy, 2002; Karthika, Radhakrishnan and Kalaichelvi, 2016).

2.3.2 Homogeneous Ice Nucleation

According to Vali et al., homogeneous ice nucleation is defined as the "*Ice nucleation without any foreign substance aiding the process*" (Vali *et al.*, 2015). It's a stochastic process in which a stable ice nucleus (germ) emerges at random due to internal fluctuation (Sassen and Dodd, 1988; Koop, 2004; Knopf and Lopez, 2009; Chukin, Pavlenko and Platonova, 2010; Kärcher and Seifert, 2016). The temperature range in which

homogeneous freezing occurs is determined by many factors, including droplet size, cooling rate, and water purity (Pruppacher, Klett and Wang, 1998).

Before ice clusters become stable throughout the nucleation process, they must reach a critical size (Pruppacher, Klett and Wang, 1998). This critical size can be reached at temperatures below -35°C in the case of homogeneous freezing. The ability to form a stable cluster is dependent on the liquid content, as in large water volumes, and nucleation is expected to occur near the ice melting point. On the other hand, water in tiny droplets is supercooled to about -37°C (Krämer *et al.*, 1999; Murray, Knopf and Bertram, 2005; Stan *et al.*, 2009). Turnbull was the first to examine ice nucleation in a closed system in 1952 (Turnbull and Vonnegut, 1952). To prevent heterogeneous nucleation, he examined homogeneous nucleation with tiny droplets. In general, homogeneous nucleation experiments are difficult to conduct because it is nearly impossible to maintain conditions with low enough impurities to prevent heterogeneous nucleation. Recent techniques like electrodynamic levitation and oil emulsion, on the other hand, can restrict heterogeneous nucleation centers, allowing ice to form through a homogeneous nucleation method (T. Li *et al.*, 2011).

The quantitative and mechanistic understanding of homogeneous ice nucleation in water is a difficult task. Some soluble organics obstruct homogeneous freezing, affecting the ice nucleation method (Cziczo *et al.*, 2004; Kärcher and Koop, 2004; Daskalakis and Hadjicharalambous, 2014). Other findings revealed that some supercooled organic-aqueous solutions form glasses (Murray, 2008). Recent research has shown that ice crystallites can form in the atmosphere by homogeneous nucleation in preexisting liquid aerosols (Russo, Romano and Tanaka, 2014). The role of the glassy phase in enhancing homogeneous ice nucleation has been tested in the lab. Furthermore, strong supersaturations at the tropical tropopause may be explained by glassy aerosol particles. However, there is a continuing controversy about the precision of humidity measurements at low temperatures and pressures (Knopf, Alpert and Wang, 2018).

2.3.2.1   *The classical description of homogenous ice nucleation*

The Gibbs free energy (ΔG) for a cluster formation containing n water molecules with CNT can be determined using the classical nucleation theory and is the sum of the Gibbs

energy required for the formation of the ice-supercooled water interface (ΔG_S) and the energy released by bond formation (ΔG_B):

$$\Delta G = \Delta G_S + \Delta G_B \qquad \text{Eq. 8}$$

A cluster of n molecules of radius, r_n, has formation energy of

$$\Delta G_c = 4\pi r_n{}^2 \gamma_{sl} \qquad \text{Eq. 9}$$

where γ_{sl} denotes the ice-supercooled water interface's interfacial tension.

The bonding formation's Gibbs free energy is determined by

$$\Delta G_B = (\mu_s - \mu_l)n \qquad \text{Eq. 10}$$

where μ_s and μ_l are the solid and liquid phase chemical potentials, respectively.

The chemical potentials can be formulated as

$$-(\mu_s - \mu_l) = kT \ln S \qquad \text{Eq. 11}$$

The Boltzmann constant is k, the temperature is T, and the liquid water saturation is S.

The number of molecules, n, is

$$n = \frac{4\pi r_n{}^3}{3v} \qquad \text{Eq. 12}$$

where v is the molecular volume of water;

The total Gibbs energy can be expressed as:

$$\Delta G = 4\pi r_n{}^2 \gamma_{sl} - \frac{4\pi r_n{}^3}{3v} kT \ln S \qquad \text{Eq. 13}$$

The two terms of Eq. 13 are opposing, so the free energy of ice formation passes through a maximum, as shown in Figure 5. The maximum value corresponds to the size of the critical nucleus, r_c.

The radius of the critical cluster, r_c can be calculated by differentiating Eq. 13 and setting $d\Delta G/dr_n = 0$,

$$r_c = \frac{2\gamma_{sl}}{kTlnS} \qquad \qquad \textbf{Eq. 14}$$

Eq. 14 can be used to calculate the temperature dependence of the critical radius size.

Furthermore, the Gibbs energy of a new critical-sized cluster at T, ΔG_{hom}, can be measured as follows:

$$\Delta G_{hom} = \frac{16\pi\gamma_{sl}{}^3 v^2}{3(kTlnS)^2} \qquad \qquad \textbf{Eq. 15}$$

This equation emphasizes the nucleation energy barrier's reliance on interfacial energy.
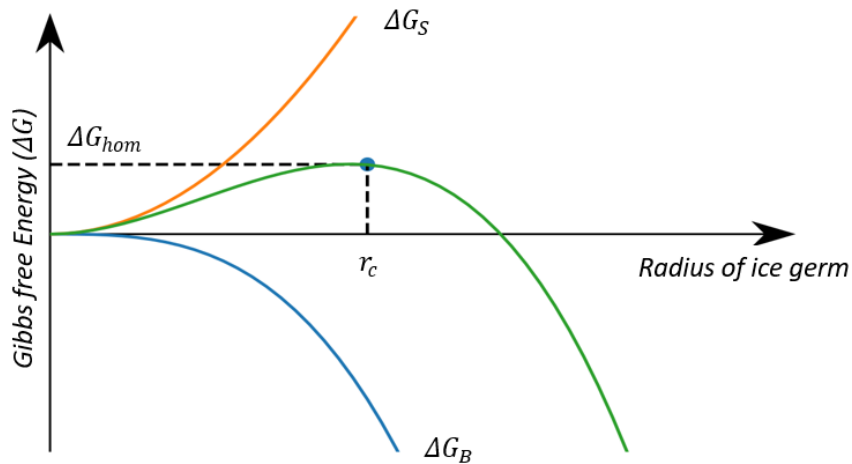
Figure 5: Gibbs free energy vs. radius diagram. The orange line shows the Gibbs energy required to shape the ice-supercooled water interface (ΔG_S), the blue line shows the energy released during bond formation (ΔG_B), and the green line shows the total Gibbs free energy (ΔG).

The nucleation rate coefficient (J_{hom}) is connected to the Gibbs energy required to form a critical cluster and can be determined by an Arrhenius form:

$$J_{hom} = A exp\left(-\frac{\Delta G_{hom}}{kT}\right)$$

<div align="right">**Eq. 16**</div>

Where A is the pre-exponential factor. Combing Eq. 15 and Eq. 16:

$$ln J_{hom} = \ln A - \frac{16\pi\gamma_{sl}{}^3 v^2}{3(kT ln S)^2}$$

<div align="right">**Eq. 17**</div>

Therefore, homogeneous ice nucleation is more possible in large volumes of water. A freezing rate $R(t)$ can be calculated in an experiment with a large number of identical droplets (held at constant temperature) where a single nucleation event within a droplet is expected to crystallize that droplet.

$$R(t) = \frac{1}{N_0 - N_f}\frac{dN_f}{dt}$$

<div align="right">**Eq. 18**</div>

where, N_f is the total number of freezing droplets at time t and N_0 is the total number of droplets present.

If the droplets are nucleated via the homogenous mechanism, then

$$J_{hom} = J_V = \frac{R(t)}{V}$$

<div align="right">**Eq. 19**</div>

where V is the volume of the droplets and J_V, the volume nucleation rate.

2.3.3 Heterogeneous ice nucleation

Since the basic microphysical processes that control the interaction between aerosol particles and water molecule clusters are still unknown, heterogeneous ice nucleation is a difficult case to research. Several methods to measure the ice nucleation efficiencies of various aerosol species have been investigated and evaluated in recent decades due to this lack of fundamental understanding. Heterogeneous ice nucleation is defined by Vali et al. (2015) as follows: "*Ice nucleation aided by the presence of a foreign substance (ice nucleating particle, INP)*" (Vali *et al.*, 2015).

Although homogeneous ice nucleation is catalyzed by a solid surface, such as an insoluble amorphous organic aerosol particle, heterogeneous ice nucleation is catalyzed by a solid

surface (Pruppacher, Klett and Wang, 1998). IN for temperatures between 0 and -35°C or ice supersaturation at temperatures below 0°C, cause heterogeneous ice nucleation. In the presence of particles, the formation of ice in nature is almost heterogeneous.

The ability of a particle to act as an ice nucleus is summarized by Pruppacher and Klett (Pruppacher, Klett and Wang, 1998) in the following five physical characteristics:

1. *Physical state*: Ice embryo formation requires a solid substrate, as particles that dissolve in wet conditions cannot function as IN.

2. *Particle size*: Since smaller particles are soluble, size is critical for the efficiency of an IN. Unsurprisingly, ice nucleation occurs more frequently on larger aerosols, especially those with diameters greater than 0.01 - 0.1 m. The chemical composition and supersaturation of the atmosphere determine the size of an IN.

3. *Hydrogen bonding*: Since ice is held together by hydrogen bonds of unique polarity and strength, IN must form hydrogen bonds with water. On its surface, an effective IN would have similar bonding sites.

4. *Crystallographic arrangement*: On an IN's surface, the geometric arrangement of hydrogen bonding molecules must be identical to an ice crystal lattice.

5. *Active sites*: Due to unique physical properties, ice nucleation occurs on some active sites. Surface defects (a phase, crack, pore, or cavity) or chemical impurities at a solid's surface are active sites.

The characteristics mentioned above give a general idea of what properties could make individual particles more efficient IN. They must, however, be reconsidered. They may not entirely refer to hygroscopic solutions in a glassy state, atmospheric organic aerosol, and secondary organic aerosol, all of which have demonstrated ice nucleation capability (Murray *et al.*, 2012a). Given this, quantitative experimentation is the best way to determine the efficacy of ice nuclei.

2.3.3.1 *Modes of Heterogeneous Ice Nucleation*

Different types of heterogeneous ice nucleation of INPs occur. The fundamental distinction is made based on the process envisaged to lead to nucleation (Vali *et al.*, 2015). In 2015 Vali et al. (Vali *et al.*, 2015) published a technical note outlining the terminology

dealing with ice nucleation. The definitions described in this section are based on this document.
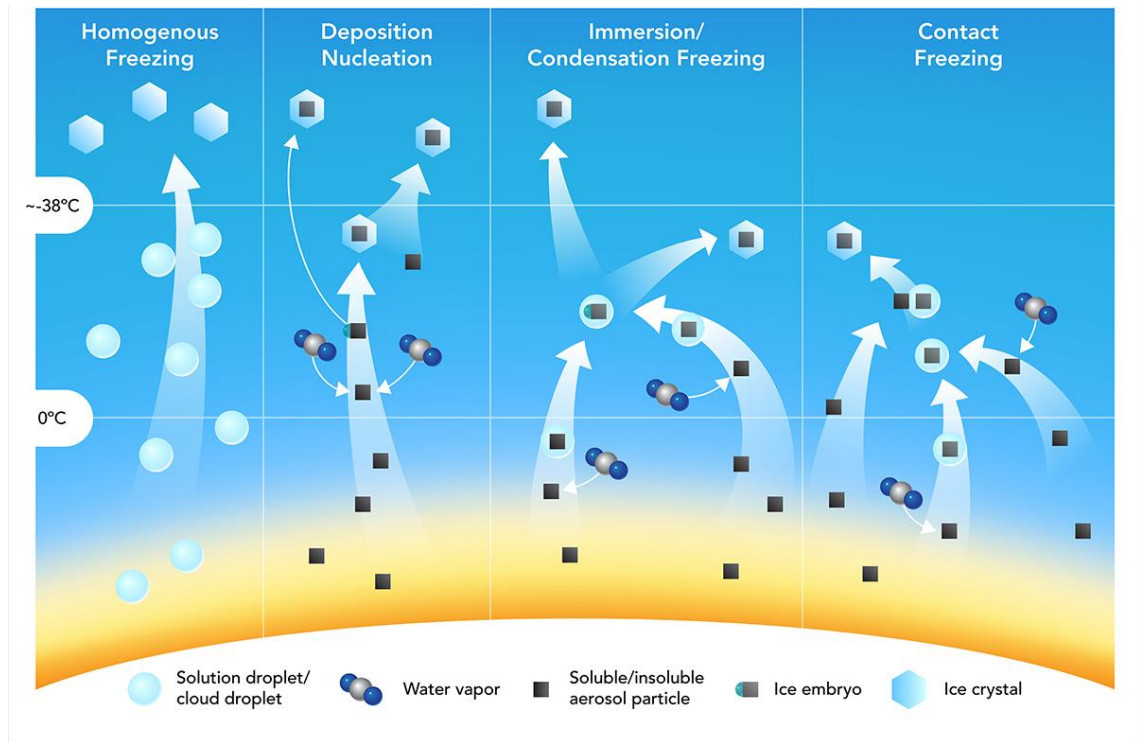
Figure 6: Schematic diagram of ice nucleation mechanisms as defined by Vali et al. (Vali *et al.*, 2015).

The two overarching modes of ice nucleation are deposition and freezing (see Figure 6). Deposition nucleation is defined as "*Ice nucleation from supersaturated vapor on an INP or equivalent without prior formation of liquid*" (Vali *et al.*, 2015). It is a gas to a solid phase transition. Freezing nucleation is defined as *"Ice nucleation within a body of supercooled liquid ascribed to the presence of an INP, or equivalent"* (Vali *et al.*, 2015). It is a liquid to a solid phase transition. Freezing nucleation is further categorized into three other modes: immersion freezing, contact freezing, and condensation freezing.

Immersion freezing refers to ice nucleation within the body of liquid induced by an INP or similar. Contact freezing is initiated by an INP at the air-water interface as it encounters the liquid or forms at air-liquid–particle triple interface. Condensation freezing is defined as taking place when freezing is initiated concurrently with the initial liquid formation on a CCN at temperatures below the melting point of ice.

It is challenging to distinguish condensation freezing in a strictly physical sense from both deposition nucleation and immersion freezing. In most cases, the microscopic process of ice formation is not understood. Previous studies indicate that there is a possibility that ice formation of microscopic water amounts followed by depositional growth precedes most or all cases of deposition nucleation occurring for organic vapors (Whale, 2018). In the same way, it is not clear how condensation freezing differs from immersion freezing in cases where liquid water does form before freezing. It is thought that immersion mode freezing is likely to be the dominant freezing mode in most mixed-phase clouds (De Boer *et al.*, 2011; Wheeler and Bertram, 2012).

2.3.3.2 *Heterogeneous classical nucleation theory*

As shown below, the Arrhenius equation for homogeneous nucleation can be modified to account for the heterogeneous nucleation coefficient:

$$J_{het}(T) = A_{het}\,exp\left(-\frac{\Delta G * \varphi}{kT}\right) \qquad \textbf{Eq. 20}$$

where A_{het} is a pre-exponential factor and φ is the factor that decreases the height of the energy barrier compared to homogeneous nucleation when a solid surface is present. The ice-nucleating efficiency parameter, m, is frequently used to express this factor.

$$\varphi = \frac{(2 + m)(1 - m)^2}{4} \qquad \textbf{Eq. 21}$$

The heterogeneous nucleation rate expression is

$$\ln J = \ln A_{het} - \frac{16\pi\gamma_{sl}{}^3 v^2}{3(kT\,lnS)^2}\frac{(2 + m)(1 - m)^2}{4} \qquad \textbf{Eq. 22}$$

The above model has also been used to explain heterogeneous ice nucleation in atmospheric cloud models (Hoose and Möhler, 2012; Wheeler and Bertram, 2012).
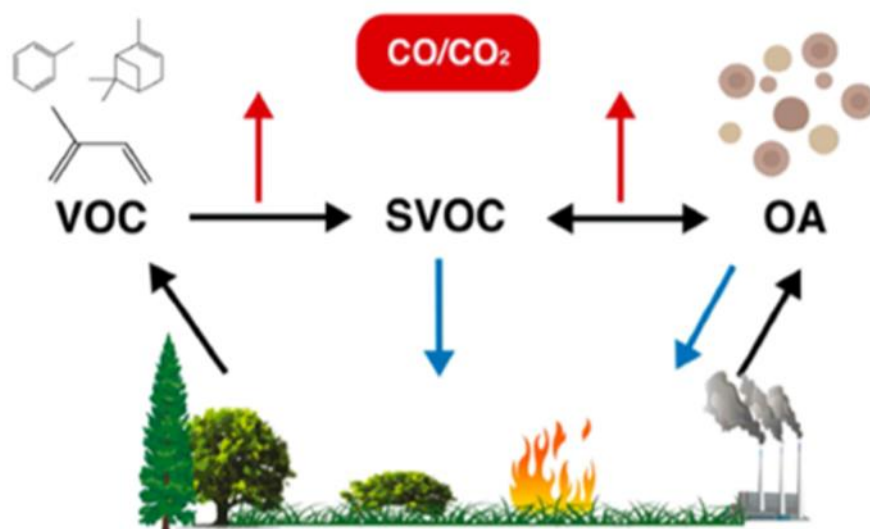
Figure 7: Organic compounds are emitted directly from natural sources, mainly vegetation, and from fossil fuel or biomass combustion into the atmosphere (taken from (Glasius and Goldstein, 2016)).

2.4 Organic Aerosols and their role in Ice Nucleation

Organic matter is ubiquitous in the atmosphere in the form of organic aerosol (OA) particles. While mineral dust particles and SSA account for the greatest aerosol mass concentrations, OA makes up a significant fraction of the ambient global tropospheric aerosol (Knopf, Alpert and Wang, 2018). The contribution of organics to the ambient particulate matter mass can be ∼20–50% at continental mid-latitudes and as high as 90% in tropical forested areas (Kanakidou *et al.*, 2005; Jimenez *et al.*, 2009). Organic compounds are emitted directly from natural sources, mainly vegetation, and from fossil fuel or biomass combustion into the atmosphere (see Figure 7).

OAs play a critical role in a variety of atmospheric and environmental issues. The volatility, solubility, and other physicochemical properties of the thousands of organic compounds critical in the atmosphere differ significantly. Despite this, the diversity of organic chemistry and the highly unpredictable physical properties of organic particles, both natural and anthropogenic, make collecting chemical data on these compounds extremely difficult. As a result of this serious obstacle, there is an incomplete picture of a potentially crucial element of atmospheric chemistry and, as a result, a lack of knowledge of organics' environmental effects (Glasius and Goldstein, 2016).

Several different pathways can activate cloud formation by organic aerosols, depending on environmental conditions and composition. At high temperatures, high humidity, and low temperatures, liquid organic particles can act as CCN and facilitate the formation of ice crystals. As seen in Figure 8, the particle phase state determines the active ice nucleation pathway. In the deposition mode, organics will nucleate ice. Partially deliquesced particles with core-shell morphologies will act as IN in the immersion mode, whereas liquid particles nucleate ice homogeneously at a much higher ice supersaturation.
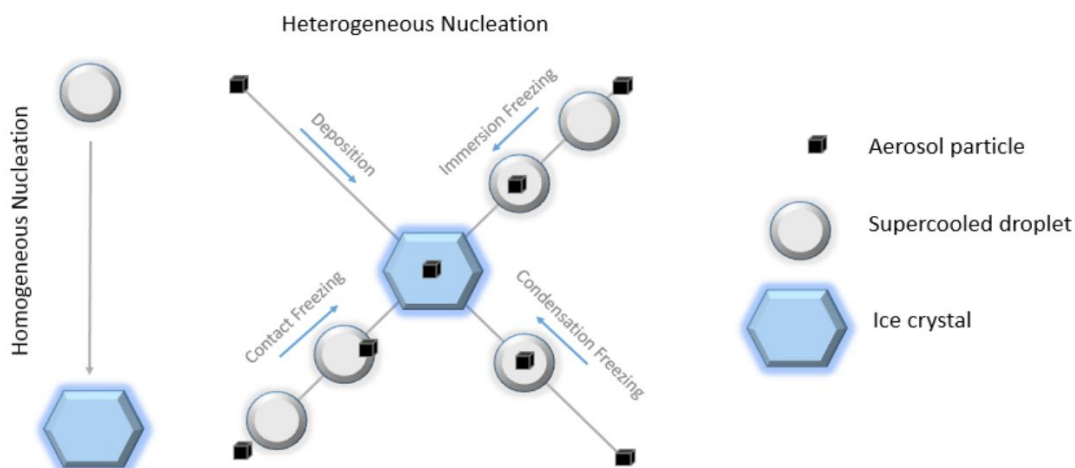
Figure 8: Schematic of Ice nucleation modes

Atmospheric OA particles come from many sources, with main and secondary formation processes. Directly from the source, primary organic aerosol (POA) is released. Secondary organic aerosol (SOA) is made up of gas-phase precursors that may have been released from natural sources or generated in the atmosphere by chemical reactions.

2.4.1   Primary organic aerosol (POA)

POAs are immediately emitted into the atmosphere by mechanical processes as a liquid or solid particles or semi-volatile vapors. Larger particles (diameter > 2.5 mm) are present. Biomass burning (e.g., household heating, forest fires, slashing and burning), fossil-fuel combustion (traffic, domestic, commercial), biological substances (microorganisms, pollen, spores, etc.), sea spray, and dissolved organic compound spray from other surface waters are the key sources (Ziemann and Atkinson, 2012).

2.4.2   Secondary organic aerosol (SOA)

SOAs are produced in the atmosphere when volatile compounds, including sulfates, nitrates, and some organics, are converted from gas to particle (Ziemann and Atkinson, 2012). If released, they form by the condensation of molecules from the gas phase or the collision of their particles (coagulation), resulting in the formation of larger yet fewer mixed chemical composition aerosol particles. Cloud droplets and wet deposition then remove these particles, allowing nucleation to form new particles. SOAs can be shaped in three different ways. The first pathway is new particle formation, in which gas-phase reactions produce semi-volatile organic compounds (SVOCs), which are involved in the nucleation and growth of new aerosol particles. The second pathway is the gas-particle partitioning pathway that produces SVOCs by gas-phase reactions and absorption by pre-existing aerosol or cloud particles. Finally, heterogeneous or multiphase reactions produce low-volatile organic compounds (LVOCs) or non-volatile organic compounds (NVOCs) due to VOC chemical reactions at the surface or in the bulk of aerosol or cloud particles (Virtanen *et al.*, 2010). The formation of SOAs is of high importance, influencing public health and the environment (Fuzzi *et al.*, 2006).

2.4.3   Glassy Organics

The atmosphere has many organic aerosol particles (Hoose and Möhler, 2012). Recent studies propose that glassy organic particles act as IN at low-temperature cirrus conditions in the deposition mode or slightly elevated temperatures in the immersion mode (Bahreini *et al.*, 2005; Fuzzi *et al.*, 2006; Zobrist, Marcolli, Pedernera, *et al.*, 2008; Mikhailov *et al.*, 2009; Saukko *et al.*, 2012). Glassy organic aerosol compound ice nucleation is still poorly known and quantified. Glassy aerosols can nucleate ice in a heterogeneous manner, preventing homogeneous freezing (B. J. Murray *et al.*, 2010). These processes require relatively low tropospheric temperatures, which would primarily affect cirrus formation. The phenomenon of irregular supersaturations at the tropopause may be explained by glass aerosol particles. Below –70°C, cubic ice nucleates in an inclination to hexagonal ice, increasing the dehydration caused by cirrus clouds (Murphy, 2003).

Amorphous substances that behave like solids are called glasses. Their chemical and physical properties are crucial in the formation of glass. There is no release of latent enthalpy during the glass transition (Zobrist, Marcolli, Pedernera, *et al.*, 2008). As a

result, it isn't a first-order step shift. In first-order phase transitions, latent heat is involved. A system absorbs or releases a large amount of energy per volume during such a transition, and the system temperature remains constant as heat is applied. When the temperature drop below the glass transition temperature T_g, glassy water (amorphous ice) will form (about 130 K at 1 bar). Although glassy water is solid, its structure displays a disordered liquid-like arrangement. At low temperatures and humidity, SOA particles may become viscous semisolid or glassy (Saukko *et al.*, 2012; Renbaum-Wolff *et al.*, 2013; Shiraiwa *et al.*, 2013). Many articles provide evidence of this in the literature based on the field (Froyd *et al.*, 2010; Knopf *et al.*, 2010; Renbaum-Wolff *et al.*, 2013; Shiraiwa *et al.*, 2013) and laboratory studies (Benjamin J. Murray *et al.*, 2010; Wagner *et al.*, 2012; Wang, Laskin, *et al.*, 2012; Baustian *et al.*, 2013; Schill, De Haan and Tolbert, 2014). The organic particles that were researched and exhibited ice nucleation vary from simple sugars and acids (Benjamin J. Murray *et al.*, 2010; Wagner *et al.*, 2012; Wang, Laskin, *et al.*, 2012; Wilson *et al.*, 2012; Baustian *et al.*, 2013) to biomass burning compounds (Wilson *et al.*, 2012; Baustian *et al.*, 2013; Schill and Tolbert, 2013), volatile aromatic compounds (Wang, Laskin, *et al.*, 2012), and aqueous particles (Schill, De Haan and Tolbert, 2014).

Glass-transition temperature (T_g) refers to the temperature range in which a glass transition occurs. It is lower than the crystalline state of a material's melting temperature (T_m). Since the thermodynamic variables entropy (S) and enthalpy (H) indicate continuity, the glass transition is a second-order transition. Upon cooling, H and S decrease in a stable liquid. If crystallization occurs without supercooling, a sudden drop in H and S can be observed at the melting point (T_m). Most liquids exhibit supercooling below T_m, as crystallization is kinetically impeded and H and S decrease continuously even below T_m (Zobrist, Marcolli, Pedernera, *et al.*, 2008; Salameh and Daskalakis, 2017)

Nucleation can happen suddenly in a supercooled liquid, and in this case, H and S decline unpredictably to their crystal values at the nucleation temperature (Zobrist, Marcolli, Pedernera, *et al.*, 2008; Salameh and Daskalakis, 2017). Upon cooling, the liquid's viscosity increases, inhibiting nucleation (Pablo G. Debenedetti and Stillinger, 2001), and in some cases, it can increase to a point where molecules are immobilized, preventing equilibration to the system's lowest energy state (Pablo G. Debenedetti and Stillinger, 2001; Zobrist, Marcolli, Pedernera, *et al.*, 2008). Glass is created at the glass transition

temperature, T_g. This process is known as vitrification. Glassy solids may nucleate ice in the deposition mode (Wang, Lambe, *et al.*, 2012). Partially deliquesced particles with core-shell morphologies will act as IN in the immersion mode, whereas liquid particles can nucleate ice homogeneously at much higher ice supersaturation (Wagner *et al.*, 2017). To nucleate ice heterogeneously glassy organic particles require temperatures below 230 K. As a result, their spectrum of atmospheric activity is restricted to the upper troposphere and lower stratosphere.

3   Molecular Dynamics Simulations

Ice nucleation is one of the most essential atmospheric processes. Despite the extensive research into heterogeneous ice nucleation, significant gaps exist in understanding the physicochemical properties of organics to form ice, reflecting thus our inability to accurately predict ice-nucleating efficiency and understand the chemical physics behind this process. Until recent years, insights into the microscopic mechanisms are obtained from various experimental techniques that quantify a given substance's ability to promote ice formation.

MD simulations can provide valuable insight and complement experimental evidence by unraveling the nucleation mechanism's aspects on different substrates at the molecular level. However, atomistic simulations of heterogeneous ice nucleation frequently face extraordinary challenges due to the complexity of the water-organic interactions and the long-time scales associated with the nucleation events (Sosso, Tribello, *et al.*, 2016). Nucleation is a rare event, and seconds can pass before the spontaneous formation of an ice nucleus with a critical size(Sosso, Chen, *et al.*, 2016). Running molecular simulations of these lengths cannot be tractable. That is why the last years, a considerable effort has been dedicated to developing enhanced sampling techniques capable of tackling this time scale problem (Bernardi, Melo and Schulten, 2015). Furthermore, equally crucial issues often go unacknowledged, such as the ability of the interatomic potentials of choice to represent the water, the substrate, the interaction between the two, or the extent to which simulations on ice nucleation are affected by various computational aspects (Sosso, Tribello, *et al.*, 2016).

The importance of MD simulations in atmospheric research has increased significantly in recent years. These simulations capture the behavior of molecules in full atomic detail and high temporal resolution. The latest improvements in simulation speed, accuracy, and accessibility, together with the proliferation of experimental structural data, have increased the appeal of simulations to researchers. Simulations have proven valuable in deciphering molecules' functional mechanisms in uncovering the structural basis of chemical and physical mechanisms. MD provides us with a powerful toolbox that enables us to follow and understand structure and dynamics in extreme detail—literally on scales where individual atoms are trackable. However, we must be careful as simulations will

not magically provide valid conclusions, but they require a skilled researcher to interpret the results correctly.

3.1 Theoretical Background

MD is a computational simulation method for studying atoms and molecules' physical movements over time based on a general model of interatomic interactions. Alder and Wainwright, considered the founding fathers of molecular dynamics research, developed the first MD simulation for a hard-sphere system in the late 1950s in the field of theoretical physics (Alder and Wainwright, 1957, 1959). Throw their work; they established the value of computer simulations in problems such as the behavior of Boltzmann's H-function, self-diffusion coefficients, collision rates, and velocity autocorrelation for simple systems of about 100 hard spheres (Battimelli and Ciccotti, 2018).

The next significant advance was made by Rahman, who carried the first simulation using a realistic potential for liquid argon in 1964 (Rahman, 1964) and then again in 1974 when he and Stillinger simulated a pragmatic system of liquid water (Stillinger and Rahman, 1974). Since then, due to the advent of high-performance computing (HPC) resources and the simplicity of the basic MD algorithm, many different applications in a wide field of science have been simulated, and simulation of large systems containing more than 100,000 atoms are now a routine.

As the number of simulation techniques has dramatically expanded, MD becomes a desired new tool for studying atmospheric applications. As atmospheric processes are complicated, MD simulations allow one to understand the underlying processes on an atomic level and to probe states of an atmospheric system not resolved experimentally. An atomic-level structure is useful and typically generates significant insight into how a molecule functions. The atoms are in constant motion, and both molecular function and intermolecular interactions depend on the dynamics of the molecules involved. MD gives us the ability to watch these molecules in action, modify them at the atomic level, and observe their response.

For the most part, the MD simulation technique is based on determining the trajectories of atoms and molecules by solving Newton's equations of motion of interacting particles in a system. While time evolves, the positions and velocities of the particles are updated

over short time steps. The interacting forces between the particles and their potential energies are frequently calculated using interatomic potentials or molecular mechanics force fields, comprising a set of potential functions and corresponding parameters.

A series of algorithms regulate MD simulations' computational procedure, including integration, periodic boundary conditions, neighbor searching, constraints, thermostats, and barostats. The *integrator* describes how the equations of motion are computed numerically. *Periodic boundary conditions* (PBC) are applied so that a microscopic simulation box can acceptably model an infinite system by replicating the simulation box in the three dimensions. The *neighbor searching algorithm* is used to quickly and efficiently find the pairs of atoms within a predefined cut-off radius. To maintain individual bonds at a constant length, we employ constraints. *Thermostats* and *barostats* keep the system under the desired temperature and pressure to mimic experimental conditions.

3.2   Basic MD Algorithm

The best way to understand MD simulations is to consider a basic and straightforward algorithm (*see* Figure 9). To construct the algorithm, we need to state the run conditions (initial temperature, number of particles, density, time step). The primary step is to initialize the system where atoms are assigned with input data like coordinates (positions) and velocities. The atom coordinates are chosen to be compatible with the structure that we want to simulate.

The basic MD loop starts after the initialization. It consists of two critical steps: the computation of atomic forces on all particles and integration. Force calculation is the most time-consuming part where the interactions between all the atoms are computed, and every force acting on an atom is calculated. We then integrate Newton's equations of motion propagating the atoms, indicating how these forces will affect the atoms' motions. Algorithms have been designed to do this. These steps are repeated until we have computed the system's time evolution for the required time. After that, the system is sampled to measure static and dynamics properties and calculate properties like total energy, temperature, pressure, relaxation time or kinetic energy, or more. The thermodynamic quantities of the system are controlled using a thermostat. The temperature is vital since it is directly linked to the motions of the atoms.

At the end of the simulation, a considerable amount of data is generated: positions, velocities, forces, energies, temperatures, and all other sample data collected during the calculation. All the generated data are evaluated, and the relevant physical properties are extracted.
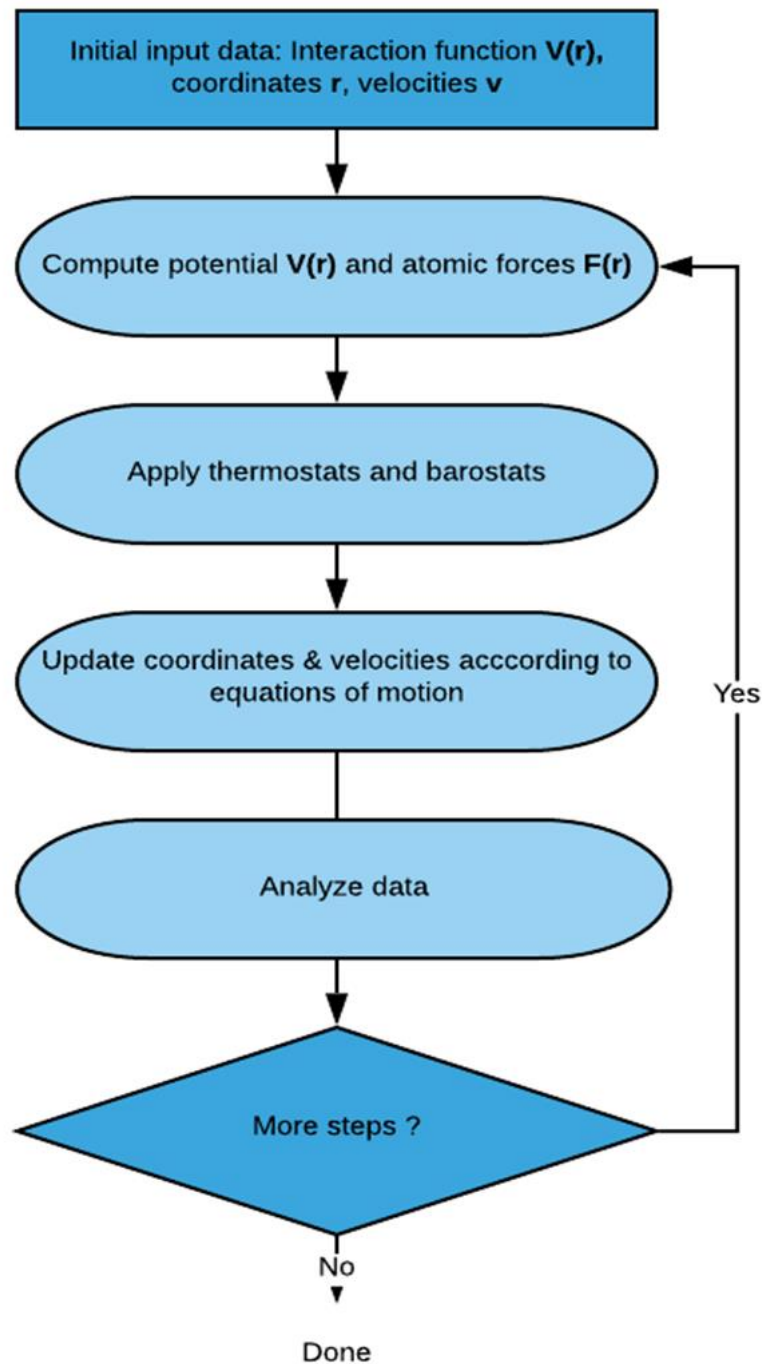
Figure 9: Basic MD Algorithm.

3.3 Equations of Motion and time Integration

As mentioned above, the time evolution of a set of interacting atoms can be followed by integrating Newton's motion equations. The equation of motion according to Newton's second law, in a system of N interacting particles with coordinates r_i, $i = 1, \dots, N$, is a second-order differential equation

$$m_i \frac{d^2 r_i}{dt^2} = F_i \qquad \text{Eq. 23}$$

where, m_i is the mass of particle i and the acting force is F_i.

It can then be extracted in terms of the gradient of a potential V_{pot},

$$F_i = -\nabla_i V_{pot} \qquad \text{Eq. 24}$$

The total energy for the system is

$$E = \sum_{i=1}^{N} \frac{m_i v_i{}^2}{2} + V_{pot} \qquad \text{Eq. 25}$$

Eq. 1Eq. 23 and Eq. 24 represent a set of $3\,N$ second order ordinary differential equations. Given a set of initial conditions for the positions $(r_1(0), \dots, r_N(0))$ and velocities $(v_1(0), \dots, v_N(0))$.

The core of an MD program is the numerical solution of Newton's equation of motion, and many different algorithms can do the numerical integration. In 1967 Loup Verlet introduced a central difference-based algorithm into molecular simulations (Verlet, 1967). In many cases, it is considered the best and simplest algorithm.

We can develop the Verlet integration algorithm by making a Taylor expansion of the position coordinates:

$$r_i(t + \Delta t) = r_i(t) + v_i(t)\Delta t + \frac{1}{2} a_i(t)\Delta t^2 + \cdots. \qquad \text{Eq. 26}$$

$$r_i(t - \Delta t) = r_i(t) - v_i(t)\Delta t + \frac{1}{2} a_i(t)\Delta t^2 + \cdots \qquad \text{Eq. 27}$$

where $a_i(t) = F_i(t)/m_i$, is the acceleration of particle i at time t.

By adding Eq. 26 and Eq. 27, we extract the equation of the Verlet Algorithm. The integrator is time-reversible with an error of the order of $\sigma(\Delta t^4)$ implied by the expansions of $r_i(t + \Delta t)$ and $r_i(t - \Delta t)$ (Verlet, 1967) as shown below

$$r_i(t + \Delta t) + r_i(t - \Delta t) = 2r_i(t) + a_i(t)\Delta t^2 + \sigma(\Delta t^4) \qquad \text{Eq. 28}$$

$$r_i(t + \Delta t) = 2r_i(t) - r_i(t - \Delta t) + a_i(t)\Delta t^2 + \sigma(\Delta t^4) \qquad \text{Eq. 29}$$

The algorithm is cantered. The two terms $r_i(t + \Delta t)$ and $r_i(t - \Delta t)$, play symmetrical roles, making the algorithm time-reversible and having excellent energy-conserving properties over long times. It is assumed that the forces only depend on the position coordinates. The velocities do not explicitly enter the algorithm; however, they are needed to estimate the kinetic energy and, hence, the temperature. The imperfection of the Verlet integrator lies in the mean-value description of the velocity $v_i(t)$ which introduces an error of the order of $\sigma(\Delta t^2)$

$$r_i(t + \Delta t) - r_i(t - \Delta t) = 2v_i(t)\Delta t + \sigma(\Delta t^3) \qquad \text{Eq. 30}$$

$$v_i(t) = \frac{r_i(t + \Delta t) - r_i(t - \Delta t)}{2\Delta t} + \sigma(\Delta t^2) \qquad \text{Eq. 31}$$

To overcome the complication of calculating the velocity, two Verlet-like integrators have been developed to obtain accurate estimates, the leapfrog method (Hockney, 1970) and the velocity-Verlet algorithm (Swope *et al.*, 1982). These algorithms are a modified version of the original Verlet integrator, and they perform over half-time steps. They are very efficient in producing positions and velocities that evolve with time.

The leapfrog method (*see* Figure 10) generates the position r_i at integer time steps and the velocity v_i at half integer time steps so that r_i and v_i are expressed as:

$$r_i(t + \Delta t) = r_i(t) + v_i\left(t + \frac{1}{2}\Delta t\right)\Delta t \qquad \text{Eq. 32}$$

$$v_i\left(t + \frac{1}{2}\Delta t\right) = v_i\left(t - \frac{1}{2}\Delta t\right) + a_i(t)\Delta t \qquad \textbf{Eq. 33}$$
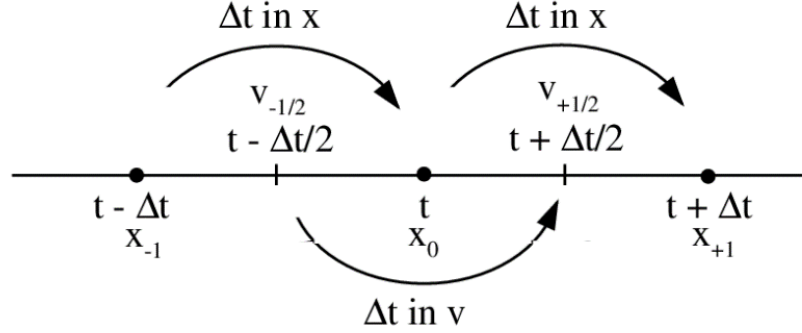
Figure 10: Leapfrog integration scheme. The position is evaluated at integral time steps, while velocity is assessed at half times.

The velocity at integer time steps is calculated as an average. The latter enables the evaluation of the kinetic energy at the same time as other physical quantities:

$$v_i(t) = \frac{1}{2}\left[v_i\left(t + \frac{1}{2}\Delta t\right) + v_i\left(t - \frac{1}{2}\Delta t\right)\right] \qquad \textbf{Eq. 34}$$

The velocity-Verlet algorithm is more commonly used. It gives both positions r_i and velocity v_i terms at integer time steps, yet through the intermediate velocity at half-integer time step

$$r_i(t + \Delta t) = r_i(t) + v_i(t)\Delta t + \frac{1}{2}a_i(t)\Delta t^2 \qquad \textbf{Eq. 35}$$

$$v_i(t + \Delta t) = v_i(t) + \frac{a_i(t) + a_i(t + \Delta t)}{2}\Delta t \qquad \textbf{Eq. 36}$$

For most MD applications, the Verlet-like algorithms are perfectly adequate, and they are implemented in the simulation packages widely used to carry out MD simulations like GROMACS (Berendsen, van der Spoel and van Drunen, 1995; Tironi *et al.*, 1995) and NAMD (Nelson *et al.*, 1996). Other higher-order algorithms exist, such as the predictor-corrector algorithm (Van Gunsteren and Berendsen, 1977) and the Runge-Kutta-Gill

method. These complex algorithms are less frequently used because of their higher computational cost (Frenkel and Smit, 1996).

3.4 Periodic Boundary Conditions and Neighbor List

MD simulations of atomic or molecular systems' main scope provide information about a macroscopic sample's properties. MD simulations are usually performed on systems containing a few thousand up to a few hundred thousand particles. However, the simulated system cannot mimic a real macroscopic system as the number of particles that MD simulations can treat is limited by the computer performance.

To simulate bulk systems, we need to choose boundary conditions that mimic the presence of an infinite surrounding bulk. This can be achieved by employing a set of boundary conditions called PBC. They are used for approximating an infinite system based on a small part called a unit cell. PBC can mimic the presence of an infinite bulk surrounding a model system. In computer simulations, the unit cell can replicate itself over the three dimensions. The particles undergo forces as though they were in a bulk solution, allowing the simulation to model an infinite system.

The N particles model is considered the primitive cell of an infinite periodic lattice of identical cells (*see* Figure 11). Each particle in a cell can interact with all other particles in the same cell and all other cells in this infinite periodic system. It is crucial to realize that the boundary of the periodic box itself has no special significance. The origin of the periodic lattice of the primitive cells may be chosen anywhere, and this choice will not affect any property of the model system under study. In contrast, the shape of the periodic cell and its orientation is fixed.

PBC is a common method for simulating homogeneous bulk structures and highly ordered crystals and solids (Frenkel and Smit, 2002). Despite this, it can cause artifacts in liquid simulations as they are much more disordered (Mandell, 1976). Luckily, the errors are usually minimal in large systems containing thousands or more atoms, and successful research results under the periodic approximation are produced.

Except for long-range electrostatic interactions, the so-called "minimum image convention" is a functional implementation of PBC. It states that each particle only interacts with the nearest image of the other particles in the system. Maintenance of the

minimum-image convention for short-range interactions also generally requires that a spherical cut-off radius r cannot exceed half the length of one side of a cubic box and the number of interacting pairs in a system containing N particles is on the order of $\sigma(N^2)$.
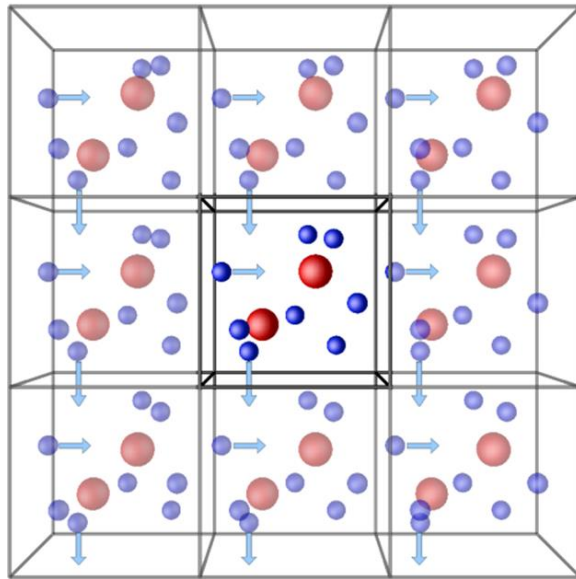
Figure 11: Schematic representation of the idea of periodic boundary conditions. The central cell is the unit cell

If the system's size is doubled, the computational cost is quadrupled, a state not desired for large-scale simulations. For this reason, the cut-off radius for short-range interactions is usually fixed at a constant value (for instance, $10 - 15$ Å in all-atom simulations), keeping the computational cost linearly dependent on N. In the case of an extensive system, the simulation box's size exceeds the cut-off radius, and to treat this efficiently, it is essential to locate the interacting neighbors within the cut-off radius for each particle.

There are mainly two types of neighbor searching methods; the Verlet list method (Verlet, 1967) and the cell list method. These methods maintain a list of all particles within a given cut-off distance of each other. The Verlet list method uses a less frequently updated neighbor list with a radius slightly larger than the cut-off radius. For large systems, we use the cell-list method, which divides the simulation box into many smaller cells so that the neighbors can be found in neighboring cells.

3.5 Constraint Algorithms

There are various time scales in molecular systems simulations like vibrational frequencies, rotations, torsional motions, and diffusion. The value of the time step determines the stability of any algorithm used. Therefore, it must be an order of magnitude smaller than the fastest motions of the system. Typically, this would be the vibration of a bond that involves a hydrogen atom with a period of the order of 10 fs, and consequently, the time step should be $1/10^{th}$. Small-time steps would lead to insufficient sampling of the phase space, whereas large-time steps would lead to instabilities in the integration algorithm and high energy overlaps.

Constraint algorithms are introduced to MD simulations to ensure that the distance between mass points is maintained and the bonds of intra-molecular interactions are at constant lengths. Using constraint algorithms, the construction of potential is simplified, allowing more efficient dynamics by neglecting motion along some degrees of freedom.

SHAKE algorithm: A typical constraint algorithm that processes all constraints one after another is SHAKE (Ryckaert, Ciccotti and Berendsen, 1977). In this algorithm, the system of non-linear constraint equations is solved using the Gauss-Seidel method, which assesses the solution of the linear system of equations using the Newton–Raphson method;

SETTLE algorithm: The SETTLE algorithm (Miyamoto and Kollman, 1992) solves the system of non-linear equations analytically. It is frequently used to constrain rigid water molecules and usually modeled using three constraints (e.g., SPC/E and TIP3P water models).

LINCS algorithm: An alternative constraint method, LINCS (Hess *et al.*, 1997), employs Lagrange multipliers to the constraint forces and solves for the multipliers by using a series expansion to approximate the inverse of the Jacobian J_σ each n step of the Newton iteration. This approximation only works for matrices with Eigenvalues smaller than 1, making the LINCS algorithm suitable only for molecules with low connectivity.

3.6 Thermostats and Barostats

In conventional MD simulations, we study the time evolution of a classical system of $\mathcal{N}$ particles in volume $\mathcal{V}$ where the total energy E is a constant of motion. If we assume that time averages are equivalent to ensemble averages, then the time averages obtained are inherently in the microcanonical ($\mathcal{NVE}$) ensemble. This does not apply in most experiments where temperature and volume or pressure are kept constant, and the canonical ($\mathcal{NVT}$) or the isothermal-isobaric ($\mathcal{NPT}$) ensemble must be generated, respectively. Consequently, the integrator requires modifications to include the influence of external temperature and pressure. In MD simulations, control over temperature and pressure is typically achieved by introducing thermostats and barostats.

To simulate the ($\mathcal{NVT}$) ensemble, a thermostat must be added to maintain a constant temperature. A thermostat can significantly affect the system's thermal fluctuations, consequently constraining the kinetic energy's fluxes that occasionally cause numerical errors (Chiu *et al.*, 2000; Morishita, 2000; D'Alessandro, Tenenbaum and Amadei, 2002; Rosta, Buchete and Hummer, 2009). Generally, for large systems, the thermostat generates a correct canonical ensemble. In MD simulations, the most used thermostats are the Nosé-Hoover thermostat (Nosé and Klein, 1983; Hoover, 1985) and the Berendsen thermostat (Berendsen *et al.*, 1984).

The Berendsen scheme mimics weak coupling with first-order kinetics to an external heat bath with a given temperature T_0. The temperature is corrected such that the deviation exponentially decays with some time constant τ according to:

$$\frac{dT}{dt} = \frac{T_0 - T}{\tau} \qquad \textbf{Eq. 37}$$

This formula means that the temperature deviation decays exponentially with τ. The advantage of this method is that it can be tailored to the user requirement. On the other hand, the Berendsen thermostat suppresses the kinetic energy fluctuations that do not generate a correct canonical ensemble. For larger systems, most ensemble averages will not be affected significantly, except for the kinetic energy distribution itself (Berendsen *et al.*, 1984).

Nosé–Hoover thermostat (Nosé and Klein, 1983; Hoover, 1985) adequately generates trajectories within the canonical ensemble. It is a deterministic algorithm that introduces a thermal reservoir and a friction term in motion equations. This friction parameter is a fully dynamic quantity with its own momentum p_ξ and the equation of motion is reformed as:

$$\frac{d^2 r_i}{dt^2} = \frac{F_i}{m_i} - \frac{p_\xi}{Q}\frac{dr_i}{dt} \qquad \textbf{Eq. 38}$$

In this case, Q is the reservoir's mass parameter. This is how the motion equation is modified:

$$\frac{dp_\xi}{dt} = (T - T_0) \qquad \textbf{Eq. 39}$$

The reference temperature is denoted T_0. While T is the current instantaneous temperature of the system. Note that using the weak-coupling scheme of Berendsen, one gets a strong exponential relaxation while using the Nosé–Hoover approach, an oscillatory relaxation is produced. This means that the actual time it takes to relax with Nosé–Hoover coupling is much larger.

To simulate the ($\mathcal{NPT}$) ensemble, a barostat is needed in addition to a thermostat. Common choices include the Parrinello-Rahman method (Parrinello and Rahman, 1981) and the Berendsen barostat (Berendsen *et al.*, 1984). This barostast can be combined with any of the temperature coupling methods mentioned above.

The Berendsen algorithm rescales the coordinates and box vectors every step, which has the effect of a first-order kinetic relaxation of the pressure towards a given reference pressure P_0 according to

$$\frac{dP}{dt} = \frac{P_0 - P}{\tau_P} \qquad \textbf{Eq. 40}$$

The Berendsen method is conceptually simple. Hence, it is very commonly used, but it is not entirely correct since this barostat does not produce the proper canonical distribution and does not yield the correct ($\mathcal{NPT}$) ensemble.

For small systems where the fluctuations in pressure or volume are significant, the ensemble must be well defined. The Parrinello-Rahman approach, in theory, gives the right $\mathcal{NPT}$ ensemble. The Parrinello-Rahman barostat works similarly to the Nosé-Hoover thermostat.

With the Parrinello-Rahman barostat, the box vectors are represented by the matrix b,

$$\frac{db^2}{dt^2} = VW^{-1}b'^{-1}(P - P_{ref}) \qquad \textbf{Eq. 41}$$

The box's volume is denoted V, and W is a matrix parameter that determines the strength of the coupling. The matrices P and P_{ref}, are the current and reference pressures, respectively. The equation of motion is also changed,

$$\frac{d^2_{r_i}}{dt^2} = \frac{F_i}{m_i} - M\frac{dr_i}{dt}$$

$$M = b^{-1}\left[b\frac{db'}{dt} + \frac{db}{dt}b'\right]b'^{-1}$$

Eq. 42

The Parrinello-Rahman time constant is not equal to the Berendsen pressure coupling algorithm's relaxation time for the Nosé–Hoover thermostat. Most of the time, a larger time constant is needed.

3.7   Force Field and Interatomic Interactions

The interactions between the atoms determine the time evolution of a system starting from an initial configuration. Therefore, the interactions must be an accurate model of how real atoms interact. A force field (FF) is a mathematical expression used to describe the forces between atoms. Specifically, in MD simulations, the FF describes the functional form and parameter sets used to compute the potential energy $U(r_1, r_2, \ldots, r_N)$. The parameters are typically derived from *ab initio* or semi-empirical quantum mechanical calculations or by fitting to experimental data. The atoms are represented bonded together by simple harmonic forces. Ideally, an FF must be simple enough to be evaluated quickly but appropriately detailed to reproduce the required properties of the system studied.

Usually, the basic functional form of the potential energy contains bonded terms for atoms that are linked by covalent bonds and non-bonded terms that describe the long-range

electrostatic and van der Waals forces. In the bonded interactions group, all intramolecular interactions (such as bonds, angles, and dihedrals) are considered. A general form for the total energy can be written as

$$U_{total} = U_{bonded} + U_{nonbonded} \qquad \textbf{Eq. 43}$$

Moreover, the covalent and noncovalent terms are given by the following sums:

$$U_{bonded} = U_{bond} + U_{angle} + U_{torsions} + U_{improper} \qquad \textbf{Eq. 44}$$

$$U_{nonbonded} = U_{electrostatic} + U_{van\,der\,Waals} \qquad \textbf{Eq. 45}$$

There are many force fields in the literature, having numerous degrees of complexity and orientation to treat different systems. However, a typical expression for an FF is:

$$
U = \sum_{bond} \frac{1}{2} k_{b,ij}(r_{ij} - r_{ij,0})^2 + \sum_{angle} \frac{1}{2} k_\theta (\theta - \theta_0)^2
$$
$$
+ \sum_{torsions} \frac{V_n}{2} [1 + \cos)n\varphi - \delta] + \sum_{improper} V_{imp} \qquad \textbf{Eq. 46}
$$
$$
+ \sum_{vdw} 4\epsilon_{ij} \left(\frac{\sigma_{ij}^{12}}{r_{ij}^{12}} - \frac{\sigma_{ij}^6}{r_{ij}^6} \right) + \sum_{elec} \frac{q_i q_j}{r_{ij}}
$$

3.7.1 Bonded Interatomic Interactions

Bonded interactions are constructed on a fixed list of atoms and occur between atoms linked through one to three bonds. There is bond stretching (2-body), angle bending (3-body), and torsional motion defined by dihedral angle (4-body) interactions. Also, there is a particular type of dihedral interaction called improper dihedral, which is applied to constrain atoms to remain on a plane or inhibit the transition to an opposite chirality configuration.

Harmonic functions approximate bond stretching and angle bending with a potential minimum at their reference bond length and angle (*see* Figure 12a,b). The bond stretching is a bonded interaction between two particles i and j with interaction potential

$$U_{b,ij} = \frac{1}{2}k_{b,ij}(r_{ij} - r_{ij,0})^2 \qquad \textbf{Eq. 47}$$

This interaction may be thought of as a very stiff linear spring between i and j. The spring has a neutral length $r_{ij,0}$ and a spring constant $k_{b,ij}$. The force of this interaction is given by

$$\boldsymbol{F}_i = -k_{b,ij}(r_{ij} - r_{ij,0})^2/(\boldsymbol{r}_{ij}/r_{ij}) \qquad \textbf{Eq. 48}$$
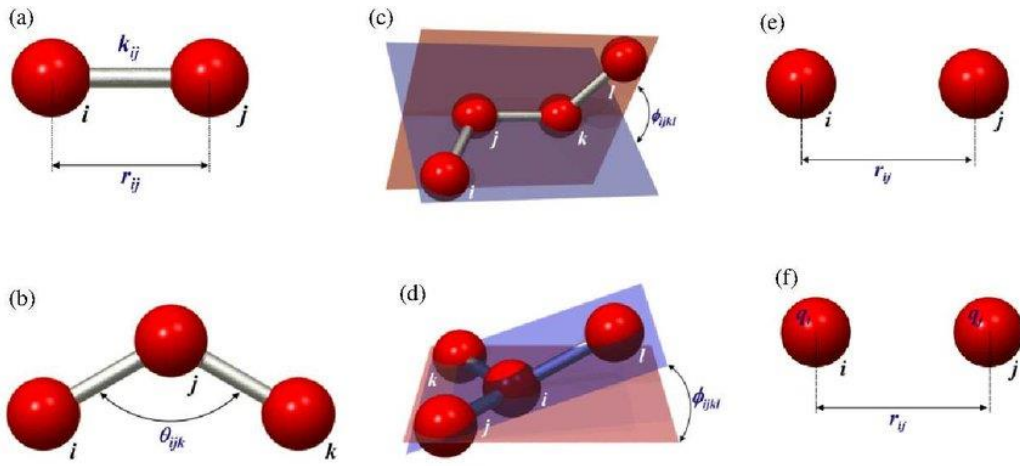
Figure 12: Schematic representation for covalent bonding (a), bond angle interactions (b), proper torsion potential (c), improper dihedral angles (d), long-range Van der Waals (e), and electrostatic interactions (f).

The angle interaction is a three-particle interaction between i, j, k with interaction potential

$$U_{a,ij} = \frac{1}{2}k_{\theta,ijk}(\theta_{ijk} - \theta_{ijk,0})^2 \qquad \textbf{Eq. 49}$$

with $\theta \equiv \arccos(\boldsymbol{r}_{ij}\boldsymbol{r}_{kj}/r_{ij}r_{kj})$

In any molecule containing more than four atoms in a row, we need to include a dihedral or torsional term (*see* Figure 12c). Dihedral angles are essential factors that determine the conformation of a molecule, and the rotations of dihedral angles have much lower frequencies comparing with the vibrations of bonds and angles.

The dihedral-angle interaction $V(\varphi)$ is a 4-particle interaction between $i; j; k; l$. The sum of several cosine functions can appropriately describe a dihedral angle potential term

$$U_{d,ijkl} = \sum_{dihedral} k_{d,ijkl}[1 + \cos(n\varphi_{ijkl} - \varphi_{ijkl,0})] \qquad \text{Eq. 50}$$

Finally, improper dihedral angles are needed to ensure the planar structures in double bonds or aromatic rings (*see* Figure 12d). They can also be used to ensure that a chiral center will not flip over to its stereoisomer. Improper dihedral angles can be portrayed by potential harmonic functions, analogous to bonds and angles,

$$U_{imp,ijkl} = \frac{1}{2} k_{imp,ijkl}(\varphi_{ijkl} - \varphi_{ijkl,0})^2 \qquad \text{Eq. 51}$$

3.7.2 Non-Bonded Interactions

As stated above, non-bonded interactions are the acts between atoms that are not connected by covalent bonds. Force fields divide non-bonded interactions into two groups: electrostatic and Van der Waals interactions.

The electrostatic interaction results from the unequal distribution of charge in a molecule and is usually modelled by a Coulomb potential between two-point charges (*see* Figure 12f). An alternative methodology used in some force fields is to model the electrostatics using point dipoles on the atoms or bonds. The Coulombic interaction is given by

$$U_{elec} = \sum_{elec} \frac{q_i q_j}{4\pi\varepsilon_0 r_{ij}} \qquad \text{Eq. 52}$$

where ε_0 is the permittivity of free space, q_i and q_j are the atomic charges, and r_{ij} is the distance between i and j.

The second non-bonded interaction is the van der Waals interaction (*see* Figure 12e). It consists of all the interactions between atoms (or molecules) that are not covered by the electrostatic interaction, and it can be modelled by the Lennard-Jones potential (LJP) (*see* Figure 13).
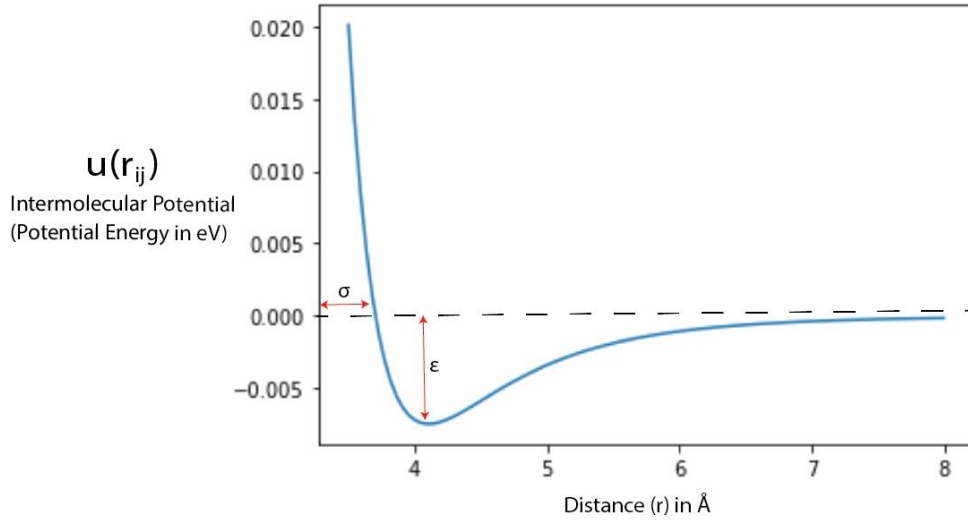
Figure 13: Schematic of the Lennard-Jones Potential curve

The LJP is a mathematically simple model that approximates the intermolecular potential energy between a pair of neutral atoms or molecules. LJP is expressed by

$$U_{LJ} = 4\varepsilon_{ij} \left(\frac{\sigma_{ij}^{12}}{r_{ij}^{12}} - \frac{\sigma_{ij}^{6}}{r_{ij}^{6}} \right) \qquad \text{Eq. 53}$$

where ε_{ij} is the depth of the potential well, σ_{ij} the finite distance at which the inter-particle potential is zero and, r_{ij} is the distance between the particles. In MD simulations, the parameters σ_{ij}^{12} and σ_{ij}^{6} depend on pairs of atom types, and they are taken from a matrix of LJ parameters. In the Verlet cut-off scheme, the potential is shifted by a constant such that it is zero at the cut-off distance.

In FF, both the Van der Waals and electrostatic interactions between atoms with more than three bonds (>1-4) are treated in the same way as if they were intermolecular. In contrast, interactions between 1-2 and 1-3 pairs are dismissed to prevent any numerical problems, as the potential can become intensely repulsive or attractive due to the small distances involved. Furthermore, the interactions between those atoms are already correctly described by the intramolecular terms.

/

4 Correlation between Surface Tension - Bulk Dynamics in Salty Atmospheric Aquatic Droplets

4.1 Introduction

Water is an excellent polar solvent due to its chemical composition and physical attributes. The solvent properties of water are vital and play a key role in atmospheric (X. Li *et al.*, 2011; Li *et al.*, 2013) and biological systems (Nymeyer and Zhou, 2008; Nucci, Pometun and Wand, 2011). Can these solvent properties be changed when surface-active organic species are present at the liquid-gas interface? The injection of salty oceanic water into marine regions rich in organic or biological material has a major impact on CCN formation and size distribution, so this issue is particularly important in atmospheric processes (O'Dowd *et al.*, 2004). This effect is linked to the properties of the liquid-gas interface in the presence of surface-active organic or biological material, and it's a key question in cloud microphysics and condensation/evaporation dynamics on these particles (Shulman *et al.*, 1996; Facchini *et al.*, 1999; Sorjamaa, Raatikainen and Laaksonen, 2004; Prisle *et al.*, 2008; Sareen *et al.*, 2013). Water is also special because of its complex interactions and numerous anomalous properties, making it an appealing research goal for computer simulations. Despite its significance, predicting its interactions in various systems is still a controversial issue (Nilsson and Pettersson, 2015) and a necessary step in understanding the relationship between surface and bulk physical properties in biological and electrochemical systems (Levy, Andelman and Orland, 2012; Gavish and Promislow, 2016). The various interaction potentials developed to characterize water's dynamical properties, such as surface tension and dielectric constant, confirm the difficulty in evaluating its properties (Vega and Abascal, 2011). Even though the surface tension of salty or pure water clusters has been studied before (Zakharov, Brodskaya and Laaksonen, 1997; Sun *et al.*, 2012) and the static dielectric constant of various concentrations of ionic solutions is well-characterized (Levy, Andelman and Orland, 2012), for polar solvents and mostly aquatic systems, there is no observed association between surface behavior, which defines the properties of the liquid-gas interface, and the static dielectric constant. A relationship between surface tension and dielectric constant has been stated in a previous study, but only for nonpolar liquids (Holmes, 1973).

The atmospheric particle system, which contains water, salt, and surface-active organic matter, is ideal for studying the above association (OM). The activation of this particle to form a CCN and then a cloud droplet is dependent on the amount of water present and the particle size. In comparison, there is still a lot of debate about surface-active OM's function (Shulman *et al.*, 1996; Facchini *et al.*, 1999; Sorjamaa, Raatikainen and Laaksonen, 2004; Prisle *et al.*, 2008; Sareen *et al.*, 2013; Daskalakis *et al.*, 2015). Anions such as sulfate or bisulfate are combined with ammonia or amine species in the atmosphere to stabilize embryonic clusters and form an initial nucleus in the new particle formation (NPF) processes (Kurtén *et al.*, 2008; Loukonen *et al.*, 2010). Ammonia salts are low-volatility gaseous compounds that can aid in the formation of some of these particles. As water vapor condenses on the latter or related salt atmospheric particulates, a CCN is formed, which then activates to form cloud droplets. The activation is based on equilibrium thermodynamics proposed by Köhler in 1936, and the dynamics are related to surface tension and water activity (Köhler, 1936). The OM's effect can be linked to the surface tension of these droplets.

On the other hand, the static dielectric constant may significantly impact the structure and dynamics of ions and water in salty solutions (Köhler, 1936; Sun *et al.*, 2012; Renou *et al.*, 2014). The contribution of water to the static dielectric constant could present a measure of the water activity (water availability) for hydration processes in atmospheric aquatic droplets. The relative importance of surface tension depression or decreased water activity concerning CCN activation and cloud droplet development is a matter of great debate (Ruehl, Davies and Wilson, 2016). Water activity parametrization (Good *et al.*, 2010; Yakobi-Hancock *et al.*, 2014) predicts droplet sizes under supersaturated conditions for non-surface-active compounds. Still, it fails to correctly account for the cloud droplets that form in the presence of surface-active species (Ruehl, Davies and Wilson, 2016).

Recent chamber experiments have shown that the ubiquitous atmospheric trace gases, methylglyoxal, and acetaldehyde, can enhance aerosol CCN activity, upon uptake, by decreasing the critical CCN activation diameter at a given critical supersaturation (Sareen *et al.*, 2013). Both organic species can be found in aquatic environments and are active on the surface (Fu *et al.*, 2008; Millet *et al.*, 2010). Surface-active species may exist in bulk and on a wet atmospheric aerosol surface, with a surface/bulk partitioning ratio that

varies depending on the aerosol's size and composition, but this is still a point of contention (Nozière, Baduel and Jaffrezo, 2014). As clusters form into nuclei of a new phase, knowledge of cluster properties, including surface tension and the static dielectric constant, is needed to understand phase transition and nucleation processes and how surface tension affects cluster dynamics. This research clarifies the function of surface-active organic matter and its impact on water droplet properties like surface tension and bulk static dielectric constant, which are important parameters in understanding CCN formation, size distribution, and content (Renou *et al.*, 2014). The response and organization (water activity) of water molecules in the bulk of an aquatic droplet to the presence of surface-active organic matter on a liquid-gas interface are described in this chapter. Using MD simulations in spherical droplets containing water, salt (ammonium bisulfate), and organic matter as methylglyoxal and acetaldehyde, this response is presented as a connection between surface behavior and the water contribution to the static dielectric constant. The association is linked to changes in water orientation, which affects water activity, and the salt structure within the droplet, which assesses the dynamical response of the bulk to the droplet's liquid-gas interface surface tension depression.

4.2   Computational Methodology

4.2.1   Systems Setup

Neutral nuclei of the general formula $[(NH_4^+HSO_4^-)_x(OM)_y]$ were constructed from individual molecules of ammonium bisulfate salt and surface-active OM. The OM being either methylglyoxal[1] (M-MTG), acetaldehyde[2] (A-ACH), or an equimolecular combination of the two (AM).

---

[1] Methylglyoxal is the organic compound with the formula CH_3CCHO. It is a reduced derivative of pyruvic acid. It is produced industrially by degradation of carbohydrates using overexpressed methylglyoxal synthase.

[2] Acetaldehyde is an organic chemical compound with the formula $CH_3 CHO$, sometimes abbreviated by chemists as MeCHO. It is one of the most important aldehydes, occurring widely in nature and being produced on a large scale in industry

Methylglyoxal (M-MTG) *Acetaldehyde (A-ACH)*
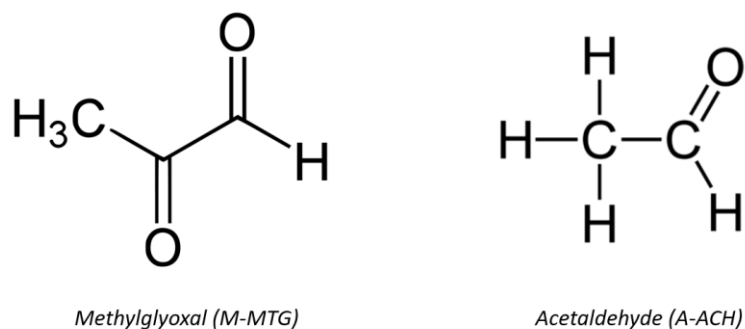
Figure 14: Molecular Formula of methylglyoxal (M-MTG) and acetaldehyde (A-ACH).

To ensure neutrality, the protonated form of sulfate (bisulfate) was used in combination with an equimolecular NH_4^+ content for model simplicity. This allows one to draw conclusions that are not influenced by the ionic species ratio. The number of molecules in each nucleus is represented by x and y, with values ranging from 0 to 128 for x and 0 to 240 for y. The neutral nuclei were solvated in approximately 7000 TIP4P (Jorgensen *et al.*, 1983) water molecules and positioned in the center of a cubic simulation box with dimensions $15 \times 15 \times 15$ nm^3.

Table 1: The contents of each sample probed in this study. The Laplace Radii RS is shown in brackets, in nm.

S	A	M	AM
neat water [3.57]	AM [3.60]	2(AM) [3.62]	4(AM) [3.71]
S [3.60]	SA [3.56]	SM [3.56]	SAM [3.60]
2S [3.59]	2(SA) [3.64]	2(SM) [3.62]	2(SAM) [3.63]
4S [3.67]	4(SA) [3.65]	4(SM) [3.72]	4(SAM) [3.79]

Producing in this way $[(NH_4^+HSO_4^-)_x(OM)_y(H_2O)_{6907}]$ droplets, with final concentrations between 0.0 to 1.0 M (salt) and 0.0 to 2.0 M (OM). Since our models are

smaller than experimental conditions, higher concentrations were used to improve each species' impact (Shulman *et al.*, 1996; Mitsche, Wang and Small, 2010; Li *et al.*, 2013; Sareen *et al.*, 2013). The simulation cell's neutrality does not prohibit the formation of smaller clusters with negative or positive total charge within the same simulation cell but accepts that the sum of the simulation cell charges remains zero. In total, 16 samples, as shown in

Table 1, were probed along with their contents and the respective Laplace radii R_S. The contenents S, A, M, and AM are related to 0.25 M salt, 0.25 M acetaldehyde, 0.25 M methylglyoxal, and 0.5 M OM (equimolecular combination of acetaldehyde and methylglyoxal), respectively.

4.2.2 Sample equilibration and initial structures

The systems were put in a simulation unit cell of $15 \times 15 \times 15$ nm^3 and subjected to energy minimization by 2000 steps of the steepest-descent method at a 5.0 kJ tolerance and by Brownian dynamics at 10K for 200ps with temperature coupling (t_C) constant of 10^{-3}ps. A short 25ps run in constant density and temperature (NVT) ensemble followed at 10K with the weak-coupling Berendsen thermostat (Berendsen *et al.*, 1984; Berendsen, van der Spoel and van Drunen, 1995) and a t_C of 0.1 ps. Initial sampling was carried out in adapted sawtooth cycles using the Simulated Annealing (SA) process (Kirkpatrick, Gelatt and Vecchi, 1983; Daskalakis *et al.*, 2015) followed the previous equilibration and relaxation steps.

Table 2: The sawtooth cycles for the Simulated Annealing (SA) runs in pairs of time (ns) and temperature (K)

Time (ns)	0	0.1	0.3	0.5	1	1.5	2	2.5	4.5	5	15
Temperature (K)	10	100	100	200	200	278	278	460	460	600	600
Time (ns)	20	21	21.1	29.1	33.1	34.1	34.2	40.6	43.8	46	50

Temperature (K)	278	278	460	460	278	278	370	370	298	278	278

The following procedure was used to obtain the starting structures for the production runs at 278 K. After equilibration–relaxation, the temperature of each sample was increased and decreased in steps at the NVT ensemble for 50ns with a t_C value of 1.0ps and the v-rescale thermostat (Bussi, Donadio and Parrinello, 2007), with a time step of 1fs. The SA sequence is described in Table 2. The initial structures were extracted at the end of the sawtooth cycles at 278K for each sample. The RF/cut-off (Tironi *et al.*, 1995) or PME schemes (Bussi, Donadio and Parrinello, 2007) employed for the electrostatics use the same parameterization throughout both the equilibration and the production runs for each sample.

4.2.3   Force Field

The OPLS-2005 force field (FF) (Banks *et al.*, 2005) was used to characterize interaction potentials for both inorganic (ionic) and organic species. The choice of FF for the NH_4HSO_4/ water interaction is not trivial (Aragones, Sanz and Vega, 2012). Previous studies have successfully used OPLS-2005 FF to probe halide clusters in free or aquatic solutions, providing crucial information about halide salt and cluster structures (Heyda *et al.*, 2010). The OPLS-2005 FF has been developed to work with the TIP4P water model (Horn *et al.*, 2004), where potential parameters for nonbonded interactions have been fitted to reproduce correct solvation energies (see below). OPLS-2005 has also successfully been used for interactions between methylglyoxal, acetaldehyde or esters, nitriles, and nitro compounds with water (Price, Ostrovsky and Jorgensen, 2001; Daskalakis *et al.*, 2014, 2015).

All production simulations were carried out at a temperature of 278 K. This temperature is especially important for surface-activity measurements in the ambient environment, New Particle Formation (NPF), particle growth, and CCN activation (Shulman *et al.*, 1996; Facchini *et al.*, 1999; Sorjamaa, Raatikainen and Laaksonen, 2004; Prisle *et al.*, 2008; Sareen *et al.*, 2013). Even with a nonpolarizable water potential, the systems are defined at low temperatures (278 K), making polarization effects and van der Waals interactions less important in producing liquid water's correct physical properties (Sokhan *et al.*, 2015).

The experimental value of the surface tension of a water droplet ($75.4 \, mN/m$ at $275 \, K$) is better reproduced by the TIP4P family of water models (Chen and Smith, 2007; Vega and De Miguel, 2007), whereas for the experimental static dielectric constant ($\varepsilon_1 = 71.7$ at 300 K) (Vega and Abascal, 2011) it is found less accurate, while TIP4P captures its temperature dependence accurately and provides an adequate level of accuracy (Elton and Fernández-Serra, 2014). However, since it is difficult to find a single water model that accurately reproduces both the experimental surface tension and the dielectric constant while also being computationally effective, the TIP4P water model was chosen because it is consistent with the OPLS-2005 FF and is less computationally intensive for the large systems investigated in this study. The TIP4P model can, however, accurately replicate the critical water/ion and water/surface-active organic matter interactions, as well as the hydrogen bonding networks involved in modifying the properties (surface tension and dielectric constant) of a water droplet (Price, Ostrovsky and Jorgensen, 2001; Heyda *et al.*, 2010; Topper *et al.*, 2011; Sun *et al.*, 2012; Daskalakis *et al.*, 2014, 2015). As a result, no conclusions were drawn based on absolute values of surface tension or static dielectric constant, but rather on their relative changes as the salt and OM content of the water droplets probed changed.

4.2.3.1   *Solvation Free Energies*

-To evaluate the FF, we calculated the Solvation Free Energies (SFE) for each complex (acetaldehyde, methylglyoxal, and ammonium/bisulfate) based on established procedures in the literature (Villa and Mark, 2002; Christ, Mark and Van Gunsteren, 2010; Pohorille, Jarzynski and Chipot, 2010) using the Gromacs software (Berendsen, van der Spoel and van Drunen, 1995). The free energy change associated with a transition from state A to state B (ΔG_{AB}) is a function of a coupling parameter, λ, that describes the extent to which the Hamiltonian has been perturbed and the system has been altered (Perturbation Theory). Simulations were conducted at different values of λ between 0 (state A) to 1 (state B) at 0.05 steps and ΔG_{AB} was derived from the $\vartheta H/\vartheta \lambda$ curve. State A defines the respective compound solvated in around 580 SPC or TIP4P waters (Mark and Nilsson, 2001) in a ~17.5 nm^3 cubic simulation unit cell. We decouple each compound for both van-der-Waals and Coulombic interactions for λ=0 (state A) to λ=1 (state B) to calculate the SFE. In the 1ps production runs, Langevin dynamics with a time stage of 2fs for 20 different values and temperature and pressure coupling constants of 1ps were used. Using

the Parinello-Rahman barostat, we kept the temperature at 298K and the pressure at 1.0 atm (Parrinello and Rahman, 1981). The Particle-Mesh-Ewald (PME) summation model was used to deal with long-range coulombic interactions (Darden, York and Pedersen, 1993) with an order of 6 and a tolerance of 10^{-6}. The van-der-Waals and short-range Coulombic interactions were truncated at a cut-off of 1.2nm. A potential shift with the Verlet cut-off scheme was selected, and dispersion corrections were applied for the energies and pressure, improving the cut-off scheme's accuracy (Cisneros *et al.*, 2014). The SETTLE algorithm (Miyamoto and Kollman, 1992) applied constraints on the C-H, O-H stretching modes, and the HOH water angles, eliminating quick motions and quantum effects (Pluhařová, Vrbka and Jungwirth, 2010). The LINCS (Hess *et al.*, 1997) algorithm was employed to constrain bonds that include hydrogen atoms for the rest of the molecules. A force constant of 1000 kJ mol^{-1}nm^{-2} was used for the constraints.

Table 3: Solvation Free Energies (SFE) at 298K in TIP4P or SPC waters, calculated in kJ/mol for the species studied herein.

compound	solvation in TIP4P *(this work)*	solvation in SPC *(this work)*	experimental/ ab-initio *(literature)*
acetaldehyde	-24.78 ± 0.68	-24.29 ± 0.86	-17.45 (Tong *et al.*, 2006)
methylglyoxal	-22.12 ± 1.63	-19.90 ± 0.37	-15.90 (Krizner, De Haan and Kua, 2009)
bisulfate HSO$_4^-$ /ammonium NH$_4^+$	-720.52 ± 0.97	-712.13 ± 2.14	-672.00 (Muller, Florián and Warshel, 1997)

The calculated SFE values are in reasonable agreement with the literature (Muller, Florián and Warshel, 1997; Tong *et al.*, 2006; Krizner, De Haan and Kua, 2009) (*see* Table 3). They capture the strong ionic (bisulfate and ammonium) interactions in both TIP4P and SPC water. The SFE for the neutral combination of the monovalent cation (NH$_4^+$) and

anion (HSO_4^-) is defined and measured as the sum of relative (or conventional) solvation free energies based on the absolute SFE of the proton. This comes in line with ref (Kelly, Cramer and Truhlar, 2006) with the proton's absolute SFE to cancel out in the sum of the free energies. Also, the OM behavior (acetaldehyde and methylglyoxal) as surface-active species is correctly reproduced with Absolute Solvation Free Energies (ASFE) a few kJ below the experimental values.

The resolution in the λ values used for the SFE calculations might account for any deviations compared to the experimental values, especially in the presence of strong h-bonding interactions for the compounds probed. Nevertheless, even if we calculate a deviation from the experimental SFE values (more considerable for the ionic species), we can accept these values, as the primary goal of this work was to qualitatively capture the effects from a surface-active organic species on the surface of a droplet that is communicated to the salt containing bulk. Moreover, the calculated SFE values exhibit the correct trend based on the experimental values: ionic species $\ll$ acetaldehyde $<$ methylglyoxal. We also note that, in line with a comparative study (Shivakumar *et al.*, 2010, 2012), the solvation free energies do not differ significantly for the solvation in SPC or TIP4P waters and show the same trend.

4.2.4 Water contribution to the static dielectric constant

The contribution of water to the droplets' static dielectric constant was determined using a published procedure (Simonson, 1996). In detail, we assume an inner spherical region of each droplet as a microscopic cavity of radius r_1, and the remaining outer region as a dielectric continuum (radius R), itself surrounded by vacuum. The mean square dipole of the inner region $\langle M_1^2 \rangle$ is associated with the dielectric constants of the inner (ε_1) and the outer (ε) regions by the following equation, where k_B is the Boltzmann's constant and T the simulation temperature (278K):

$$\frac{\langle M_1^2 \rangle}{k_B T r_1^3} = \frac{(\varepsilon_1 - 1)\left[(1 + 2\varepsilon)(2 + \varepsilon) - 2\left(\frac{r_1}{R}\right)^3 (1 - \varepsilon)^2\right]}{(\varepsilon_1 + 2\varepsilon)(2 + \varepsilon) - 2\left(\frac{r_1}{R}\right)^3 (1 - \varepsilon)(\varepsilon_1 - \varepsilon)} \qquad \textbf{Eq. 54}$$

For each droplet/ sphere the r_1 radius is chosen between 0.8-2.7nm every 0.1nm and the respective calculated time-dependent $\varepsilon_1(r_1)$ values are averaged at each time frame. From the resulting ε_1 profile, we use only the values over a 60-100ns time window out of the

production runs to calculate a time-averaged ε_1 value, with the standard deviation to represent the error. The r_1 is chosen not too close to the droplet's radius R to achieve a nearly bulk-like screening of the outer region's inner sphere dipole fluctuations. For $r_1 < 0.8\ nm$ there are too few waters for reliable statistics, while for $r_1 > 2.7\ nm$ we calculate static dielectric constants that deviate considerably from the ones calculated for the $0.8 - 2.7nm$ inner spheres due to the outer shell becoming too thin to be viewed as a continuum.

For solving Eq. 54, we assume $\varepsilon_1 = \varepsilon$. By choosing $\varepsilon = 50$, the TIP4P bulk static dielectric constant (Vega and Abascal, 2011), the results are not affected, as it is the case also for larger ε values tested (up to 10^3). In fact, the choice of the value of ε has a minor effect on the calculated average ε_1 values (Simonson, 1996), as long as r_1 remains small compared to R.

4.3 Molecular Dynamics Simulations

The $[(NH_4{}^+HSO_4{}^-)_x(OM)_y(H_2O)_{6907}]$ models simulate small aquatic, atmospheric droplets, in the presence and absence of surface-active OM, as in the NPF processes. Initial sampling was performed by the simulated annealing (SA) method in adapted sawtooth cycles after equilibrating and relaxing the systems (Kirkpatrick, Gelatt and Vecchi, 1983; Topper *et al.*, 2011; Daskalakis *et al.*, 2015). Brownian Dynamics at 10K for 200ps were employed along with two short 24ps runs in NVT and NPT ensembles at 10K with the weak-coupling Berendsen thermostat-barostat (Berendsen *et al.*, 1984).

The constant density and temperature (NVT) ensemble run with the Nose−Hoover thermostat (Nosé and Klein, 1983; Hoover, 1985) and a large simulation unit cell ($15 \times 15 \times 15$ nm^3) simulates pure or salty water droplets of spherical geometry in the ambient environment (Sun *et al.*, 2012). The temperature coupling constant was set at 0.2 ps, and we maintained the system temperature at 278 K with an RMSD of 1.8 and error estimation of 0.032K. The simulation cell volume was chosen to allow at least a 4.0 nm distance between molecules and the simulation cell sides and was extended indefinitely in all directions under 3D PBC. This latter minimizes the interactions of the nuclei with their images under the 3D PBC scheme adopted (Sun *et al.*, 2012), and the nucleus assumes a spherical shape (droplet) (Sun *et al.*, 2012; Daskalakis *et al.*, 2015). Newton's equations of motion were integrated for 100 ns for each production trajectory per sample. All simulations (equilibration, relaxation, SA, and production) were performed using the

Gromacs 5.0.4 MD package (Berendsen, van der Spoel and van Drunen, 1995). Coulombic interactions were treated using the reaction-field method, as implemented in Gromacs (Berendsen, van der Spoel and van Drunen, 1995; Tironi *et al.*, 1995), while van-der Waals interactions using the cut-off scheme. All nonbonded interactions were truncated at 1.4 nm. A potential shift with the Verlet cut-off scheme was selected, and dispersion corrections were applied for the energies, improving accuracy (Cisneros *et al.*, 2014). The reaction-field method was used for computational efficiency (Lin *et al.*, 2009). A large number of water molecules (6907) ensures the existence of a bulk-like structure within each water droplet, where truncation schemes (like the reaction-field method) score very well, also providing a good convergence for the dielectric constant (Cisneros *et al.*, 2014). Several methods exist for the detailed account of long-range electrostatic interactions, with the most prominent PME method (Darden, York and Pedersen, 1993). For selected samples only, the long-ranged Coulombic interactions were treated using PME to compare the results. Newton's motion equations were integrated using a time step of 1.0 fs and the velocity-Verlet algorithm (Swope *et al.*, 1982) for all production runs. The SETTLE algorithm (Miyamoto and Kollman, 1992) applied constraints on the C−H, O−H stretching modes, and the HOH water angles, eliminating quick motions and quantum effects (Pluhařová, Vrbka and Jungwirth, 2010). The LINCS (Hess *et al.*, 1997) algorithm was employed to constrain bonds that include hydrogen atoms for the rest of the molecules. A force constant of 1000 kJ mol^{-1}nm^{-2} was used for the constraints.

4.4   Results and discussion

4.4.1   Density Distributions

The radial distributions of the center of mass of all constituents (water, salt, and OM) for the samples probed can be used to measure the density distributions. The radial distributions are averages of the last 20 ns of the 100 ns output trajectories. The OM molecules are mainly found on the surface of the spheres in a Gaussian-shaped distribution, even in the samples without salt, AM, 2(AM), and 4(AM) (Figure 15a). A representative spherical shape of a sample (SAM) is shown in (Figure 15b). All samples are probed in a large NVT box ($15 \times 15 \times 15$ nm^3), which minimizes the interactions with their mirror images under the 3D PBC employed, and thus, they assume a spherical shape (Sun *et al.*, 2012; Daskalakis *et al.*, 2015).

The spheres throughout the production trajectories were centered in the simulation unit cell box for all post-run processing and data analysis reported herein. We have to note that some water or organic matter molecules escape from the sphere liquid phase and migrate into the gas phase in dynamical equilibrium. The mean radius calculated from

Table 1 is at $3.63 \pm 0.06 \, nm$, whereas the mean spherical volume is at $200.4 \pm 9.9 \, nm^3$, with the greater deviations for the samples with a large number of organic molecules within. The spherical particles are usually compressed when ions, like in halide salts (e.g., NaCl), are present (Sun *et al.*, 2012). Still, due to the bulky size of the ammonium bisulfate salt and surface-active OM, we expect deviations from this rule, as shown in

Table 1.
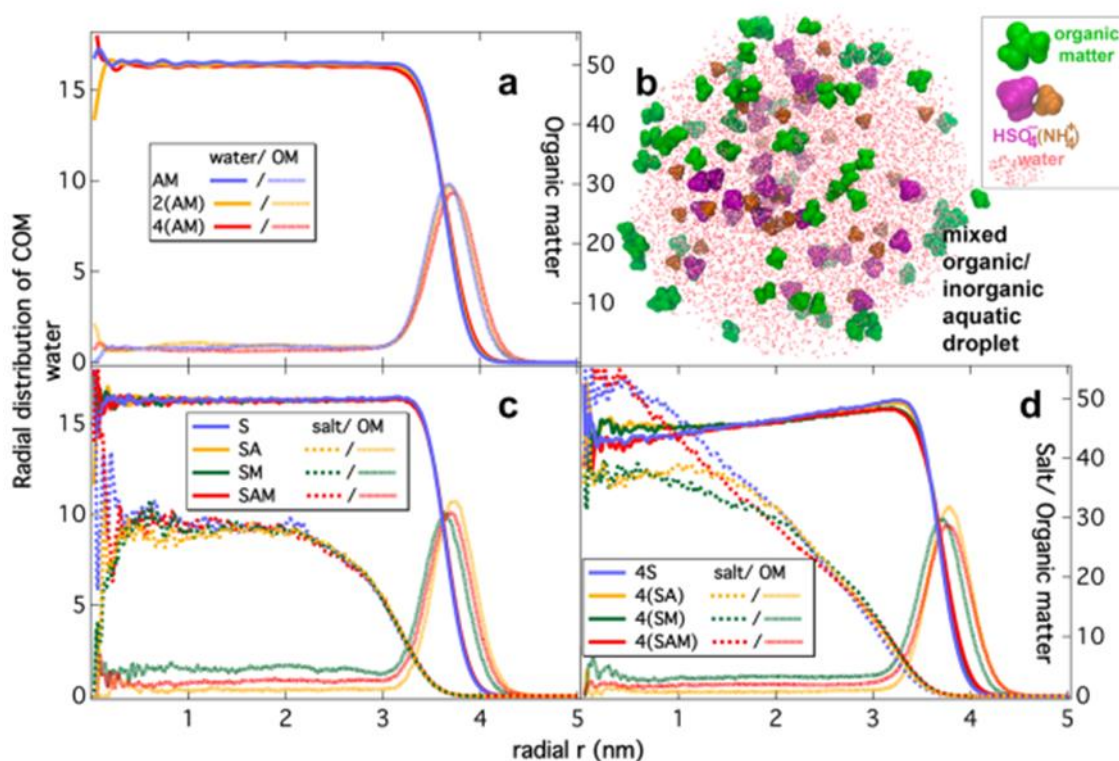
Figure 15: Graphs a,c,d: the radial distributions of the center of mass (COM) of the water (left axis), salt, and organic matter (right axis) molecules for the aquatic droplets. Graph b: the spherical structure of the water (pink sticks) droplet enriched with organic matter (green) and ammonium (orange) bisulfate (magenta) salt.

The density distributions for the 2S, 2(SA), 2(SM), and 2(SAM) samples are almost identical to those of the S, SA, SM, and SAM, respectively, in Figure 15c. The presence of salt could reduce the OM solubility in a salting-out effect and explain the Gaussian-shaped distributions for the OM on the surface (Figure 15c,d). However, given the OM surface distribution, even in the absence of salt (Figure 15a), the OM is shown to exhibit surface activity. The respective Laplace radii shown in

Table 1 are in agreement with the spherical radii as observed from the radial distributions in Figure 15a,c,d, defined around the peak of the Gaussian-shaped OM distribution or at the radius corresponding to roughly half the height of the water distribution in the absence of OM. All samples contain the same number of water molecules whose radial distribution is similar for the samples with 0.25−0.5 M salt but differs for the 1.0 M salt samples. The salt is mainly found in the center of the spherical shapes, forming a core for the latter. For the 0.25−0.5 M salt samples, there is an almost homogeneous distribution of water and salt in the bulk of the spheres (between radials 0.0−2.7 nm). For the 1.0 M salt samples, the inhomogeneity is more pronounced with the salt concentration decreasing. The molarity of water is increasing in bulk at the radials between 0.0 and 2.7 nm.
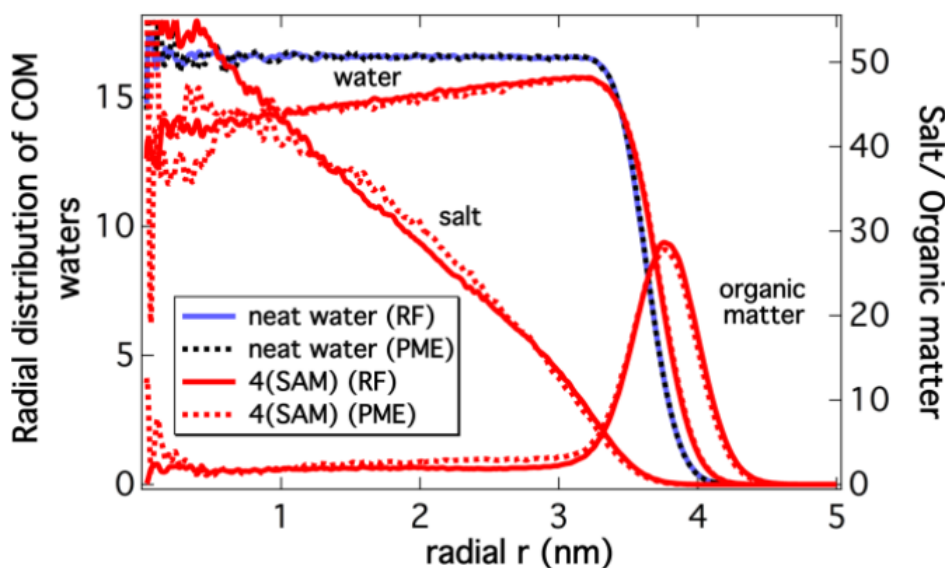
Figure 16: The Radial Distributions of the Center of Mass (COM) of the water (left axis), salt and organic matter (right axis) molecules for the aquatic droplets of neat water, and the droplet with the highest concentration of salt (1.0M) and organic matter (2.0M) probed in this study. Two

different methods have been used to treat long-range electrostatic interactions; the PME and RF methods

We note that the electrostatics treatment by the RF or the PME methods exerts no considerable effect on the radial distributions; thus, the structures probed appear the same (Figure 16). We have chosen two extreme cases for this latter comparison: one droplet of neat water and the sample with the highest salt concentration (1.0 M) and OM (2.0 M). The long-range electrostatics are treated by two different methods (PME and RF) for comparison. As observed from the distributions, the two methods' results are consistent, even for the two extreme concentration cases (0-1M salt, 0-2M organic matter).

Without compromising the samples' structural features, we have chosen to use the RF approach to treat electrostatics because of the computational advantage. We note that OM has a considerable effect on the salt structure within the high salt (1.0M) content droplets (Figure 15d). This effect has also been reported previously for high salt content samples (172). Surface-active OM (either acetaldehyde or methylglyoxal) induces morphology transitions for the salt within the droplet (172). In the 4(SA) and 4(SM) droplet samples, the salt seems to be solvated in the bulk of the droplet, exerting a more homogeneous distribution and order (Figure 15d, green and orange dotted lines), compared to the uncontaminated by OM, 4S sample, with a more distinct form of a concentrated salt core in the center of the droplet that gradually dissolves in bulk (blue dotted line).
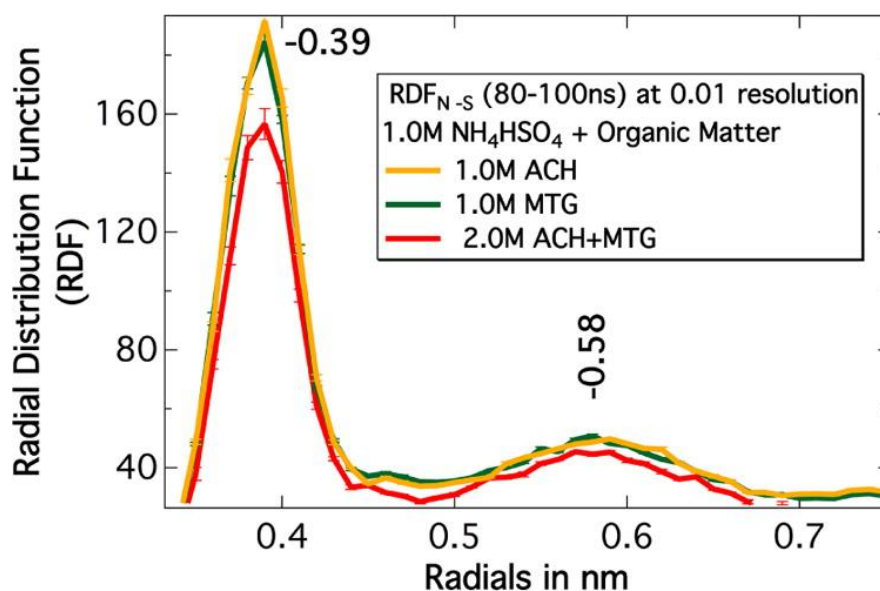
Figure 17: Nitrogen (N)−sulfur (S) radial distribution function (RDF) for the salt within the samples of high salt concentration (1.0 M NH4HSO4) over the 80−100 ns time window of the production trajectories. Error bars are shown for the calculated RDF profiles as the standard deviation of the average value of the RDF profiles at 5 ns intervals over the 80−100 ns time window of the production trajectories.

Further increase of the OM concentration from 4(SA) or 4(SM) to 4(SAM) seems to work against the previous trend. Still, we need to consider that the higher OM content (acetaldehyde + methylglyoxal) in the 4(SAM) sample might introduce a higher concentration of OM in the bulk and alter the bulk to surface ratio. Thus the change in salt distribution to a more disordered morphology (211–214). This latter can be deduced by looking at the nitrogen−sulfur radial distribution functions (RDF$_{N–S}$) for the salt within the high concentration sample in Figure 17, calculated for the 80−100 ns time window of the production trajectories to achieve equilibrium in the salt morphology. Lower order is observed for the high salt and the highest OM content sample (Figure 17, red line) compared to the rest of the high salt content and low OM content (green−methylglyoxal and orange−acetaldehyde contamination).

4.4.2   Surface Tension of the Spherical Droplets

In droplets, the interfacial tension acts in such a way to minimize the contact area between the droplet and the surrounding media. This results in spherical shapes (Figure 15b). The surface tension γ of the aquatic droplets was calculated based on published procedures using the local stress tensor code (LTS) (Ollila *et al.*, 2009; Vanegas, Torres-Sánchez and Arroyo, 2014; Torres-Sánchez, Vanegas and Arroyo, 2015). The tangential $p_T(r)$ and the radial $p_{rr}(r)$ components of the pressure tensor were used to calculate the surface tension of each droplet−sample. A 5 ns window from each production trajectory is used to calculate the surface tension. A larger cut-off (2.0 nm) was employed for the LTS code to rerun the production trajectories in 5 ns time windows and calculate both the tangential $p_T(r)$ and the radial $p_{rr}(r)$ components of the pressure tensor. The relatively short window is chosen as both positions and velocities have to be recorded for each particle in the NVT box, for the LST code to calculate the $p_T(r)$ and $p_{rr}(r)$ values, leading to huge amounts of output data, in addition to high computational demand by the increase in the

cutoff value. These short windows (5 ns) are adequate to achieve convergence. In detail, the surface tension is given Eq. 55 (Buff, 1955; Rickayzen, 1983; Ollila *et al.*, 2012), where r is the distance from the origin of the coordinate system (the center of the sphere/droplet), and R_S is the Laplace radius.

$$\gamma = -\int_0^\infty \left(\frac{r}{R_S}\right)^2 [p_T(r) - p_{rr}(r)]dr \qquad \text{Eq. 55}$$

where,

$$R_S{}^3 = \frac{\int_0^\infty r^2 [p_T(r) - p_{rr}(r)]dr}{\int_0^\infty r^{-1}[p_T(r) - p_{rr}(r)]dr} \qquad \text{Eq. 56}$$

In practice, it is assumed that $p_T(r) - p_{rr}(r) = 0$ in the bulk region of each droplet. All of the above integrals are calculated for radials between $r = 2.4$ and $r = 7.0\,nm$, having in practice convergence even at shorter distances for the upper limit (at around 4.0 nm). The upper limit (7.0 nm) is close to half the unit cell box length in x, y, and z dimensions (7.5 nm). The results are not changed in practice when the integral limits are expanded from 0.0 to 7.5 nm.

The pressure tensor components (tangential $p_T(r)$ and radial $p_{rr}(r)$) were derived from the molecular dynamics trajectories, as described in detail elsewhere with the default parametrization (Ollila *et al.*, 2009; Vanegas, Torres-Sánchez and Arroyo, 2014; Torres-Sánchez, Vanegas and Arroyo, 2015). As an example, Figure 18 depicts the components of the pressure tensor as a function of the distance from the droplet center for two extreme concentration cases; the neat water droplet (0.0M) and the droplet with the highest concentration of salt (1.0M) and OM (2.0M). In theory, the droplets need to exert a bulk region both inside and outside to have a correct definition of the interfacial tension. This is shown to be a reasonable case for all the droplets probed herein, with the integrals of Eq. 55 to be close to zero in the bulk regions (Ollila *et al.*, 2012). In the bulk phase of the droplet, the $p_{rr}(r)$ / $p_T(r)$ curves are flatter. The $p_{rr}(r)$ / $p_T(r)$ absolute values and fluctuations in the bulk should decrease as the size of the droplet increases, and the effect of surface tension on the bulk phase becomes smaller. Because of the relatively small size of our droplets, these fluctuations are still apparent. A peak of the $p_T(r) - p_{rr}(r)$ near the surface of the droplet is exhibited, as expected, in Figure 18. This is in accordance with the fact that surface molecules are under strong tension, with water having a large

surface tension and a low vapor pressure under the ambient conditions simulated. Because of the very large fluctuations of pressure in a simulation, the average values of the tangential $p_T(r)$ and radial $p_{rr}(r)$ components are only of interest. The errors and fluctuations are omitted from the plots similar to Figure 18 (Ollila *et al.*, 2009, 2012).

The calculated surface tension for each droplet probed in this study is shown in Table 4 based on the convergence of the integrals of Eq. 55 over the 5 ns time windows. The error in the absolute values can be calculated in terms of this convergence. We split the 1−5 ns frames used for the averaging into three groups (1−3, 1−4, and 1−5 ns) and use the variation between the mean obtained from each group to get a standard deviation. The standard deviation out of the averaging, thus, provides the error. We exclude the 0−1 ns frames group, as the system might not have reached equilibrium in the early stages, and also, we exclude the 1−2 ns frames group, as there are not enough frames within this group for the statistics. We did not obtain convergence within that shorter time window. This is also the case for the calculation of the errors in the Laplace radii of

Table 1. Although runs with PME electrostatics were also considered, in this case, there will be an additional error from using a cut-off in the local stress calculation code. A relative local stress value (between the vacuum and the droplet) is calculated, and thus, this error likely cancels out.
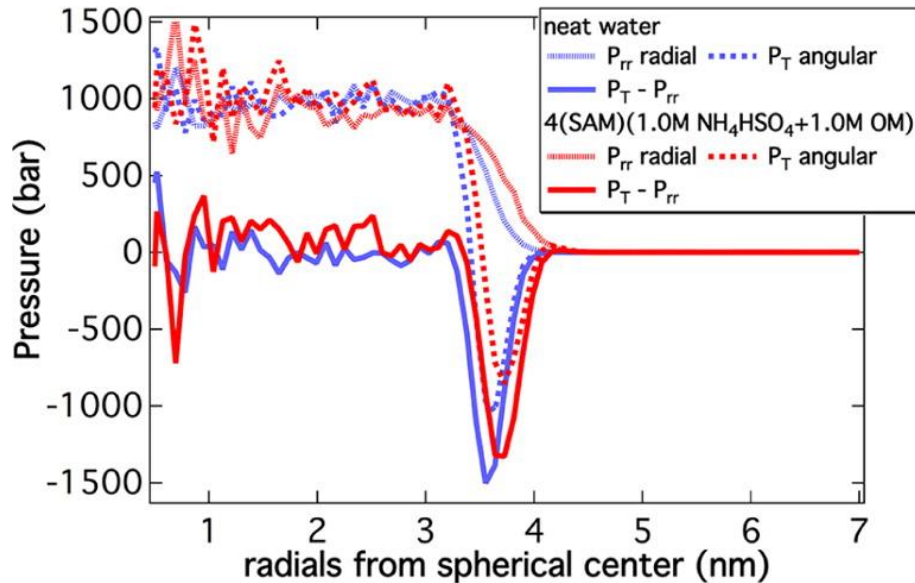
Figure 18: Tangential, or angular $p_T(r)$ and radial $p_{rr}(r)$ constituents of the pressure tensor as a function of the distance from the center of the droplet r for the neat water sample and the sample with the highest concentration of salt and organic matter. The positive or negative signs on the

absolute pressure values have been assigned based on the requirement to calculate a positive surface tension from Eq. 55. The absolute pressure values should be considered for any physical meaning.

Nevertheless, more calculations with different cut-off values would be needed to estimate the associated error on the surface tension's resulting value when PME electrostatics are employed. The LTS code employed calculates the pressure tensor components employing the RF or plain cut-off methods only. Thus, artifacts might be present when switching to the PME method instead of the original trajectory before the LTS rerun. To test this is beyond this study's scope, as the PME runs were performed for reference only and should be taken into account only to calculate the dielectric constants compared to the RF method.

Table 4: Surface Tension in mN/m or mJ/m^2, Calculated for All Samples Probed in This Study (Shown in Brackets), along with the Standard Deviation.

neat water [53.9 ± 0.7]	AM [53.9 ± 0.5]	2(AM) [52.7 ± 0.5]	4(AM) [49.3 ± 0.4]
S [52.4 ± 0.4]	SA [53.8 ± 0.3]	SM [56.2 ± 0.5]	SAM [52.3 ± 0.6]
2S [53.1 ± 0.3]	2(SA) [49.6 ± 0.3]	2(SM) [53.0 ± 0.6]	2(SAM) [50.0 ± 0.8]
4S [51.2 ± 0.4]	4(SA) [51.2 ± 0.4]	4(SM) [47.0 ± 1.0]	4(SAM) [47.7 ± 1.2]

In general, as is the case for calculating the static dielectric constant (*see* below), interfacial tension measurements can be done only for macroscopic droplets of a volume between 25 and 45 mm^3 (Mitsche, Wang and Small, 2010). Thus, a systematic error should also be considered for our droplets due to the smaller volume. Still, this error cannot be easily calculated, as experimental data are not available for all our samples. Nevertheless, we have to note that the surface tension is less pronounced in a sphere than in a planar interface, so lower surface tension values are calculated compared to the

experimental values. The smaller the sphere, the less prominent the effect of surface activity would be. Experimental data give a higher value for the planar pure water liquid−gas interface (75.4 mN/m at 275 K) (Chen and Smith, 2007; Vega and De Miguel, 2007). However, it is common for water models to give surface tensions different from the experimental values. Despite that, the system's general behavior is not affected (Hede *et al.*, 2011).

Nevertheless, we see that the surface tension we calculate for the neat water TIP4P droplet (53.9 mN/m) is in reasonable agreement with the calculated TIP4P value for a large flat surface (59.0 mJ/m^2) (Vega and De Miguel, 2007). Also, we observe that as the OM concentration on the surface of the droplet is increased from the neat water to the 4(SM) (1.0 M NH$_4$HSO$_4$ and 1.0 M MTG) or 4(SAM) sample (1.0 M NH$_4$HSO$_4$ and 2.0 M OM), the surface tension of the droplet drops down by around 13%. For the droplets without any salt within, the same drop is calculated to approximately 8.5% from the neat water to the 4(AM) sample of 2.0 M OM. From Table 4, we can deduce that the surface tensions calculated are quite the same for the samples of low salt or OM concentrations, but for the higher salt or OM content samples, shown in bold, there is a considerable change. There is a need for high OM concentration for the changes in surface tension and their effects to show, especially in the presence of salts. This agrees with experimental studies (Ruehl, Davies and Wilson, 2016)(Sareen *et al.*, 2013).

4.4.3   Water Contribution to the Static Dielectric Constants

The water contribution to the static dielectric constant of the droplets was also calculated based on a published procedure, employing the method described by T. Simonson (Simonson, 1996). Each droplet is divided into concentric spheres of inner radials between $r = 0.8$ to $2.7\ nm$ and the mean square water dipoles of the inner region $\langle M_1^2 \rangle$ are associated with the dielectric constants of the inner-bulk (ε_1) and outer-surface (ε) regions.

In Figure 19a, we show the $\varepsilon_1(r)$ convergence for the different radials r between $0.8 - 3.2nm$ in the neat water sphere for reference. For the larger ($r = 2.8 - 3.2nm$) radials we identify a significant increase of the $\varepsilon_1(r)$ values, as we approach the surface of the sphere. The neat water ε_1 value throughout the production trajectory (depicted in Figure 19b, c, d, e, and f as a light blue dashed line) is derived by averaging the $\varepsilon_1(r)$ values

corresponding to the radials $r = 0.8 - 2.7nm$. The same procedure has been used for all the samples. The time-independent values shown in the insets are time averages of the ε_1 values in windows of $20 - 30ns$ (Figure 19b) or 60-100ns (Figure 19 c, d, e and f) to ensure convergence. The standard deviation out of the averaging provides the error.
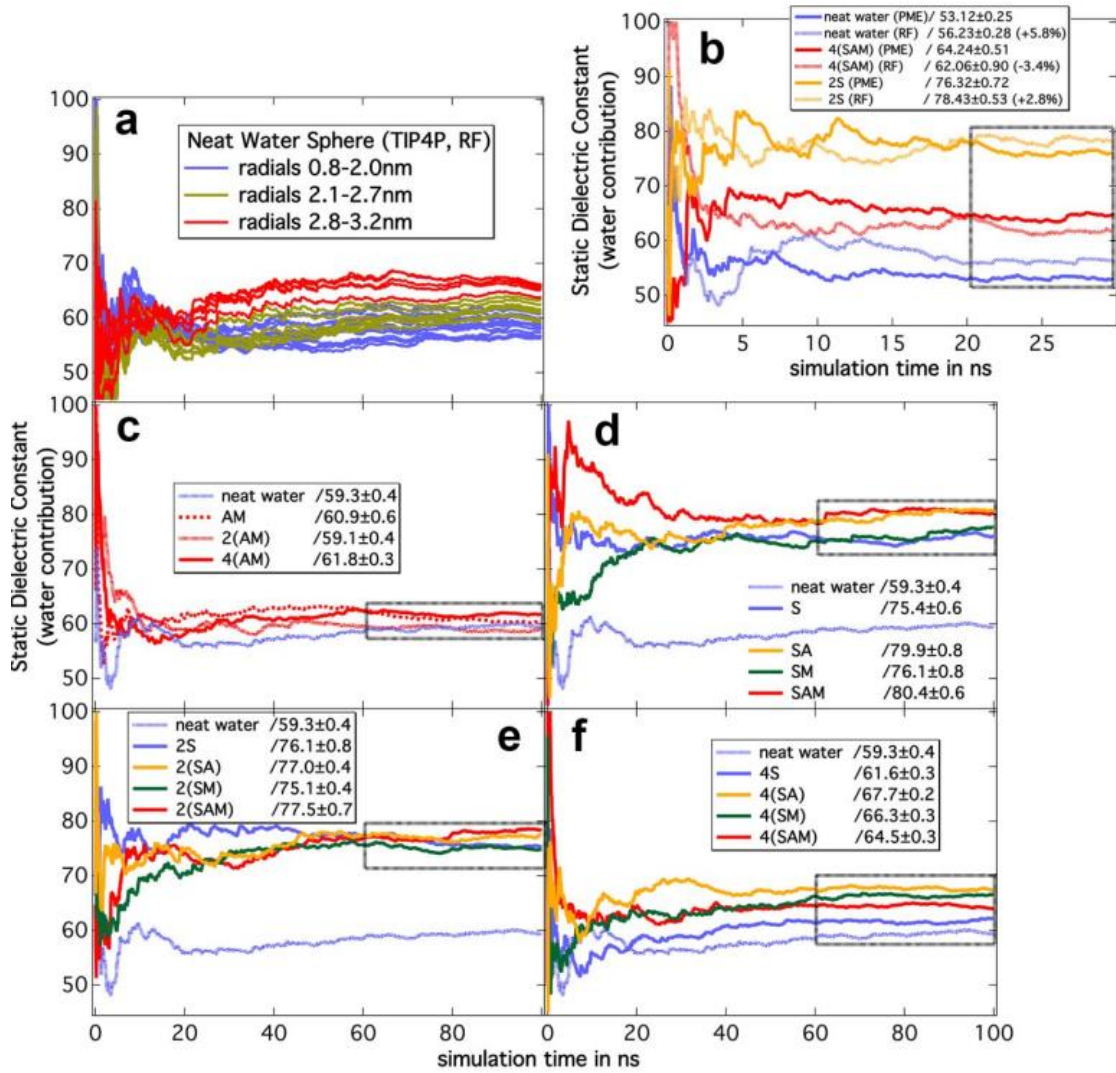
Figure 19: The convergence of the static dielectric constants ε_1 throughout the production trajectories for all the samples. Graph a. The $\varepsilon_1(r_1)$ values for the neat water sphere. Graph b. The ε_1 values averaged over the different $\varepsilon_1(r_1)$ in cases where the electrostatics have been treated by either the Reaction Field (RF) or the Particle-Mesh Ewald (PME) method for selected samples. The % change in the mean ε_1 value is also calculated, and shown in the inset when the electrostatic interactions are treated by RF, compared to the PME method. Graphs c-f. The ε_1 values averaged over the different $\varepsilon_1(r_1)$ for the different samples probed. The respective time average values are

shown for each sample and the calculated error, where applicable. Rectangular boxes indicate the time windows for this time, averaging

The ε_1 values, along with their errors, are shown in Table 5. The errors have been calculated from the averaging in the last $40\,ns$ of the $100\,ns$ production trajectories. Compared to the RF method, shorter trajectories were also run based on the PME method due to the former's very high computational resources requirements. As was the case for the radial distributions of the droplet constituents (Figure 15a,c,d), selected samples were probed with the electrostatics treated by either the RF or the PME method but exert minor differences on the calculated time-averaged ε_1 values (*see* Figure 19b). We note that ε_1 convergence for the neat water samples is achieved even at shorter times (30 ns) in the RF trajectories within 3 units (absolute value 56.2) compared to the convergence achieved toward the end of the 100 ns trajectory (absolute value 59.3).

Table 5: Water Contribution to the Static Dielectric Constant, Calculated for All Samples Probed in This Study (Shown in Brackets), along with the Standard Deviation

neat water	AM	2(AM)	**4(AM)**
[59.3 ± 0.4]	[60.9 ± 0.6]	[59.1 ± 0.4]	**[61.8 ± 0.3]**
S	SA	SM	SAM
[75.4 ± 0.6]	[79.9 ± 0.8]	[76.1 ± 0.8]	[80.4 ± 0.6]
2S	2(SA)	2(SM)	2(SAM)
[76.1 ± 0.8]	[77.0 ± 0.4]	[75.1 ± 0.4]	[77.5 ± 0.7]
4S	4 (SA)	**4(SM)**	**4(SAM)**
[61.6 ± 0.3]	[67.7 ± 0.2]	**[66.3 ± 0.3]**	**[64.5 ± 0.3]**

Deviations are expected from the calculated value for the neat TIP4P in bulk at 300 K (ε_1 = 50) (Vega and Abascal, 2011) as we are probing water droplets as finite systems, where the ε_1 values are dependent on the number of water molecules, even for the neat water

droplet, as well as the constituents. In addition, our calculations are performed at 278 K, and an increase in the ε_1 value is expected as temperature drops (Elton and Fernández-Serra, 2014). The ε_1 value for a neat water droplet should approach that of the bulk when the number of water molecules increases (Morrow and Smith, 1990). The 6907 water molecules contained in our systems give an ε_1 value for the neat water droplet ($\varepsilon_1 = 56.2$, 20−30 ns time window) at a very reasonable agreement with that of the bulk value. The runs based on the PME method give a slightly better result with $\varepsilon_1 = 53.1$ (20−30 ns time window). Despite the slightly increased ε_1 value calculated for the neat water droplet using the RF method, we make this compromise instead of allocating a huge amount of computational resources for the runs with PME. We anticipate that there will be a systematic error to the RF based calculated ε_1 value that does not compromise the validity of our results or our conclusions in the comparison between samples with the electrostatics treated at the same method (RF). Even for the sample of the highest salt and OM content, the RF method scores very well, giving a ε_1 value of 62.06 compared to 64.24 employing the PME method. The latter system appears the least homogeneous, where the RF method would normally fail; instead, the method gives reasonable ε_1 values.

We observe that the presence of OM in the samples affects the calculated time-averaged ε_1 values only for the droplets with salt content within (S contains samples in Table 5). On the contrary, the presence of OM on a neat water sphere (neat water, AM, 2(AM), and 4(AM) samples in Table 5) has a minor effect on the calculated ε_1 values, even at high concentrations (2.0M). In detail, for the neat water and OM-only contaminated samples (first row of Table 5), the average ε_1 value is at 60.3 with a standard deviation of 1.3. To the contrary, when moving to the salt-contaminated samples (rows 2−4 of Table 5), the average ε_1 values are calculated at 78.0 ±2.6 (0.25 M salt), 76.4 ± 1.1 (0.5 M salt), and 65.0 ± 2.6 (1.0 M salt), exerting double the dispersion for the low and high salt content droplets, compared to the OM-only-contaminated aquatic droplet. This dispersion is higher than the calculated errors in the absolute ε_1 values of Table 5. The lower dispersion in ε_1 of the medium content (0.5M) salt samples might be due to opposing effects from the salt (*see* below). Nevertheless, the average ε_1 value of the 0.5 M salt samples exhibits still a larger deviation from that of the neat water droplet. Given that the OM is mainly found on the surface of the probed droplets, we propose that the presence of OM affects salty water droplets in terms also of the salt structure within.

This variant salt structure among different samples polarizes the water molecules in different ways by producing a local electric field (Levy, Andelman and Orland, 2012), leading to the orientation of the water dipoles and further contribution of the water molecules to the static dielectric constant. The increase of the static dielectric constant has been observed upon increasing salt content (from neat water to the $0.25-0.5$ M salt samples herein), which has also been observed experimentally. The size of the ions matters (Wei, Chiang and Sridhar, 1992). It also seems that as the concentration of the salt within the droplets increases further, the calculated ε_1 value decreases by almost 20%, from an average of 75.8 (0.25 M or 0.5M) to 61.6 (1.0M). This latter can be due to the orientation of the water dipoles on the stronger electric field produced by the higher concentration of salt (Levy, Andelman and Orland, 2012) within the droplet or the lower number of water molecules used for the calculation of the $\langle M_1^2 \rangle$, given the inhomogeneity, observed in the bulk of the higher salt content sample (Figure 15d). The decrease in the static dielectric constant, in increasing salt concentration, correlates with experimental and theoretical results; the response of dipoles to an external field is smaller in the presence of ions, leading to a reduction in the dielectric constant (Levy, Andelman and Orland, 2012). The high salt content disrupts the overall hydrogen bonding network, increasing the water dipole fluctuations (Elton and Fernández-Serra, 2014). Opposing effects, thus, might be present for the medium salt content (0.5M) samples, as reported before, leading to the small dispersion of the average ε_1 value (76.4 ± 1.1). This disruption of the hydrogen bonding network is evident from the radial distribution of the center of mass of waters in the high salt content samples, where the bulk region turns less homogeneous (Figure 15d).

4.4.4 Correlation

The correlation between the surface tension values and the water contribution to the static dielectric constants for all samples probed in this study is depicted in Figure 20. Only the relative percentage changes are shown, based on a reference sample (termed "ref" in the legend) of each different salt concentration. This ensures that the level of homogeneity of the aquatic droplets does not interfere with the correlation due to the different salt concentrations within. Differences in sample homogeneity are drawbacks when using the RF method to treat long-range electrostatic interactions (Van Der Spoel, Van Maaren and Berendsen, 1998). Forcing us in this way to refrain from directly comparing or correlating

between the absolute values of surface tension or static dielectric constant of all samples of varying salt content. Also, the absolute values calculated for the surface tension γ or the dielectric constant ε_1 for each sample deviate from the experimental values when available (i.e., $\gamma = 75.4$ mN/m at 275 K and $\varepsilon_1 = 71.7$ at 300 K for the neat water) (Chen and Smith, 2007; Vega and Abascal, 2011; Elton and Fernández-Serra, 2014).

However, we overcome the drawback above by using the relative changes shown in Figure 20. Linear fitting is used to show correlation trends. The solid black line fit includes all samples, whereas the solid red line fit excludes the SA, 2(SA), and 4(SA) samples for fitting. The solid blue line shows the fitted correlation for the samples without salt within the droplet bulk. The calculated slopes of the fitting lines are also shown adjacent to each line for the correlation. All of the slopes that include data in the presence of both surface-active organic matter and salt are negative.
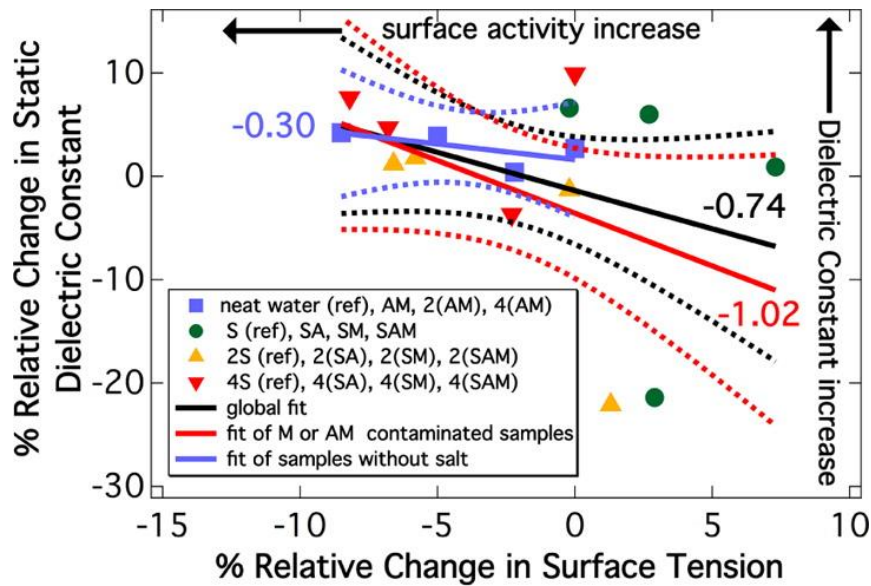
Figure 20: Correlation between the aquatic droplets' two macroscopic physical properties: the surface tension and the static dielectric constant out of the water contribution. The relative percentage changes (%) based on a reference (termed ref) sample are shown. The slopes for the linearly fitted data are also depicted for reference for the solid lines. The dotted lines correspond to 95% confidence bands for the fitting as an estimation of the error.

In contrast, the absence of salt within the droplet bulk (solid blue line) exhibits a weaker correlation sign. Even if we consider the confidence bands (95%) of the fitting, we see a pronounced negative correlation, especially when the samples SA, 2(SA), and 4(SA) are

not included (solid red line). This pronounced negative correlation is evident for samples containing salt and OM concentration, while it vanishes in the absence of salt. We propose that the depression of the surface tension is more pronounced in the presence of methylglyoxal or a mixture of methylglyoxal and acetaldehyde. Compared to larger concentrations needed for the acetaldehyde-only-contaminated samples (SA, 2(SA), and 4(SA)) to show such a behavior. Because of acetaldehyde's higher vapor pressure, its presence on the aquatic droplets' surface is reduced, hence the less pronounced reduction in the surface tension (Daskalakis *et al.*, 2015). It should be stressed that this correlation could be disrupted in the presence of other (no surface-active) organic or inorganic species in the liquid phase. Nevertheless, it seems to capture the bulk response to the presence of surface-active OM. It is not within the errors for the calculated surface tension or static dielectric constant absolute values.

4.4.5   Implications of the Correlation and Model Evaluation

The spherical aquatic droplets studied herein, with a high degree of curvature, are realistic representations of atmospheric particulates compared to simulations of a planar interface. A significant fraction of aerosol particles is mainly composed of sea salt with a coating of organic compounds (Leck and Bigg, 2005). The process by which water vapor condenses upon such particulates to form liquid cloud droplets is based on equilibrium thermodynamics proposed by Köhler, and the dynamics are related to surface tension and the water activity, as previously stated (Köhler, 1936). Thus, to gain fundamental insight into droplet growth, one has to study microscopic properties of aqueous interfaces, such as those between ionic solutions and the air in atmospheric aerosols, involving surface and bulk dynamics, related to surface tension and water activity, respectively. An increase in surface-active OM presence can decrease the particulate matter's surface tension (Ruehl *et al.*, 2012) and reduce the vapor pressure needed for CCN activation, followed by growth (Sareen *et al.*, 2013). Cloud droplets of smaller or larger sizes could thus be favored depending on the conditions (Shulman *et al.*, 1996; Facchini *et al.*, 1999; Sareen *et al.*, 2013). However, the water activity of the solution, a term in Köhler theory (X. Li *et al.*, 2011), defines the availability of the water molecules to interact with solutes in hydration schemes giving rise to new parametrization called the k-Köhler scheme (Petters and Kreidenweis, 2007). A water activity value of unity implies pure water, whereas zero indicates the total absence of free water molecules. We propose that as the surface tension

in an aquatic droplet is decreased in the presence of surface-active OM, the water activity is affected as well. This is evident by the increased dielectric constant of the water in the bulk as the surface tension is decreased, and the water dipoles are oriented based on the salt morphology within the droplet. We therefore suggest that the surface tension depression can be accompanied by the water activity change, related to CCN activation and the cloud droplet growth (Ruehl, Davies and Wilson, 2016). Water-activity-only-based parametrization predicts droplet sizes under supersaturated conditions for non-surface-active compounds, but when cloud droplets form in the presence of surface-active species,[23−25] we propose that the correlation between water activity and the surface tension depression comes also into effect.

Two competing phenomena are acting in the liquid water phase in the presence of ions: (a) the disruption of the hydrogen-bonding network that leads to an increase in the water dipole fluctuations and (b) the orientation of water dipoles around ions, a process that decreases dipole fluctuations (Renou *et al.*, 2014). Thus, the water contribution to the static dielectric constant is crucial to understand before assessing water structure around ions or water activity. Beyond previous research, we have characterized the change in static dielectric constant, closely related to aquatic droplets' water activity, due to the presence of surface-active OM, which should also change the scavenging capability of atmospheric species as these species become solutes. More importantly, it should alter the OM surface-to-bulk ratio and disrupt the hydrogen bonding network in different ways (Li *et al.*, 2013; Nozière, Baduel and Jaffrezo, 2014). This surface-to-bulk ratio has an impact also on the Rault term in Köhler theory (Köhler, 1936). Thus, we propose that the orientational arrangement of the water molecules or their availability (water activity) is affected by OM's presence, observed via OM's effect on the water contribution to the droplets' dielectric constant. This effect is not independent of the surface-active OM, which could explain the literature's differences and the importance of surface tension depression over a water activity-only parametrization model. For example, methylglyoxal or a mixture of methylglyoxal/ acetaldehyde coated droplets seems to exert a stronger negative correlation between surface tension and the water contribution to the static dielectric constant contrast a pure acetaldehyde coating.

The varying behavior of the organic matter can be based on the fact that the solubility of a foreign compound in water droplets can be determined by its ability to form hydrogen

bonds or to interact with the water dipole, and it is an important property that affects atmospheric physicochemical processes. Also, the vapor pressure of the organic matter should also affect this varying behavior. In detail, in the presence of surface-active OM, the compressed-filmed model (Jura and Harkins, 1946) describes the correlation between surface tension depression and organic surface coverage in atmospheric droplets correctly. A compressed film on the surface of a droplet occurs in the case of an increased surface concentration of organics leading to a lower droplet's surface tension. If the OM surface concentration drops, then the organics can be considered in the gas phase and almost noninteracting with the droplet surface tension to match that of the neat water. This latter conclusion agrees with our results, as high concentrations of OM are needed for a considerable surface tension depression to occur in the model droplets.

At CCN activation, the compressed film transitions to a gaseous state. The droplet's surface tension becomes nearly equal to that of pure water, but this should depend on the organic species coating. The model proposed in ref (Ruehl, Davies and Wilson, 2016) shows that most organic material is at the droplet surface, in line with our results. Our results also point to the significance of the surface-active OM coating mechanism and the various effect on the water activity in droplets of mixed organic/ inorganic aerosol. Thus, they can provide an additional qualitative dimension to the parametrization of cloud droplet formation.

This study found that the correlation between surface tension depression and water activity is related to the salt structure within the droplet affected by the OM presence on salty aquatic droplets' liquid-gas interface. Thus, we propose that the salt structure within the droplet changes and that, in turn, the water network can become stiffer and not available for other hydration processes, exerted as a decrease in water activity (Chen *et al.*, 2016). We have to consider that OM can also influence water activity or water availability to participate in hydration processes by altering the water dipole orientation within an aerosol. This should be of particular importance to the secondary organic aerosol (SOA) formation processes by hydration (e.g., the formation of glyoxal or methylglyoxal hydrates) (Hastings *et al.*, 2005; Tan *et al.*, 2010), where the availability of water to hydrate the organic matter should be reduced in the presence of salts. This could consist of a negative feedback mechanism, as the surface-active OM (glyoxal, methylglyoxal) concentration is increased on the droplet surface, the surface tension

depression correlates with water activity, and thus, alters the number of water molecules that are available for the hydration.

The size of our model systems ideally characterizes NPF structures. However, this study also assesses a fundamental question on how a droplet surface's properties can induce changes in the bulk of a droplet and surface a correlation between two crucial properties of ionic solvents to add to the debate role of organic matter in NPF and CCN activation.

4.5 Conclusions

This study presents a correlation between surface activity and water contribution to the static dielectric constant of ionic aquatic droplets. We identify changes to this contribution even for samples with the same water molarity due solely to the presence of different organics or concentrations of organic matter on the surface. These changes are attributed to different salt structures within the droplets that lead to different orientations of the water dipoles. A significant application resides in NPF and CCN activation dynamics in the atmosphere. The effect of aerosol properties on cloud dynamics and the atmosphere's radiative balance relies on cloud droplet formation parametrizations. Such parameterization is based on Köhler theory, but there is considerable debate in the literature based on the importance of factors like the surface tension depression or the water activity decrease. We have given insight into the dynamics of aquatic droplets at a level of detail not accessible experimentally (due to the small size). Thus, we have provided evidence for the correlation between their surface tension depression and the water activity decrease for droplets of radials at the ~3.6 nm scale related to NPF. Even with a weak surface tension−dielectric constant (water activity) correlation, the effects can be considerable on the droplet growth dynamics. Hence, this correlation is a fundamental property to consider when assessing NPF and the Köhler theory in CCN formation.

Despite the plethora of available data in the scientific literature, we calculate the surface tension and dielectric constants of salty water clusters in this study. However, to correlate these properties, it was necessary to calculate both under precisely the same conditions and use the exact system sizes and methods to show an unbiased result. Of course, we have to note that electrolyte solutions are highly complex systems and that there are too many aspects to consider in assessing their dynamical properties, especially water/ ion-

pair interactions, reaction-field effects, water/ organic interactions, and, more importantly, the decrease in water molarity as ionic concentration increases. Thus, it is quite challenging to achieve experimental evidence where too many interactions are present in an atmospheric aerosol particle, as its composition often becomes complicated and unconstrained. It has also been proposed that the properties of the interface regulate the adsorption and reaction of trace gases, thus changing the chemical composition of the aerosol particles on the fly (Medders and Paesani, 2016). The correlation between physical properties is an essential insight for cloud droplets. A plethora of interacting species within the droplet's macroscopic properties and the competition or correlation between physical properties give rise to direct or indirect effects. To conclude, the control of an aquatic droplet's bulk properties by the amount of surface-active organic matter on the liquid−gas interface could also have biochemical implications and research for drug delivery and lipid bilayer−water interactions in terms of the water activity and dynamics within.

5 The Effect of Glassy Organic Aerosols on Ice Nucleation

5.1 Introduction

The formation of ice in the atmosphere plays a vital role in Earth's climate and other atmospheric processes such as cloud formation, sunlight scattering, radiative transfer, and atmospheric chemical reactions (Kärcher and Koop, 2004; Murray, 2008; Russo, Romano and Tanaka, 2014). Ice nucleation proceeds on aerosols (Murray *et al.*, 2012a). While atmospheric particles contain salt, soot, metals, and crystal oxides, they also hold many organic compounds (Cui *et al.*, 2006; De Boer *et al.*, 2011; Whale, 2018). One of the least known atmospheric aerosols components is organic aerosols that add from 30 to 80 % aerosol mass (De Boer *et al.*, 2011). Although less hygroscopic than inorganic salts, organic aerosols have been shown to absorb water depending on the particle size, composition, and RH (Wheeler and Bertram, 2012). Also, many studies have highlighted the effect of chemical composition on the physical state of atmospheric aerosols and the resulting impact of this aerosol state on ice nucleation (Jimenez *et al.*, 2009; Glasius and Goldstein, 2016; Knopf, Alpert and Wang, 2018). As such, droplets containing various soluble organic compounds can become highly viscous or glassy at low temperatures and low relative humidity. The organic fraction can contain polycarboxylic acids, polyols, ketones, polyphenols, aromatic aldehydes, acids, and sugars (Hallquist *et al.*, 2009; Kuwata and Martin, 2012; Ziemann and Atkinson, 2012; Glasius and Goldstein, 2016; Whale, 2018). Many different atmospheric particles made almost entirely of organic compounds can induce ice nucleation, allowing clouds and precipitation to develop more easily. They play an important role in both direct and indirect aerosol forcing (Hoose *et al.*, 2010; Koop *et al.*, 2011; Shiraiwa, Pöschl and Knopf, 2012; Slade and Knopf, 2014; Berkemeier *et al.*, 2016).

Organic aerosols are generally considered liquid, exhibiting instantaneous equilibrium conditions in gas-particle partitioning (Virtanen *et al.*, 2010). In response to changes in temperature (T) and RH, organic aerosol particles may present an amorphous (semi-) solid or glass phase state, according to recent research (RH) (Bahreini *et al.*, 2005; Fuzzi *et al.*, 2006; Zobrist, Marcolli, Pedernera, *et al.*, 2008; Mikhailov *et al.*, 2009; Perraud *et al.*, 2012). The term glassy state describes an amorphous, highly viscous state with a dynamic viscosity greater than 10^{12} pa.s (Roth, Goss and Schwarzenbach, 2005) and the

mechanical properties (Saukko *et al.*, 2012). The molecules of glassy solids lack the long-range order that is characteristic of crystals. This characteristic forms when a liquid is cooled to a temperature at which the molecules stop diffusing. Its viscosity increases resulting in them being held in a "liquid-like" amorphous state. The glassy state can appear by quench cooling, rapid drying of organic or aqueous solutions, or vapor phase deposition at low temperatures (Bahreini *et al.*, 2005). Glassy aerosols act as heterogeneous ice nuclei affecting ice clouds and cloud droplets' properties, affecting ice nucleation, chemical reactions, and water uptake of aerosols by altering processes evaporation, reactivity, and diffusion time scales (B. J. Murray *et al.*, 2010). Glassy aerosol particles serve as heterogeneous IN through the immersion, contact, and depositional freezing modes when present at conditions advantageous to ice formation (Glasius and Goldstein, 2016). (Berkemeier *et al.*, 2016) simulations revealed that glassy states could persist, allowing heterogeneous ice nucleation to dominate homogeneous ice nucleation in the deposition and immersion modes.

A glassy state is a metastable state. It is thermodynamically nonergodic and unable to rearrange to the ground state (Koop *et al.*, 2011). This phenomenon will set kinetic constraints on water transport to and from the particle during condensation and evaporation. To characterize a glassy state, one must look at a key property termed dynamic viscosity (η). An increase in the dynamic viscosity leads to decreased macroscopic transport properties and molecular transport processes such as diffusion (D). The Stokes-Einstein equation gives the relation between D and η:

$$D = \frac{kT}{6\pi\eta r} \qquad\qquad \textbf{Eq. 57}$$

where k is the Boltzmann constant, T is the absolute temperature; η is the dynamic viscosity, and r is the apparent radius of the molecule. Based on the viscosity values, one can classify components into liquids ($< 10^2\ Pa\ s$), semi-solids ($10^2 - 10^{12}\ Pa\ s$) and glasses ($> 10^{12}\ Pa\ s$) (Pablo G. Debenedetti and Stillinger, 2001).

The formation of glass depends strongly on a given substance's chemical and physical properties and its mixing state (Murray, 2008). Aerosol particles present as glasses significantly influence the physical and chemical processes in the atmosphere like ice nucleation, ice growth, water uptake, evaporation, diffusion, sorption, and chemical aging

(Zobrist, Marcolli, Pedernera, *et al.*, 2008; Cappa and Wilson, 2011; Shiraiwa *et al.*, 2011; Bones *et al.*, 2012). In glassy aerosols, the water uptake from the gas phase can be inhibited, reducing the direct aerosol effect and affecting the aerosol particles' ice nucleation efficiency (Murray, 2008; Schill and Tolbert, 2013). Many observations suggest a connection between particle phase state and the resulting predominant ice nucleation pathway (Benjamin J. Murray *et al.*, 2010). Certain organic species can undergo this glass transition under atmospheric conditions, and those organic glasses can nucleate ice heterogeneously. SOA particles can exhibit a viscous semisolid or glassy state at low temperature and low humidity (Renbaum-Wolff *et al.*, 2013). Evidence of this is provided in the literature on the field (Froyd *et al.*, 2010; Knopf *et al.*, 2010, 2014) and laboratory studies.

However, existing studies make it difficult to observe the complex and microscopic ice nucleation process by glassy organics. There is no proposed mechanism at the atomic level to describe ice nucleation on glassy organic aerosol. Because diverse experimental techniques respond differently to transition and the T_g value varies depending on how it is obtained. The most common way to determine T_g is calorimetry, a technique sensitive to the change in isobaric heat capacity associated with glass transition (Zobrist, Marcolli, Pedernera, *et al.*, 2008).

Information on the diffusion rates of water and organic molecules within SOAs is essential to predict cloud condensation and ice nucleation (119,120,232,235–238) and size distributions and growth rates of these particles (Lignell, Hinks and Nizkorodov, 2014; Davies and Wilson, 2015; Houle, Hinsberg and Wilson, 2015; Wang *et al.*, 2015; Hinks *et al.*, 2016). A particle's ability to engross water and activate as a CCN can be influenced by slow diffusion in the glassy process (Tong *et al.*, 2011) and the particle's ice nucleation capabilities (Wang, Laskin, *et al.*, 2012; Wilson *et al.*, 2012; Schill and Tolbert, 2013). Diffusion-limited growth occurs in semi-solid aerosol, resulting in a different size distribution than that created by quasi-equilibrium growth in liquid aerosol (Zhang *et al.*, 2012).

Glassy organic aerosol's actual impact on the environment is still far from being completely understood and quantified due to insufficient knowledge of its shape, structure, properties, and processes. Glassy organic aerosol's effects on weather are indirect affecting water droplet and ice crystals formation, evaporation, and deposition

with consequences to cloud formation and precipitation. To better understand their function in the atmosphere, ice nucleation on glassy organic aerosols requires quantitative characterization. Experiments to parameterize the nucleation activity in the presence of glassy organics over a broad temperature range are needed. This latter is essential because some water-soluble organic compounds demonstrate a strong temperature dependence of water activity for aqueous mixtures of constant composition (Zobrist, Weers and Koop, 2003). Such enhancements will significantly minimize model uncertainty in future modeling studies.

The effect of glassy organics on ice nucleation mechanisms, on the other hand, has yet to be determined. Due to the high heterogeneity and complexity of organic aerosols, computer simulation modelling of simple structures appears to be an attractive first step towards a deeper understanding of aerosol behavior. Using computational methods like MD simulations, valuable insight can be provided for the glass atmospheric organic compounds' ability to form IN (Sanz *et al.*, 2013; Carignano, Kachmar and Hutter, 2015). However, ice nucleation events are rare and demand long simulation times, reaching μs time scale (Li, Donadio and Galli, 2013). Despite this, the improvement in computational power and efficiency of today's computers and the combination of innovative computational methods can provide significant information about the structural and physicochemical properties of glassy organic aerosols.

5.2 Computational Methodology

5.2.1 Systems Setup

We carried out MD simulations for 12 organic species with different structures/ functional groups considered proxies for atmospheric organic aerosols depicted in Table 6. The organics under study were divided into three groups: organics with $-O-/-OH$ functional groups corresponding to oxygen-containing compounds, alcohols, and phenols (Figure 21a), organics with only $-CH_2-$ functional groups corresponding to hydrocarbons, alkynes and cycloalkanes (Figure 21b) and organics with $-NH_2/-CN$ functional groups corresponding to nitrogen-containing compounds – amines and nitriles (Figure 21c).

Table 6: Chemical structures of the organics considered proxies for atmospheric aerosols

Functional Group	Molecular name	Molecular Formula
-O-/-OH	Dimethyl Ether	C_2H_6O (or CH_3OCH_3)
	Ethanol	C_2H_6O (CH_3CH_2OH)
	Ethylene oxide	C_2H_4O
	1,2 - Dioxetane	$C_2H_4O_2$
	Vinylhydroperoxide	$C_2H_4O_2$
	PEG-06	$C_{12}H_{26}O_7$
-CH₂-	Propyne	C_3H_4
	Cyclopropene	C_3H_4
-NH₂/-CN	3-aminopropyne	C_3H_5N
	1-Propyn-1-amine	C_3H_5N
	Glycine	$C_2H_5NO_2$
	Propanenitrile	C_3H_5N

5.2.2   Force Field

To describe the interactions between molecules, we used the OPLS-AA (FF) (Banks *et al.*, 2005) along with the TIP4P/2005 water model (Abascal and Vega, 2005) in each case. The TIP4P/2005 model is a re-parameterization of the original TIP4P potential for water simulations and consists of a Lennard-Jones site for the oxygen atom and three charge sites (Abascal and Vega, 2005). We use the non-polarizable water model TIP4P/2005 (Abascal and Vega, 2005). It is a simple empirical model that reproduces many experimental results at a reasonable computational cost and gives a computational insight into ice nucleation (Frenkel and Smit, 1996). In combination with classical simulations, it seems to be reasonably successful in describing the experimental values of the nucleation rates and the interfacial free energies and dynamic properties of real water (Mandell, 1976). The OPLS-AA (FF) has been developed to work with the TIP4P family

of water models, where the parameters for nonbonded interactions have been fitted to reproduce correct solvation energies (P G Debenedetti and Stillinger, 2001).

5.2.2.1 *Evaluation of Force Fields – Free energy of Solvation*

The choice of the force field was validated by computing the free energy of hydration (ΔG_{hyd}) of the organics under study (Ryckaert, Ciccotti and Berendsen, 1977) following the protocol of Shirts et al. (Shirts *et al.*, 2003). Each organic was simulated in a cubic simulation box ($2.5 \times 2.5 \times 2.5$ nm^3) holding 500 water molecules. The transitions between two states were carried along with a coupling parameter, λ, indicating the level of change that has taken place between an initial state ($\lambda = 0$) and a final state ($\lambda = 1$). The transitions were divided into 21 sets of λ-vectors, and each step was simulated. For each value of λ, a workflow of steepest descend minimization, L-BFGS minimization, *NVT* equilibration, *NPT* equilibration and data collection under an *NPT* ensemble were conducted. The value of ΔG_{hyd} was calculated by adding the free energy differences of each λ-step, resulting in $\vartheta\mathcal{H}/\vartheta\lambda$, where $\mathcal{H}$ is the system's Hamiltonian.

5.2.3 Calculation of Mean Square Displacement MSD and Diffusion Coefficient

To elucidate the dynamic aspects of the studied clusters under supercooling conditions, we calculated the mean square

In statistical mechanics, MSD assess the deviation over time of a particle's position concerning a reference position. It is used to evaluate whether a particle moves primarily due to diffusion or due to an advective force. The molecular water motions are described by their long-time diffusion rate, computed by the diffusion coefficient D. This parameter is related to the MSD of any fixed point in each molecule. The following equation can be used:

$$MSD = u^2(t) = \frac{1}{N}\left\langle \sum_i |r_i(t_0 + t) - r_i(t_0)|^2 \right\rangle \qquad \textbf{Eq. 58}$$

where the brackets indicate an average over different time origins, t_0. In a long time limit, the slope of $u^2(t)$ gives the diffusion coefficient, D according to the Einstein equation:
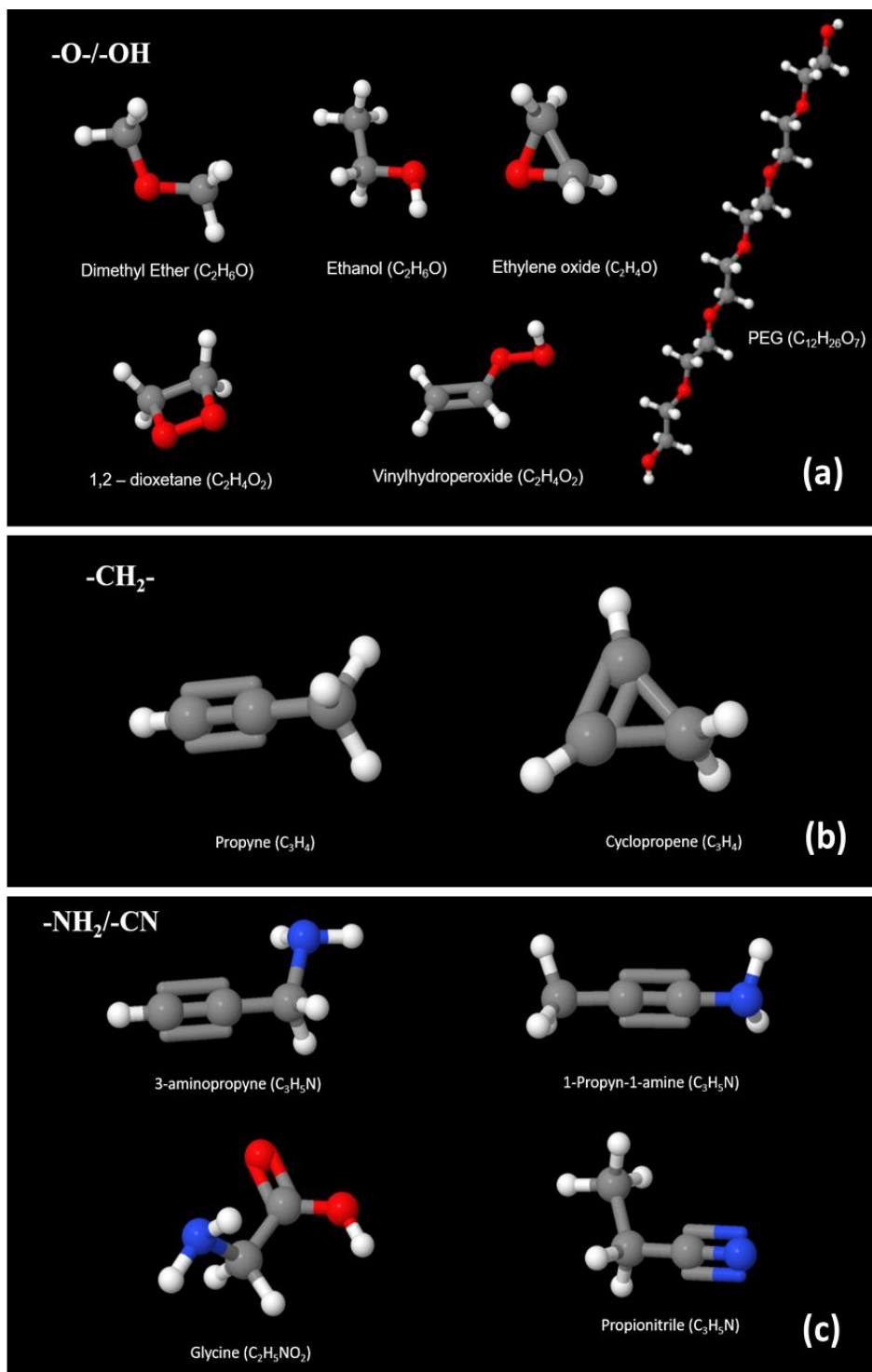
Figure 21: 3D representation of organics under study: (a) organics with -O-/-OH function groups corresponding to oxygen-containing compounds, alcohols, and phenols, (b) organics with -CH$_2$-function groups corresponding to hydrocarbons, alkynes, and cycloalkanes, and (c) organics with -NH$_2$/-CN function groups corresponding to nitrogen-containing compounds – amines and nitriles.

$$D = \lim_{t \to \infty} \frac{u^2(t)}{6t}$$

Eq. 59

where $r_i(t_0 + t)$ is the position at time t of the center of mass, and $\langle \sum_i |r_i(t_0 + t) - r_i(t_0)|^2 \rangle$: an average over both time origins and individual water molecules.

The MSD and D are calculated by the algorithm gmx msd using the analysis tools within the GROMACS package (Berendsen, van der Spoel and van Drunen, 1995). The MSD is averaged over these atoms using an index file containing atom numbers. For multi-atom molecules, r_i is taken as the centre of mass positions of the molecules.

In detail, gmx msd computes the MSD of atoms from a set of initial positions. This provides an easy way to calculate the diffusion constant using the Einstein relation. The D is calculated by least-squares fitting a straight line ($Dt + c$) to the $MSD(t)$.

5.2.4 Steinhardt order parameter

To monitor the ice nucleation potential within the water clusters, MD simulations focused on obtaining the local Steinhardt Q3, Q4, and Q6 parameters during cluster supercooling in the presence of organic matter (Steinhardt, Nelson and Ronchetti, 1983; Reinhardt *et al.*, 2012). In observing a nucleation process, a quantitative method is usually required as an order parameter. In the nucleation literature, particles' classification as solid-like or liquid-like is often based on the Steinhardt classification parameter. Steinhardt parameters are bond-based order parameters that have been widely used to describe the crystal packing of atoms, highly symmetric molecules, or more objects with a geometry that can be approached as a sphere. The definition of the Steinhardt order parameters is founded on the concept of bonds that do not necessarily correspond with that of a chemical bond, and the bond between two fundamental particles is defined when their distance is below a certain threshold. The local Steinhardt parameters are the correct order parameters to study the phase transition and identify both the F.C.C. (face-centered cubic) and the B.C.C. (body-centered cubic) ice during ice nucleation processes.

The local Steinhardt parameters are computed as the magnitude of the vector sum of the local parameters averaged over all i particles in the system,

$$q_l(i) = \left[\frac{4\pi}{2l + 1} \sum_{m=-1}^{+l} |q_{lm}(i)|^2 \right]^{1/2}$$

<div align="right">**Eq. 60**</div>

where $q_l(i)$ is based on the arrangement of the nearest neighbors of particle i, calculated as follow

$$q_{lm}(i) = \frac{1}{N(i)} \sum_{j=1}^{N(i)} Y_{lm}(\theta_{ij}, \varphi_{ij})$$

<div align="right">**Eq. 61**</div>

$Y_{lm}(\theta_{ij}, \varphi_{ij})$ are the spherical harmonics, θ and φ are the polar angles and $N(i)$ is the number of neighbors of particle i.

5.2.5 Autocorrelation function

To further check the system equilibration and organic state (glassy-liquid-solid), we computed and monitored the autocorrelation function (ACF) of specific vectors within the organic molecules in the simulation boxes. The ACF of the angle generated by the position vectors of a pair of atoms within each molecule under investigation is a useful tool for characterizing glassy states in MD simulations (Sun *et al.*, 2016). The rotational mobility of molecules is essential for ice nucleation since higher water mobility can represent a kinetic advantage for ice nucleation (Matsumoto, Saito and Ohmine, 2002). The method is implemented within the GROMACS molecular simulation package.

When ACF approaches a constant value above zero, this suggests a somewhat frozen system. Meaning that the internal structure evolves too slowly for the ACF angle to drop to zero, in contrast to liquid-like systems for which this ACF would rapidly disappear.

For any dynamic variable $A(t)$, such as bond lengths or dihedral angles, the $ACF(t)$ is defined as $ACF(t) = \langle A(t) A(0) \rangle$. This function measures the correlation of the property $A(t)$ to itself at two separate times with a time interval t, averaged over the whole trajectory. In practical terms, the autocorrelation function is obtained by averaging the terms $\langle A(s + t) A(s) \rangle$ while sliding along the trajectory. An essential property of the $ACF(t)$ is that by taking its Fast Fourier transform (FFT), one gets a spectral decomposition of all the frequencies that contribute to the motion (Becker *et al.*, 2001).

5.3 Molecular dynamics simulations

MD simulations were performed to examine complex organics' ability to form a glassy state and enhance Ice Nucleation in low temperatures (220-96K). All MD simulations (equilibration, relaxation, simulated annealing, and production) were performed using the Gromacs 5.0.4 program package (Berendsen, van der Spoel and van Drunen, 1995). To generate the molecular trajectories, a time step of 2 fs was used.

For the production, we employed supercooling dynamics (from 220K to 96K) for 100ns (*see* Figure 22). The constant density and temperature (NVT) ensemble run employed the Nosé−Hoover thermostat (Nosé and Klein, 1983; Hoover, 1985). We performed SA run after equilibrating and relaxing each system for the initial sampling performed. The temperature coupling constant was set at $0.2\ ps$ for all thermostats.
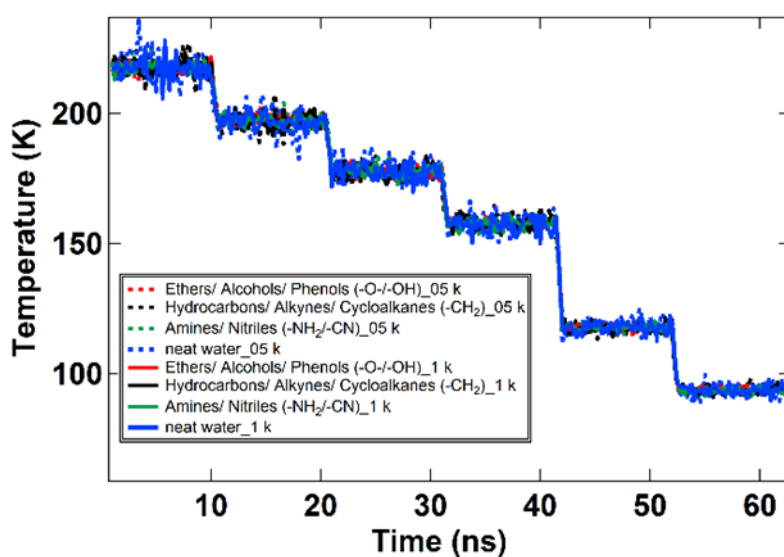
Figure 22: Time evolution of the temperature during supercooling dynamics (from 220K to 96K) for the organic molecules solvated in 500 TIP4P/2005 water and 1000 TIP4P/2005

The Coulombic interactions were treated using the reaction field method, as implemented in Gromacs (Berendsen, van der Spoel and van Drunen, 1995; Tironi *et al.*, 1995), while van-der-Waals interactions were using the cut-off scheme. The cut-off distances for the Coulombic and van der Waals interactions were set to 1.2 nm. The particle mesh Ewald summation method (Darden, York and Pedersen, 1993) was applied to compute the long-

range Coulombic interactions. A potential shift with the Verlet cutoff-scheme was selected, and dispersion corrections have been implemented for the energies, improving accuracy (Cisneros *et al.*, 2014). The LINCS (Hess *et al.*, 1997) algorithm was employed to constrain bonds that include hydrogen atoms for the rest of the molecules. A force constant of $1000 \, \text{kJ mol}^{-1}\text{nm}^{-2}$ was used for the constraints. While the SHAKE algorithm (Ryckaert, Ciccotti and Berendsen, 1977) is implemented to constrain the O–H distance and H–O–H angle (Pluhařová, Vrbka and Jungwirth, 2010).

5.4   Results and discussion

5.4.1   Free energy of Solvation

To evaluate our accurate models (and especially the employed FF), we computed the Gibbs free energy of solvation for the twelve organic molecules, using a combination of the OPLS/AA FF and a TIP4P/2005 water model. The results are given in Table 7. For many of the organics, there was a lack of experimental data, so a comparison with similar molecules was performed. Our simulations have a high degree of statistical precision, indicating that the force fields used can correctly describe the systems probed's organic-water interactions.

5.4.1   Mean-square displacement (MSD)

To determine the supercooling dynamics and potential phase changes from liquid to solid, MSD calculations were performed. We calculated the TIP4P/2005 water MSD for all clusters at low temperatures from 220 down to 96 K. The computed results for the water clusters reveal the effect of organic presence on the mobility of water molecules. Figure 23 shows the results of the MSD of the pure water in a system of 500 and 1000 molecules at different temperatures. For the 500-molecule system, it can be observed that the slope increases with time for temperatures >180 K, while when the temperature decreases to <180 K, the slopes fluctuate around a constant value since the system is trapped in a solid-like state. For larger clusters with 1000 molecules, we can observe that the slopes show more stability and fluctuate around a mean value, indicating that it is easier to overcome the liquid-solid barrier in a larger system, and a phase transition event is possible.

Table 7: Experimental (NIST 2011) and Calculated Hydration Free Energies ΔGhyd (kcalmol^{-1}) at T=293 K for the 20 organic molecules using the OPLS/AA force field and TIP4P/2005 water model.

Molecular Name	Molecular Formula	OPLS/AA-TIP4P/2005	Experimental
Dimethyl Ether	C_2H_6O	-0,78 ± 0,19	-1.45
Ethanol	C_2H_6O	-2,95 ± 0,25	-3.94
Ethylene oxide	C_2H_4O	-1,90 ± 0,18	-2.31
1,2 - Dioxetane	$C_2H_4O_2$	-4,38 ± 0,15	-
Vinylhydroperoxide	$C_2H_4O_2$	-2,39 ± 0,37	-5.32
PEG-06	$C_{12}H_{26}O_7$	-	-
Propyne	C_3H_4	1,99 ± 0,22	-2.49
Cyclopropene	C_3H_4	-1,09 ± 0,02	-0.77
3-aminopropyne	C_3H_5N	-4,01 ± 0,26	-3.67
1-Propyn-1-amine	C_3H_5N	-7,44 ± 0,17	-
Glycine	$C_2H_5NO_2$	-13,80 ± 0,36	−14.5
Propanenitrile	C_3H_5N	-3,94 ± 0,34	-6.28*
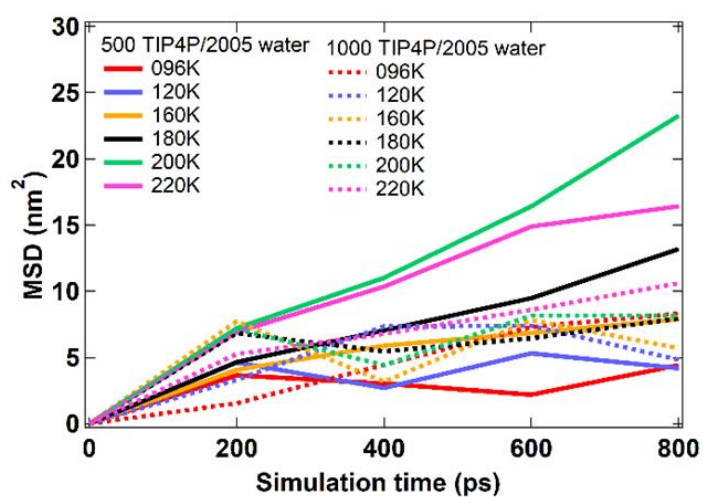
Figure 23: MSD for clusters of 500 and 1000 water molecules
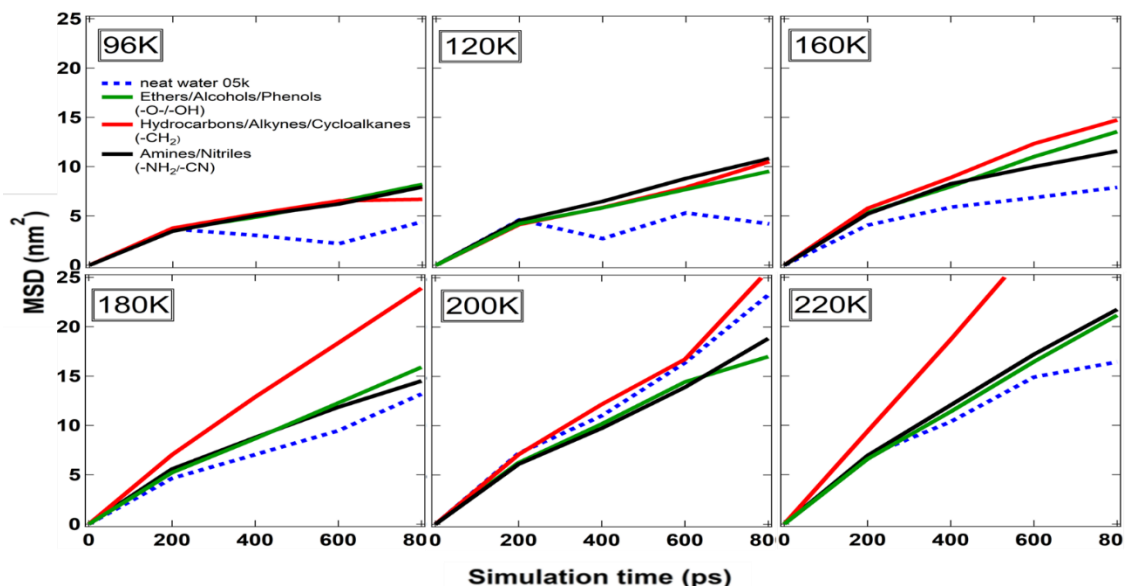
Figure 24: Mean square displacement (MSD) curves of the organic clusters solvated in 500 TIP4P/2005 water at different temperatures (96, 120, 160, 180, 200, and 220 K). Each line is an average of each function group. Green: ethers/ alcohols/ phenols, red hydrocarbons /alkynes /cycloalkanes, and black amines / nitriles.
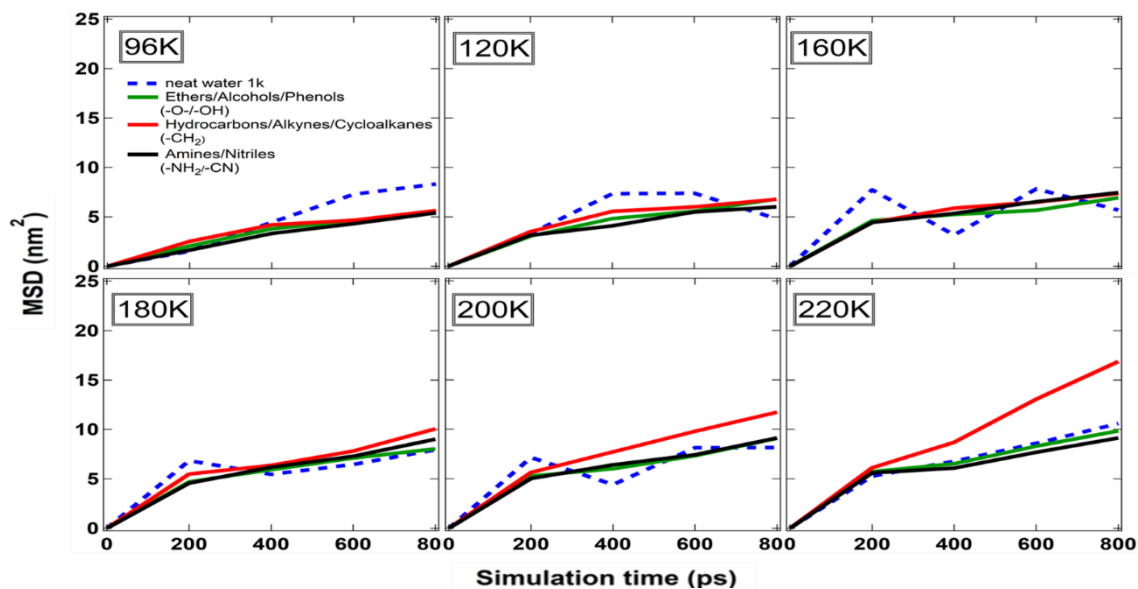
Figure 25: Mean square displacement (MSD) curves of the organic clusters solvated in 1000 TIP4P/2005 water at different temperatures (96, 120, 160, 180, 200, and 220 K). Each line is an average of each function group. Green: ethers/ alcohols/ phenols, red hydrocarbons/ alkynes/ cycloalkanes, and black amines/ nitriles.

5.4.2 Diffusion coefficient

The dynamical properties of the supercooled clusters were also examined by calculating the diffusion coefficient (D). We measured TIP4P/2005 water D in all model clusters representing organic aerosol as a temperature function. The computational setup used captured the system's correct dynamical properties simulated within the NPT ensemble (Shiraiwa, Pfrang and Pöschl, 2010; Price, 2013).

The results are illustrated in Figure 26 and show water diffusivity for all organic compounds and the diffusion coefficient for pure (neat) water. The results obtained are calculated for the clusters of 500 and 1000 TIP4P/2005 water. The values for D have a similar magnitude for all compounds. In general, the reduction of water diffusivity can be interpreted as a result of delayed interactions with water that may indicate a glassy phase resulting in inhibition of droplets' ability to act as IN (Benjamin J. Murray *et al.*, 2010; Cappa and Wilson, 2011; Price *et al.*, 2015). However, based on these results, we cannot present any significant differences to the organics' macroscopic physical property. No identification of a glassy state can be claimed as no experimental data to back up our results. However, we see that different organics exert a variable effect on the water dynamics.

5.4.3 Steinhardt Order Parameters

A criterion based on the Steinhardt local bond-order parameters Q3, Q4, and Q6 is employed to monitor ice nucleation events. These parameters were selected to label each water molecule in the system as liquid or solid. MD runs were performed at different temperatures (220, 200, 180, 160, and 96 K), and all values of the water TIP4P/2005 Steinhardt parameters were calculated for each organic system. The results are summarized in Figure 27 for Q4-Q6 and Q6-Q3 correlation, respectively. We used a 500/1000 TIP4P/2005 water ice cube with geometry obtained from previous simulations and calculated the Steinhardt parameters to compare the results with reference systems. The system was then melted (Simulated annealing run from 220K up to 300K and down to 96K), and the Steinhardt parameters were re-calculated. The results are also presented for reference to identify the configurational space in Q4-Q6 and Q6-Q3 coordinates related to ice-like or liquid-like structures. Only the results at 96K are shown, as this is

the lowest temperature of the Supercooling dynamics and should therefore represent the ice-like or (supercooled) liquid-like structure at the end of the dynamics.

As shown in the graphs Figure 27, there is a tendency from several of the organics to form ice crystals matching the reference for ice. Specifically, ethers/ alcohols (Red dots) and amines and nitriles (green dots) can induce ice nucleation. However, the results obtained show that most organic components do not promote ice nucleation. Instead, organic-rich aquatic particles preferentially remain unfrozen. These results suggest that emissions of organic species have the potential to influence aerosol-cold cloud interactions.
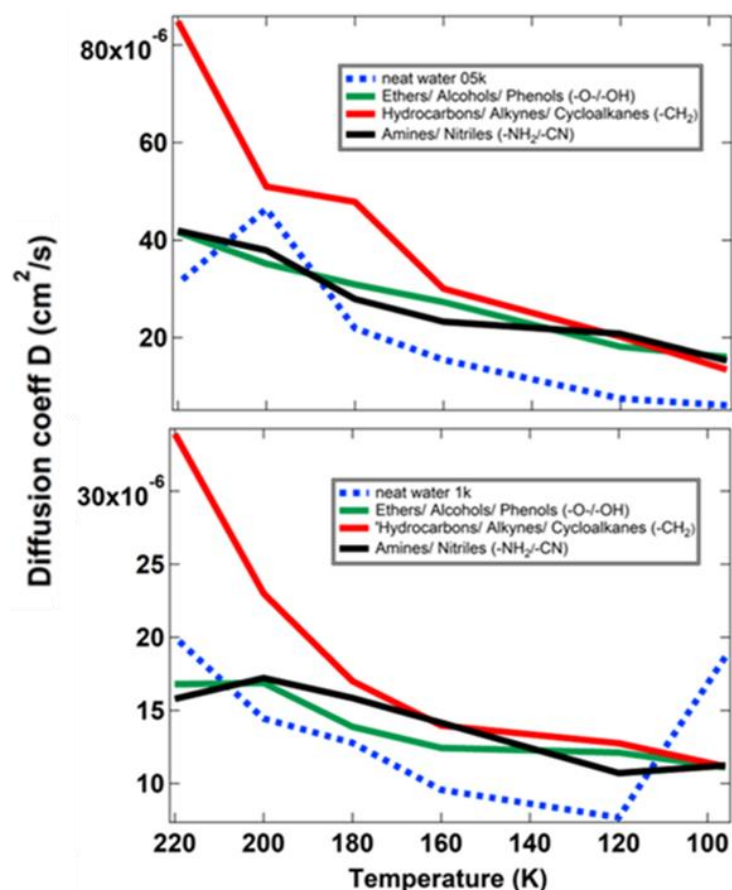
Figure 26: Plot of the water diffusion coefficient of the organic solvated in 500 and 1000 TIP4P2005 water clusters displayed as a function of inverse temperature. The blue lines are the self-diffusion coefficient of neat water. Green lines correspond to ethers/alcohols/phenols (-O-/-OH), red lines correspond to hydrocarbons/alkynes/cycloalkanes (-CH$_2$-), and black lines correspond to amines/ nitriles (-NH$_2$/-CN)
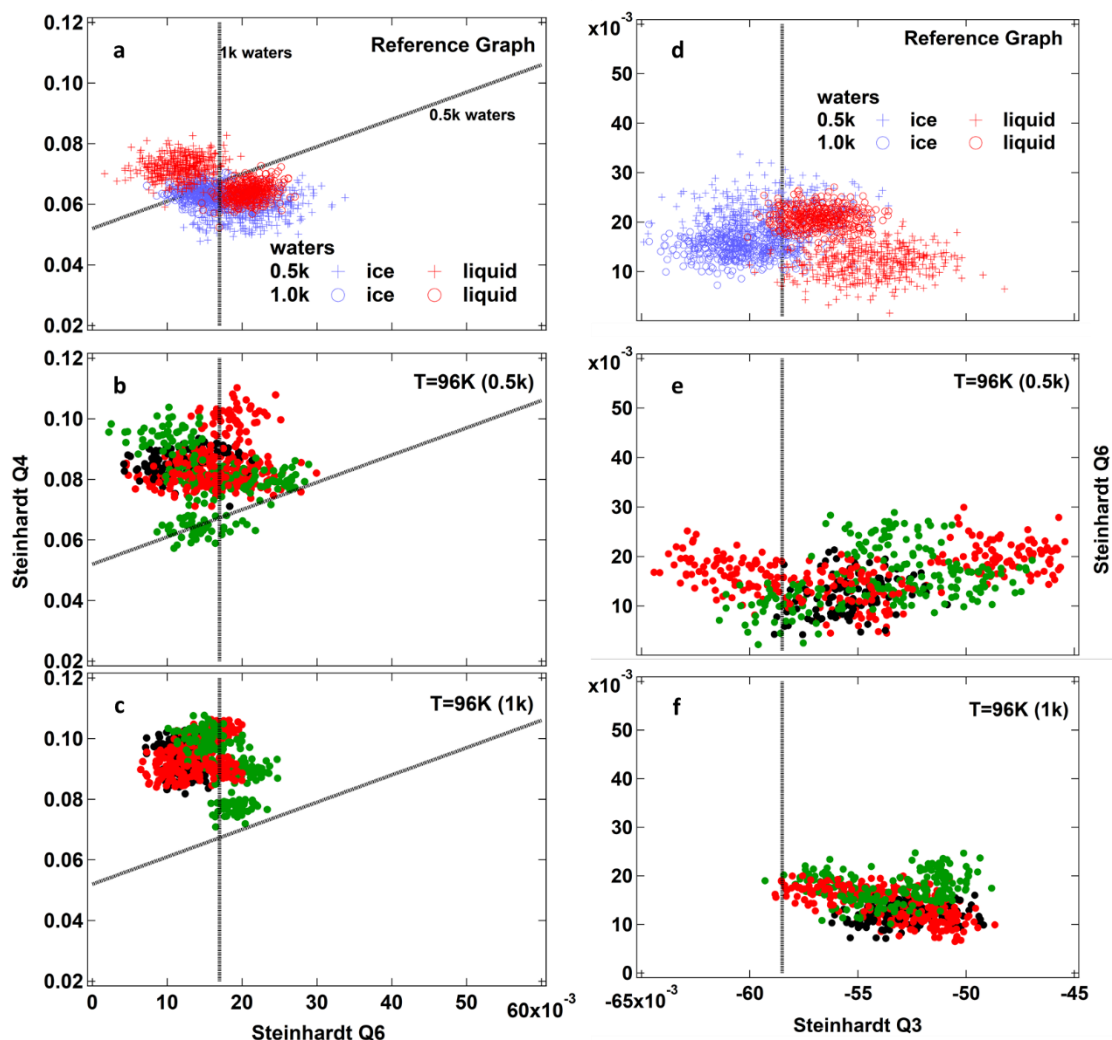
Figure 27: 2D scatter plot of values of Steinhardt order parameters Q4/Q6 and Q6/Q3 obtained for the clusters of all organics solvated in 500 and 1000 TIP4P2005. To the right (a) is the reference plot for Q4/Q6, and to the left (d) is the reference plot for Q6/Q3. Red dots correspond to ethers, alcohols, or phenols, green dots correspond to amines and nitriles, and black dots correspond to hydrocarbons (alkynes and cycloalkanes).

5.4.4 Autocorrelation function

The average rotational autocorrelation function of the three organic molecular groups investigated was calculated to represent organic molecules' flexibility. In Figure 28, the corresponding curves clearly exhibit a glassy-like behavior for the organics under study. In detail, Figure 28 shows that the autocorrelation functions decay relatively quickly, but then they fluctuate around zero for all organic groups. The rate with which ACF drops to zero is a measure of how fast the chosen pair of molecules or ions forgets its initial

configuration during the simulation. Therefore, it provides a measure of the degree of the system's relaxation rate and could also measure the formation of a glassy organic state.
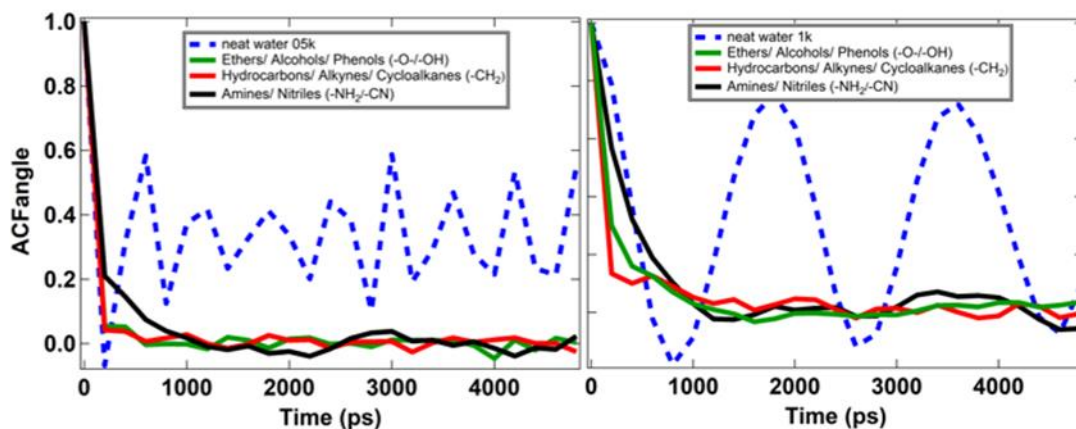
Figure 28: Average rotational autocorrelation function of the three organic groups studied, ethers/alcohols/phenols (green), hydrocarbons/alkynes/cycloalkanes (red), and amines/ nitriles (black)

For all organics examined, ACF is initially equal to one and drops rapidly, fluctuating around a constant value around zero. This indicates a somewhat frozen system whose internal microstructure evolves too slowly. In soft matter physics, such sluggish dynamics are typically displayed by glassy systems. The internal microstructure gets arrested at a local minimum of the potential energy. The fast decay of ACF initially is due to the fast dynamics of organic molecules at the nanoparticle's free surface.

5.5 Conclusions

Molecular dynamics simulations were carried out with a primary scope to assess organics solutions' ability to form glasses. From the organic systems investigated in this study, glass formation was more likely in aqueous organic solutions containing glycine, propanenitrile, 1,2 – dioxetane, and vinylhydroperoxide. These organics correspond to ethers, alcohols or phenols, amines, or nitriles, suggesting that these organic groups may persist in a glassy state, thus facilitating heterogeneous ice nucleation. For the rest of the organics studied, the results obtained show that they do not promote ice nucleation, and organic-rich particles preferentially remain unfrozen. The correlation of Q4-Q6 and Q6-

Q3 Steinhardt parameters for the water shows this distinct behavior. Meanwhile, the slow diffusion rates may indicate inhibition of ice nucleation and/ or ice growth. This suggests that emissions of organic species have the potential to influence aerosol-cold cloud microphysics and dynamics in different ways, even if nucleation is not observed for all the organics probed.

Glassy organic aerosols affect ice crystals formation with a consequence to cloud formation and precipitation. The study of atmospheric organic aerosols is a complicated discipline demanding in-depth research for a comprehensive understanding. Limitations exist, and they are mainly due to the obscure insight into the glassy organic aerosol formation, composition, properties, and processes. More experiments and simulations to parameterize the nucleation activity in the presence of glassy organics over a broad temperature range are needed. This latter is essential because some water-soluble organic compounds show a strong temperature dependence of water activity for aqueous mixtures of uniform composition. Such knowledge would reduce the model uncertainty in future modeling studies substantially. Furthermore, it may impact the set off semi-volatile compounds, decrease the occurrence of heterogeneous chemical reactions, influence aerosol particles' ability to accumulate water, act as ice nuclei, and change the particles' lifetime.

6   Summary and Future Outlook

Ice nucleation (IN)/cloud condensation nuclei (CCN) formation study has gotten a lot of attention in the last decade. Many critical research goals and unanswered questions must be addressed and used to close the gaps in our knowledge of such processes and their impact on atmospheric dynamics. Our overall goal was to highlight the importance of molecular dynamics simulations and modeling in understanding ice nucleation processes/ CCN formation and events in this research. In particular, the MD simulation technique was employed to study two principal objectives. The first was related to CCN formation in terms of the correlation between surface tension and the static dielectric constant in particles consisting of water, salt (ammonium bisulfate), and surface-active organic matter. The second was to understand organic species' ability to form glassy phases and initiate ice nucleation in low temperatures.

In the first case, we present a correlation between surface activity and water contribution to the static dielectric constant of ionic aquatic droplets. We identify changes to this contribution due solely to different organics or organic matter concentrations on the surface. These changes are attributed to different salt structures within the droplets that lead to different orientations of the water dipoles. We provide evidence for the association between their surface tension depression and the water activity decrease for droplets of radials at the 3.6 nm scale that can be attributed to New Particle Formation (NPF) at a level of detail that is not accessible experimentally. In the second case, we assess organics solutions' ability to form glasses related to IN formation. We show that organic species emissions can influence aerosol-cold cloud microphysics and dynamics in different ways, even if nucleation is not observed for all the organics probed. From the organic systems investigated in this study, glass formation was more likely in aqueous organic solutions corresponding to ethers, alcohols or phenols, amines, or nitriles, suggesting that these organic groups may persist in a glassy state, thus facilitating heterogeneous ice nucleation. On the other hand, we show that organic-rich particles preferentially remain unfrozen and do not promote ice nucleation.

6.1 Future Work

The research outlined in this study points to a variety of potential research directions. As noted in chapter 5, glassy organic aerosol's impact on the climate is indirect. It affects water droplet and ice crystal formation, evaporation, and deposition due to cloud formation and precipitation. Future work on this thesis will involve MD experiments to parameterize the nucleation activity in the presence of glassy organics over a broader temperature range and in larger particles to enable efficient nucleation. This is significant since, for aqueous mixtures of constant composition, at least some water-soluble organic compounds display a strong temperature dependence of water behavior. (Zobrist, Weers and Koop, 2003). In future modeling research, such changes will reduce model uncertainty. Another uncertainty is the lack of information about the exact microphysical mechanism by which amorphous organics compounds nucleate ice heterogeneously. Glassy particles have a wide variety of recorded ice nucleation onsets and are the most probable material or substance type (Wilson *et al.*, 2012). The study of heterogeneous ice nucleation requires, as a first step, the distinction of fundamental classes of properties of the substance added to the water that affects the nucleation rate of ice. Here, models with different accuracy levels (quantum, empirical) could help bridge the gap between fundamental theories and experiments. As a result, further laboratory experiments are needed to uncover information about the ice nucleation mechanism and make predictions of ice nucleation capacity for various substances.

Given our experience and the protocols employed in the above studies, another fascinating new research target is identifying and studying ice-nucleating particles containing biological species in the atmosphere using MD Simulations techniques. Biological ice nuclei are a distinctive category of INPs due to their capability of facilitating ice crystal formation in clouds at relatively warm temperatures (Huang *et al.*, 2021). Particles related to biological origins can initiate ice nucleation at a temperature range between $-2℃$ and $-10℃$ critical for secondary ice formation (Hoose and Möhler, 2012; Murray *et al.*, 2012b). Active biological INPs are ubiquitous in the atmosphere. They include bacteria, fungal spores, pollen, algae, lichens, archaea, viruses, and biological fragments (e.g., leaf litters, insects) and molecules (e.g., proteins, polysaccharides, lipids) (DeMott and Prenni, 2010; Knopf *et al.*, 2011; Després *et al.*, 2012; Fröhlich-Nowoisky *et al.*, 2015; Felgitsch *et al.*, 2018; Zhai *et al.*, 2018; Guo *et al.*,

2020). The most efficient ice-nucleating substance discovered so far comes from the protein produced by the plant pathogenic bacterium *Pseudomonas syringae*, capable of freezing water at temperatures up to -2 °C (Maki *et al.*, 1974; Monteil, Bardin and Morris, 2014; Karimi *et al.*, 2020). Field observations and model simulations have indicated that biological INPs affect cloud and precipitation formation and regulate regional or global climate. However, there are considerable uncertainties in modeling and large gaps between the observed and model-simulated biological particles' contribution to atmospheric INPs.

6.2 Final Remarks

MD simulation is a powerful and useful technique that allows us to study the statistical and dynamical properties of complex systems and examine the atomistic scale's physiochemical processes. Our research contributed towards a fundamental understanding of nucleation. The investigation of realistic systems has provided findings directly relevant to problems of considerable significance. Therefore, it is safe to assume that MD simulations have been and will continue to be an excellent complement to experiments. However, simulations are currently affected by many drawbacks, which impede a credible comparison with experimental nucleation rates and restrict nucleation studies to structures and/or environments that are frequently far from those experimentally examined. These shortcomings can be divided into two major categories: deficiencies related to the precision of the numerical model used to describe the system; and weaknesses attributable to the computational methods used to simulate nucleation events.

Ab initio calculations would be an ideal study tool to study ice nucleation events in a perfect universe. Unfortunately, the timescale problem makes ab initio simulations unfeasible. We must focus our energies on enhancing existing classical force fields and creating novel classical interatomic potentials since this will be the status quo for the next few decades. While simulations of basic systems are feasible, when particles interact within more realistic systems where the interface description requires transferable and stable force fields, they tend to fall apart. Machine learning algorithms are developed as possible partners to the classical MD simulations with an accuracy similar to first-principle calculations, such as neural network potential (Behler, 2014; Handley and

Behler, 2014; Noé *et al.*, 2020). Nevertheless, the field is actively searching for other alternatives that can bring simulations closer to reality.

MD simulations allow for an impartial investigation of nucleation incidents, but the timescale issue restricts this method to a small number of structures, most of which are far removed from practical materials. Although brute force MD cannot provide a complete characterization of the nucleation mechanism, it can still provide valuable insight into nucleation events. Enhanced sampling techniques are rapidly evolving and have the potential to take the field to the next level. However, free energy methods do not give access to nucleation kinetics, and, in the case of complex systems, they are strongly dependent on the choice of the order parameter. On the other hand, it seems that path sampling methods can provide a more comprehensive picture of crystal nucleation. However, these strategies are computationally costly, and a general implementation is not yet available, despite recent consistent efforts. One of the most important challenges ahead, we believe, is the advancement of efficient enhanced sampling methods unique to crystal nucleation.

Nucleation models are limited to small (10^2-10^4 particle) complex structures, most commonly in idealized conditions. Because of the inherent challenges in modeling and experimentally characterizing them, it is impossible to consider impurities or defects very often present in experimental systems. These are key factors that almost always influence experimental measurements and should be used in simulations. MD simulations can also provide microscopic analysis and useful observations, and a general understanding of various systems.

Finally, it has been shown in this study that MD simulations have proved to be critical in unraveling the microscopic information of nucleation mechanisms. At the current stage, the disadvantage is that MD simulations' time scale is usually limited to hundreds of nanoseconds or microseconds, which may not be sufficient to sample the rare events fully. Improving the current limitations of computational models and techniques will enable simulations of far larger systems over much longer timescales, with a precision level that would allow for a far more fruitful comparison with experiments. To do so, we will need to improve our computational and theoretical skills. We should develop the classical interatomic potentials available and the current enhanced sampling techniques to allow accurate simulations of nucleation events for systems of practical importance.

97

Consequently, with the fast development of computer hardware and new emerging algorithms, MD simulations' computational accuracy and efficiency will be pushed to new frontiers in the future. MD simulations will undoubtedly constitute an essential part of both academic and industrial research in the coming era of computer modeling.

REFERENCES

Abascal, J. L. F. and Vega, C. (2005) 'A general purpose model for the condensed phases of water: TIP4P/2005', *Journal of Chemical Physics*, 123(23), p. 234505.

Alder, B. J. and Wainwright, T. E. (1957) 'Phase transition for a hard sphere system', *The Journal of Chemical Physics*. American Institute of PhysicsAIP, 27(5), pp. 1208–1209.

Alder, B. J. and Wainwright, T. E. (1959) 'Studies in molecular dynamics. I. General method', *The Journal of Chemical Physics*, 31(2), pp. 459–466.

Andreae, M. O. and Crutzen, P. J. (1997) 'Atmospheric aerosols: Biogeochemical sources and role in atmospheric chemistry', *Science*, 276(5315), pp. 1052–1058.

Andreae, M. O. and Rosenfeld, D. (2008) 'Aerosol-cloud-precipitation interactions. Part 1. The nature and sources of cloud-active aerosols', *Earth-Science Reviews*, 89(1–2), pp. 13–41.

Aragones, J. L., Sanz, E. and Vega, C. (2012) 'Solubility of NaCl in water by molecular simulation revisited', *Journal of Chemical Physics*, 136(24).

Bahreini, R. *et al.* (2005) 'Measurements of secondary organic aerosol from oxidation of cycloalkenes, terpenes, and m-xylene using an aerodyne aerosol mass spectrometer', *Environmental Science and Technology*, 39(15), pp. 5674–5688.

Baltensperger, U. and Prévôt, A. S. H. (2008) 'Chemical analysis of atmospheric aerosols', *Analytical and Bioanalytical Chemistry*, 390(1), pp. 277–280.

Banks, J. L. *et al.* (2005) 'Integrated Modeling Program, Applied Chemical Theory (IMPACT)', *Journal of Computational Chemistry*, 26(16), pp. 1752–1780.

Battimelli, G. and Ciccotti, G. (2018) 'Berni Alder and the pioneering times of molecular simulation', *European Physical Journal H*, 43(3), pp. 303–335.

Baustian, K. J. *et al.* (2013) 'State transformations and ice nucleation in amorphous (semi-)solid organic aerosol', *Atmospheric Chemistry and Physics*, 13(11), pp. 5615–5628.

Becker, O. M. *et al.* (2001) *Computational Biochemistry and Biophysics*, *Computational Biochemistry and Biophysics*.

Becker, R. and Döring, W. (1935) 'Kinetische Behandlung der Keimbildung in übersättigten Dämpfen', *Annalen der Physik*, 416(8), pp. 719–752.

Behler, J. (2014) 'Representing potential energy surfaces by high-dimensional neural network potentials', *Journal of Physics Condensed Matter*. Institute of Physics Publishing, p. 183001.

Berendsen, H. J. C. *et al.* (1984) 'Molecular dynamics with coupling to an external bath', *The Journal of Chemical Physics*, 81(8), pp. 3684–3690.

Berendsen, H. J. C., van der Spoel, D. and van Drunen, R. (1995) 'GROMACS: A message-passing parallel molecular dynamics implementation', *Computer Physics Communications*, 91(1–3), pp. 43–56.

Berkemeier, T. *et al.* (2016) 'Ozone uptake on glassy, semi-solid and liquid organic

matter and the role of reactive oxygen intermediates in atmospheric aerosol chemistry', *Physical Chemistry Chemical Physics*. The Royal Society of Chemistry, 18(18), pp. 12662–12674.

Bernardi, R. C., Melo, M. C. R. and Schulten, K. (2015) 'Enhanced sampling techniques in molecular dynamics simulations of biological systems', *Biochimica et Biophysica Acta - General Subjects*. Elsevier B.V., 1850(5), pp. 872–877.

De Boer, G. *et al.* (2011) 'Evidence of liquid dependent ice nucleation in high-latitude stratiform clouds from surface remote sensors', *Geophysical Research Letters*, 38(1).

Bond, T. C. *et al.* (2007) 'Historical emissions of black and organic carbon aerosol from energy-related combustion, 1850-2000', *Global Biogeochemical Cycles*, 21(2).

Bones, D. L. *et al.* (2012) 'Comparing the mechanism of water condensation and evaporation in glassy aerosol', *Proceedings of the National Academy of Sciences of the United States of America*, 109(29), pp. 11613–11618.

Boucher, O. *et al.* (2013) 'Clouds and aerosols', *Climate Change 2013 the Physical Science Basis: Working Group I Contribution to the Fifth Assessment Report of the Intergovernmental Panel on Climate Change*, 9781107057, pp. 571–658.

Buff, F. P. (1955) 'Spherical interface. II. Molecular theory', *The Journal of Chemical Physics*, 23(3), pp. 419–427.

Bussi, G., Donadio, D. and Parrinello, M. (2007) 'Canonical sampling through velocity rescaling', *Journal of Chemical Physics*. American Institute of Physics, 126(1), p. 014101.

Cappa, C. D. and Wilson, K. R. (2011) 'Evolution of organic aerosol mass spectra upon heating: Implications for OA phase and partitioning behavior', *Atmospheric Chemistry and Physics*, 11(5), pp. 1895–1911.

Carignano, M. A., Kachmar, A. and Hutter, J. (2015) *Thermal effects on CH3NH3PbI3 perovskite from Ab initio molecular dynamics simulations*, *Journal of Physical Chemistry C*.

Cavalli, F. *et al.* (2004) 'Advances in characterization of size-resolved organic matter in marine aerosol over the North Atlantic', *Journal of Geophysical Research D: Atmospheres*, 109(24), pp. 1–14.

Chen, F. and Smith, P. E. (2007) 'Simulated surface tensions of common water models', *Journal of Chemical Physics*, 126(22).

Chen, Y. *et al.* (2016) 'Electrolytes induce long-range orientational order and free energy changes in the H-bond network of bulk water', *Science Advances*, 2(4), pp. e1501891–e1501891.

Chiu, S. W. *et al.* (2000) 'Collective Motion Artifacts Arising in Long-Duration Molecular Dynamics Simulations', *Journal of Computational Chemistry*, 21(2), pp. 121–131.

Christ, C. D., Mark, A. E. and Van Gunsteren, W. F. (2010) 'Basic ingredients of free energy calculations: A review', *Journal of Computational Chemistry*, pp. 1569–1582.

Chukin, V. V., Pavlenko, E. A. and Platonova, A. S. (2010) 'Homogeneous ice nucleation rate in supercooled droplets of aqueous solutions', *Russian Meteorology and Hydrology*, 35(8), pp. 524–529.

Cisneros, G. A. *et al.* (2014) 'Classical electrostatics for biomolecular simulations', *Chemical Reviews*, pp. 779–814.

Coveney, P. V. and Wan, S. (2016) 'On the calculation of equilibrium thermodynamic properties from molecular dynamics', *Physical Chemistry Chemical Physics*. Royal Society of Chemistry, 18(44), pp. 30236–30240.

Cui, Z. *et al.* (2006) 'A numerical study of aerosol effects on the dynamics and microphysics of a deep convective cloud in a continental environmental', *Journal of Geophysical Research Atmospheres*, 111(5).

Cziczo, D. J. *et al.* (2004) 'Observations of organic species and atmospheric ice formation', *Geophysical Research Letters*, 31(12), p. n/a-n/a.

D'Alessandro, M., Tenenbaum, A. and Amadei, A. (2002) 'Dynamical and statistical mechanical characterization of temperature coupling algorithms', *Journal of Physical Chemistry B*, 106(19), pp. 5050–5057.

Darden, T., York, D. and Pedersen, L. (1993) 'Particle mesh Ewald: An N·log(N) method for Ewald sums in large systems', *The Journal of Chemical Physics*, 98(12), pp. 10089–10092.

Daskalakis, V. *et al.* (2014) 'Effects of surface-active organic matter on carbon dioxide nucleation in atmospheric wet aerosols: A molecular dynamics study', *Physical Chemistry Chemical Physics*, 16(43), pp. 23723–23734.

Daskalakis, V. *et al.* (2015) 'Surface-active organic matter induces salt morphology transitions during new atmospheric particle formation and growth', *RSC Advances*, 5(78), pp. 63240–63251.

Daskalakis, V. and Hadjicharalambous, M. (2014) 'Hexagonal ice stability and growth in the presence of glyoxal and secondary organic aerosols', *Physical Chemistry Chemical Physics*. Royal Society of Chemistry, 16(33), pp. 17799–17810.

Davies, J. F. and Wilson, K. R. (2015) 'Nanoscale interfacial gradients formed by the reactive uptake of OH radicals onto viscous aerosol surfaces', *Chemical Science*, 6(12), pp. 7020–7027.

Debenedetti, P G and Stillinger, F. H. (2001) 'Supercooled liquids and the glass transition.', *Nature*, 410(6825), pp. 259–67.

Debenedetti, Pablo G. and Stillinger, F. H. (2001) 'Supercooled liquids and the glass transition', *Nature*, 410(6825), pp. 259–267.

DeMott, P. and Prenni, A. (2010) 'New Directions: Need for defining the numbers and sources of biological aerosols acting as ice nuclei', *Atmospheric Environment - ATMOS ENVIRON*, 44, pp. 1944–1945.

Després, V. *et al.* (2012) 'Primary biological aerosol particles in the atmosphere: a review', *Tellus B: Chemical and Physical Meteorology*. Taylor & Francis, 64(1), p. 15598.

Elton, D. C. and Fernández-Serra, M. V. (2014) 'Polar nanoregions in water: A study of the dielectric properties of TIP4P/2005, TIP4P/2005f and TTM3F', *Journal of Chemical Physics*, 140(12).

Facchini, M. C. *et al.* (1999) 'Cloud albedo enhancement by surface-active organic solutes in growing droplets', *Nature*, 401(6750), pp. 257–259.

Feig, M. *et al.* (2018) 'Challenges and opportunities in connecting simulations with experiments via molecular dynamics of cellular environments', in *Journal of Physics: Conference Series*. Institute of Physics Publishing.

Felgitsch, L. *et al.* (2018) 'Birch leaves and branches as a source of ice-nucleating macromolecules', *Atmos. Chem. Phys*, 18, pp. 16063–16079.

Franks, F., Mathias, S. F. and Trafford, K. (1984) 'The nucleation of ice in undercooled water and aqueous polymer solutions', *Colloids and Surfaces*, 11(3–4), pp. 275–285.

Frenkel, D. and Smit, B. (1996) *Understanding molecular simulation: From algorithms to applications*. 1st edn, *Understanding molecular simulation: From algorithms to applications*. 1st edn. USA: Academic Press, Inc.

Frenkel, D. and Smit, B. (2002) 'Monte Carlo Simulations', in *Understanding Molecular Simulation*. Elsevier, pp. 23–61.

Frenkel, J. (1946) 'Kinetic Theory of Liquids: Oxford University Press', *New York*, p. 36.

Fröhlich-Nowoisky, J. *et al.* (2015) 'Ice nucleation activity in the widespread soil fungus Mortierella alpina', *Biogeosciences*. Copernicus GmbH, 12(4), pp. 1057–1071.

Froyd, K. D. *et al.* (2010) 'Aerosols that form subvisible cirrus at the tropical tropopause', *Atmospheric Chemistry and Physics*, 10(1), pp. 209–218.

Fu, T. M. *et al.* (2008) 'Global budgets of atmospheric glyoxal and methylglyoxal, and implications for formation of secondary organic aerosols', *Journal of Geophysical Research Atmospheres*, 113(15).

Fuzzi, S. *et al.* (2006) 'Critical assessment of the current state of scientific knowledge, terminology, and research needs concerning the role of organic aerosols in the atmosphere, climate, and global change', *Atmospheric Chemistry and Physics*. Copernicus GmbH, 6(7), pp. 2017–2038.

Fuzzi, S. *et al.* (2015) 'Particulate matter, air quality and climate: Lessons learned and future needs', *Atmospheric Chemistry and Physics*, 15(14), pp. 8217–8299.

Gavish, N. and Promislow, K. (2016) 'Dependence of the dielectric constant of electrolyte solutions on ionic concentration: A microfield approach', *Physical Review E*, 94(1).

Genareau, K. *et al.* (2018) 'Compositional and mineralogical effects on ice nucleation activity of volcanic ash', *Atmosphere*. Multidisciplinary Digital Publishing Institute, 9(7), p. 238.

George, I. J. and Abbatt, J. P. D. (2010) 'Heterogeneous oxidation of atmospheric aerosol particles by gas-phase radicals', *Nature Chemistry*, 2(9), pp. 713–722.

Ghoufi, A., Malfreyt, P. and Tildesley, D. J. (2016) 'Computer modelling of the surface tension of the gas-liquid and liquid-liquid interface', *Chemical Society Reviews*. Royal

Society of Chemistry, 45(5), pp. 1387–1409.

Glasius, M. and Goldstein, A. H. (2016) 'Recent Discoveries and Future Challenges in Atmospheric Organic Chemistry', *Environmental Science and Technology*, 50(6), pp. 2754–2764.

Good, N. *et al.* (2010) 'Consistency between parameterisations of aerosol hygroscopicity and CCN activity during the RHaMBLe discovery cruise', *Atmospheric Chemistry and Physics*, 10(7), pp. 3189–3203.

Van Gunsteren, W. F. and Berendsen, H. J. C. (1977) 'Algorithms for macromolecular dynamics and constraint dynamics', *Molecular Physics*, 34(5), pp. 1311–1327.

Guo, J. *et al.* (2020) 'Characteristics of airborne bacterial communities in indoor and outdoor environments during continuous haze events in Beijing: Implications for health care', *Environment International*. Elsevier Ltd, 139, p. 105721.

Hallquist, M. *et al.* (2009) 'The formation, properties and impact of secondary organic aerosol: Current and emerging issues', *Atmospheric Chemistry and Physics*. Copernicus GmbH, 9(14), pp. 5155–5236.

Handley, C. M. and Behler, J. (2014) 'Next generation interatomic potentials for condensed systems', *European Physical Journal B*. Springer Berlin Heidelberg, 87(7), pp. 1–16.

Hastings, W. P. *et al.* (2005) 'Secondary organic aerosol formation by glyoxal hydration and oligomer formation: Humidity effects and equilibrium shifts during analysis', *Environmental Science and Technology*, 39(22), pp. 8728–8735.

Hauner, I. M. *et al.* (2017) 'The Dynamic Surface Tension of Water', *Journal of Physical Chemistry Letters*, 8(7), pp. 1599–1603.

Hede, T. *et al.* (2011) 'Model HULIS compounds in nanoaerosol clusters - Investigations of surface tension and aggregate formation using molecular dynamics simulations', *Atmospheric Chemistry and Physics*, 11(13), pp. 6549–6557.

Hess, B. *et al.* (1997) 'LINCS: A Linear Constraint Solver for molecular simulations', *Journal of Computational Chemistry*, 18(12), pp. 1463–1472.

Heyda, J. *et al.* (2010) 'Reversal of Hofmeister ordering for pairing of NH4+ vs alkylated ammonium cations with halide anions in water', *Journal of Physical Chemistry B*, 114(33), pp. 10843–10852.

Hinds, W. C. (1999) *Aerosol technology: properties, behaviour, and measurement of airborne particles.*

Hinks, M. L. *et al.* (2016) 'Effect of viscosity on photodegradation rates in complex secondary organic aerosol materials', *Physical Chemistry Chemical Physics*, 18(13), pp. 8785–8793.

Hockney, R. W. (1970) 'The potential calculation and some applications', in *Methods in Computational Physics, Vol. 9*, pp. 135–211.

Holmes, C. F. (1973) 'On the Relation between Surface Tension and Dielectric Constant', *Journal of the American Chemical Society*. American Chemical Society, 95(4), pp. 1014–

1016.

Hoose, C. *et al.* (2010) 'A classical-theory-based parameterization of heterogeneous ice nucleation by mineral dust, soot, and biological particles in a global climate model', *Journal of the Atmospheric Sciences*, 67(8), pp. 2483–2503.

Hoose, C. and Möhler, O. (2012) 'Heterogeneous ice nucleation on atmospheric aerosols: A review of results from laboratory experiments', *Atmospheric Chemistry and Physics*, 12(20), pp. 9817–9854.

Hoover, W. G. (1985) 'Canonical dynamics: Equilibrium phase-space distributions', *Physical Review A*, 31(3), pp. 1695–1697.

Horn, H. W. *et al.* (2004) 'Development of an improved four-site water model for biomolecular simulations: TIP4P-Ew', *Journal of Chemical Physics*, 120(20), pp. 9665–9678.

Hospital, A. *et al.* (2015) 'Molecular dynamics simulations: Advances and applications', *Advances and Applications in Bioinformatics and Chemistry*, 8(1), pp. 37–47.

Houle, F. A., Hinsberg, W. D. and Wilson, K. R. (2015) 'Oxidation of a model alkane aerosol by OH radical: The emergent nature of reactive uptake', *Physical Chemistry Chemical Physics*, 17(6), pp. 4412–4423.

Huang, S. *et al.* (2021) 'Overview of biological ice nucleating particles in the atmosphere', *Environment International*. Elsevier Ltd, 146, p. 106197.

Jacobson, M. C. *et al.* (2000) 'Organic atmospheric aerosols: Review and state of the science', *Reviews of Geophysics*, 38(2), pp. 267–294.

Jimenez, J. L. *et al.* (2009) 'Evolution of organic aerosols in the atmosphere', *Science*, 326(5959), pp. 1525–1529.

Jorgensen, W. L. *et al.* (1983) 'Comparison of simple potential functions for simulating liquid water', *The Journal of Chemical Physics*, 79(2), pp. 926–935.

Jura, G. and Harkins, W. D. (1946) 'Surfaces of solids. XIV. A Unitary Thermodynamic Theory of the Adsorption of Vapors on Solids and of Insoluble Films on Liquid Subphases', *Journal of the American Chemical Society*, 68(10), pp. 1941–1952.

Kanakidou, M. *et al.* (2005) 'Organic aerosol and global climate modelling: A review', *Atmospheric Chemistry and Physics*, 5(4), pp. 1053–1123.

Kanji, Z. A. *et al.* (2017) 'Overview of Ice Nucleating Particles', *Meteorological Monographs*. American Meteorological Society, 58(1), pp. 1.1-1.33.

Kärcher, B. and Koop, T. (2004) 'The role of organic aerosols in homogeneous ice formation', *Atmospheric Chemistry and Physics Discussions*, 4(5), pp. 6719–6745.

Kärcher, B. and Seifert, A. (2016) 'On homogeneous ice formation in liquid clouds', *Quarterly Journal of the Royal Meteorological Society*, 142(696), pp. 1320–1334.

Karimi, B. *et al.* (2020) 'A comparative evaluation of freezing criteria and molecular characterization of epiphytic ice-nucleating (Ice+) and non-ice-nucleating (Ice−) Pseudomonas syringae and Pseudomonas fluorescens', *Journal of Plant Pathology*. Springer, 102(1), pp. 169–178.

Karthika, S., Radhakrishnan, T. K. and Kalaichelvi, P. (2016) 'A Review of Classical and Nonclassical Nucleation Theories', *Crystal Growth and Design*, 16(11), pp. 6663–6681.

Kelly, C. P., Cramer, C. J. and Truhlar, D. G. (2006) 'Aqueous solvation free energies of ions and ion-water clusters based on an accurate value for the absolute aqueous solvation free energy of the proton', *Journal of Physical Chemistry B*, 110(32), pp. 16066–16081.

Kirkpatrick, S., Gelatt, C. D. and Vecchi, M. P. (1983) 'Optimization by simulated annealing', *Science*, 220(4598), pp. 671–680.

Knopf, D. A. *et al.* (2010) 'Heterogeneous nucleation of ice on anthropogenic organic particles collected in Mexico City', *Geophysical Research Letters*, 37(11).

Knopf, D. A. *et al.* (2011) 'Stimulation of ice nucleation by marine diatoms', *Nature Geoscience*. Nature Publishing Group, 4(2), pp. 88–90.

Knopf, D. A. *et al.* (2014) 'Microspectroscopic imaging and characterization of individually identified ice nucleating particles from a case field study', *Journal of Geophysical Research*, 119(17), pp. 10,365-10,381.

Knopf, D. A., Alpert, P. A. and Wang, B. (2018) 'The Role of Organic Aerosol in Atmospheric Ice Nucleation: A Review', *ACS Earth and Space Chemistry*. American Chemical Society, 2(3), pp. 168–202.

Knopf, D. A. and Lopez, M. D. (2009) 'Homogeneous ice freezing temperatures and ice nucleation rates of aqueous ammonium sulfate and aqueous levoglucosan particles for relevant atmospheric conditions', *Physical Chemistry Chemical Physics*. The Royal Society of Chemistry, 11(36), pp. 8056–8068.

Köhler, H. (1936) 'The nucleus in and the growth of hygroscopic droplets', *Transactions of the Faraday Society*, 32(0), pp. 1152–1161.

Koop, T. *et al.* (2000) 'Water activity as the determinant for homogeneous ice nucleation in aqueous solutions', *Nature*. Nature Publishing Group, 406(6796), pp. 611–4.

Koop, T. (2004) 'Homogeneous ice nucleation in water and aqueous solutions', *Zeitschrift fur Physikalische Chemie*. Oldenbourg Wissenschaftsverlag, 218(11), pp. 1231–1258.

Koop, T. *et al.* (2011) 'Glass transition and phase state of organic compounds: Dependency on molecular properties and implications for secondary organic aerosols in the atmosphere', *Physical Chemistry Chemical Physics*. The Royal Society of Chemistry, 13(43), pp. 19238–19255.

Krämer, B. *et al.* (1999) 'Homogeneous nucleation rates of supercooled water measured in single levitated microdroplets', *Journal of Chemical Physics*, 111(14), pp. 6521–6527.

Kreidenweis, S. M., Petters, M. and Lohmann, U. (2018) '100 Years of Progress in Cloud Physics, Aerosols, and Aerosol Chemistry Research', *Meteorological Monographs*, 59(December), pp. 11.1-11.72.

Krizner, H. E., De Haan, D. O. and Kua, J. (2009) 'Thermodynamics and kinetics of methylglyoxal dimer formation: A computational study', *Journal of Physical Chemistry A*, 113(25), pp. 6994–7001.

Kurtén, T. *et al.* (2008) 'Amines are likely to enhance neutral and ion-induced sulfuric acid-water nucleation in the atmosphere more effectively than ammonia', *Atmospheric Chemistry and Physics*, 8(14), pp. 4095–4103.

Kuwata, M. and Martin, S. T. (2012) 'Phase of atmospheric secondary organic material affects its reactivity', *Proceedings of the National Academy of Sciences of the United States of America*, 109(43), pp. 17354–17359.

Laaksonen, A. and Napari, I. (2001) 'Breakdown of the capillarity approximation in binary nucleation: A density functional study', *Journal of Physical Chemistry B*, 105(47), pp. 11678–11682.

Leck, C. and Bigg, E. K. (2005) 'Source and evolution of the marine aerosol - A new perspective', *Geophysical Research Letters*, 32(19), pp. 1–4.

Levy, A., Andelman, D. and Orland, H. (2012) 'Dielectric constant of ionic solutions: A field-theory approach', *Physical Review Letters*, 108(22).

Li, J. *et al.* (2019) 'The evolution of cloud microphysics upon aerosol interaction at the summit of Mt. Tai, China', *Atmospheric Chemistry and Physics Discussions*.

Li, T. *et al.* (2011) 'Homogeneous ice nucleation from supercooled water', *Physical Chemistry Chemical Physics*, 13(44), pp. 19807–19813.

Li, T., Donadio, D. and Galli, G. (2013) 'Ice nucleation at the nanoscale probes no man's land of water', *Nature Communications*. Nature Publishing Group, 4(May), p. 1887.

Li, X. *et al.* (2010) 'Surface-active cis-pinonic acid in atmospheric droplets: A molecular dynamics study', *Journal of Physical Chemistry Letters*, 1(4), pp. 769–773.

Li, X. *et al.* (2011) 'Glycine in aerosol water droplets: A critical assessment of Köhler theory by predicting surface tension from molecular dynamics simulations', *Atmospheric Chemistry and Physics*, 11(2), pp. 519–527.

Li, X. *et al.* (2013) 'Cloud droplet activation mechanisms of amino acid aerosol particles: Insight from molecular dynamics simulations', *Tellus, Series B: Chemical and Physical Meteorology*, 65(1), pp. 1–13.

Lignell, H., Hinks, M. L. and Nizkorodov, S. A. (2014) 'Exploring matrix effects on photochemistry of organic aerosols', *Proceedings of the National Academy of Sciences of the United States of America*, 111(38), pp. 13780–13785.

Lin, Y. *et al.* (2009) 'An image-based reaction field method for electrostatic interactions in molecular dynamics simulations of aqueous solutions', *Journal of Chemical Physics*, 131(15), p. 154103.

Lohmann, U. (2002) 'Possible aerosol effects on ice clouds via contact nucleation', *Journal of the Atmospheric Sciences*, 59(3 PT 2), pp. 647–656.

Lohmann, U. and Feichter, J. (2005) 'Global indirect aerosol effects: A review', *Atmospheric Chemistry and Physics*. European Geosciences Union, 5(3), pp. 715–737.

Loukonen, V. *et al.* (2010) 'Enhancing effect of dimethylamine in sulfuric acid nucleation in the presence of water-a computational study', *Atmospheric Chemistry and Physics*, 10(10), pp. 4961–4974.

Maki, L. R. *et al.* (1974) 'Ice nucleation induced by pseudomonas syringae.', *Applied microbiology*. American Society for Microbiology (ASM), 28(3), pp. 456–459.

Mandell, M. J. (1976) 'On the properties of a periodic fluid', *Journal of Statistical Physics*. Kluwer Academic Publishers-Plenum Publishers, 15(4), pp. 299–305.

Mark, P. and Nilsson, L. (2001) 'Structure and dynamics of the TIP3P, SPC, and SPC/E water models at 298 K', *Journal of Physical Chemistry A*. American Chemical Society, 105(43), pp. 9954–9960.

Matsumoto, M., Saito, S. and Ohmine, I. (2002) 'Molecular dynamics simulation of the ice nucleation and growth process leading to water freezing', *Nature*, 416(6879), pp. 409–413.

McFiggans, G. *et al.* (2006) 'The effect of physical and chemical aerosol properties on warm cloud droplet activation', *Atmospheric Chemistry and Physics*. European Geosciences Union, 6(9), pp. 2593–2649.

McMurry, P. H. (2000) 'A review of atmospheric aerosol measurements', *Atmospheric Environment*. Elsevier Science Ltd, 34(12–14), pp. 1959–1999.

McNeill, V. F. (2017) 'Atmospheric aerosols: Clouds, chemistry, and climate', *Annual Review of Chemical and Biomolecular Engineering*. Annual Reviews Inc., 8(1), pp. 427–444.

Medders, G. R. and Paesani, F. (2016) 'Dissecting the Molecular Structure of the Air/Water Interface from Quantum Simulations of the Sum-Frequency Generation Spectrum', *Journal of the American Chemical Society*. American Chemical Society, 138(11), pp. 3912–3919.

Mikhailov, E. *et al.* (2009) 'Amorphous and crystalline aerosol particles interacting with water vapor: Conceptual framework and experimental evidence for restructuring, phase transitions and kinetic limitations', *Atmospheric Chemistry and Physics*, 9(24), pp. 9491–9522.

Millet, D. B. *et al.* (2010) 'Global atmospheric budget of acetaldehyde: 3-D model analysis and constraints from in-situ and satellite observations', *Atmospheric Chemistry and Physics*, 10(7), pp. 3405–3425.

Mitsche, M. A., Wang, L. and Small, D. M. (2010) 'Adsorption of egg phosphatidylcholine to an air/water and triolein/water bubble interface: Use of the 2-dimensional phase rule to estimate the surface composition of a phospholipid/triolein/water surface as a function of surface pressure', *Journal of Physical Chemistry B*, 114(9), pp. 3276–3284.

Miyamoto, S. and Kollman, P. A. (1992) 'Settle: An analytical version of the SHAKE and RATTLE algorithm for rigid water models', *Journal of Computational Chemistry*, 13(8), pp. 952–962.

Monteil, C. L., Bardin, M. and Morris, C. E. (2014) 'Features of air masses associated with the deposition of Pseudomonas syringae and Botrytis cinerea by rain and snowfall', *ISME Journal*. Nature Publishing Group, 8(11), pp. 2290–2304.

Morishita, T. (2000) 'Fluctuation formulas in molecular-dynamics simulations with the

weak coupling heat bath', *Journal of Chemical Physics*, 113(8), pp. 2976–2982.

Morrow, T. J. and Smith, E. R. (1990) 'Simulation calculation of dielectric constants: Comparison of methods on an exactly solvable model', *Journal of Statistical Physics*, 61(1–2), pp. 187–201.

De Mott, P. J. *et al.* (2011) 'Resurgence in ice nuclei measurement research', *Bulletin of the American Meteorological Society*. American Meteorological Society, 92(12), pp. 1623–1635.

Muller, R. P., Florián, J. and Warshel, A. (1997) 'Semiempirical and Ab Initio Modeling of Chemical Processes', in *Biomolecular Structure and Dynamics*. Springer Netherlands, pp. 47–77.

Murphy, D. M. (2003) 'Dehydration in cold clouds is enhanced by a transition from cubic to hexagonal ice', *Geophysical Research Letters*, 30(23), p. 52-70.

Murray, B. J. (2008) 'Inhibition of ice crystallisation in highly viscous aqueous organic acid droplets', *Atmospheric Chemistry and Physics*, 8(17), pp. 5423–5433.

Murray, Benjamin J. *et al.* (2010) 'Heterogeneous nucleation of ice particles on glassy aerosols under cirrus conditions', *Nature Geoscience*. Nature Publishing Group, 3(4), pp. 233–237.

Murray, B. J. *et al.* (2010) 'Kinetics of the homogeneous freezing of water', *Physical Chemistry Chemical Physics*, 12(35), pp. 10380–10387.

Murray, B. J. *et al.* (2012a) 'Ice nucleation by particles immersed in supercooled cloud droplets', *Chemical Society Reviews*, 41(19), pp. 6519–6554.

Murray, B. J. *et al.* (2012b) 'Ice nucleation by particles immersed in supercooled cloud droplets', *Chemical Society Reviews*. The Royal Society of Chemistry, 41(19), pp. 6519–6554.

Murray, B. J., Knopf, D. A. and Bertram, A. K. (2005) 'The formation of cubic ice under conditions relevant to Earth's atmosphere', *Nature*, 434(7030), pp. 202–205.

Nelson, M. T. *et al.* (1996) 'NAMD: A parallel, object-oriented molecular dynamics program', *International Journal of High Performance Computing Applications*, 10(4), pp. 251–268.

Nilsson, A. and Pettersson, L. G. M. (2015) 'The structural origin of anomalous properties of liquid water', *Nature Communications*.

Noé, F. *et al.* (2020) 'Machine learning for molecular simulation', *Annual Review of Physical Chemistry*. Annual Reviews Inc., 71, pp. 361–390.

Norris, S. J. *et al.* (2013) 'Near-surface measurements of sea spray aerosol production over whitecaps in the open ocean', *Ocean Science*, 9(1), pp. 133–145.

Nosé, S. and Klein, M. L. (1983) 'Constant pressure molecular dynamics for molecular systems', *Molecular Physics*. Taylor & Francis Group , 50(5), pp. 1055–1076.

Nozière, B., Baduel, C. and Jaffrezo, J. L. (2014) 'The dynamic surface tension of atmospheric aerosol surfactants reveals new aspects of cloud activation', *Nature Communications*, 5, p. 3335.

Nucci, N. V., Pometun, M. S. and Wand, A. J. (2011) 'Site-resolved measurement of water-protein interactions by solution NMR', *Nature Structural and Molecular Biology*. Nature Publishing Group, 18(2), pp. 245–250.

Nymeyer, H. and Zhou, H. X. (2008) 'A method to determine dielectric constants in nonhomogeneous systems: Application to biological membranes', *Biophysical Journal*, 94(4), pp. 1185–1193.

O'Dowd, C. D. *et al.* (2004) 'Biogenically driven organic contribution to marine aerosol', *Nature*, 431(7009), pp. 676–680.

O'Sullivan, D. *et al.* (2015) 'The relevance of nanoscale biological fragments for ice nucleation in clouds', *Scientific Reports*, 5, p. 8082.

Ollila, O. H. S. *et al.* (2009) '3D Pressure field in lipid membranes and membrane-protein complexes', *Physical Review Letters*, 102(7).

Ollila, O. H. S. *et al.* (2012) 'Interfacial tension and surface pressure of high density lipoprotein, low density lipoprotein, and related lipid droplets', *Biophysical Journal*, 103(6), pp. 1236–1244.

Parrinello, M. and Rahman, A. (1981) 'Polymorphic transitions in single crystals: A new molecular dynamics method', *Journal of Applied Physics*, 52(12), pp. 7182–7190.

Perilla, J. R. *et al.* (2015) 'Molecular dynamics simulations of large macromolecular complexes', *Current Opinion in Structural Biology*. Elsevier Ltd, 31, pp. 64–74.

Perraud, V. *et al.* (2012) 'Nonequilibrium atmospheric secondary organic aerosol formation and growth', *Proceedings of the National Academy of Sciences of the United States of America*, 109(8), pp. 2836–2841.

Petersen, P. B. and Saykally, R. J. (2006) 'On the nature of ions at the liquid water surface', *Annual Review of Physical Chemistry*, 57(1), pp. 333–364.

Petters, M. D. and Kreidenweis, S. M. (2007) 'A single parameter representation of hygroscopic growth and cloud condensation nucleus activity', *Atmospheric Chemistry and Physics*, 7(8), pp. 1961–1971.

Pluhařová, E., Vrbka, L. and Jungwirth, P. (2010) 'Effect of surface pollution on homogeneous ice nucleation: A molecular dynamics study', *Journal of Physical Chemistry C*, 114(17), pp. 7831–7838.

Pohorille, A., Jarzynski, C. and Chipot, C. (2010) 'Good practices in free-energy calculations', *Journal of Physical Chemistry B*, 114(32), pp. 10235–10253.

Pöschl, U. (2005) 'Atmospheric aerosols: Composition, transformation, climate and health effects', *Angewandte Chemie - International Edition*, 44(46), pp. 7520–7540.

Prather, K. A., Hatch, C. D. and Grassian, V. H. (2008) 'Analysis of atmospheric aerosols', *Annual Review of Analytical Chemistry*. Annu Rev Anal Chem (Palo Alto Calif), pp. 485–514.

Price, H. (2013) *Quantifying diffusion coefficients in glassy aerosol*.

Price, H. C. *et al.* (2015) 'Water diffusion in atmospherically relevant α-pinene secondary organic material', *Chemical Science*. Royal Society of Chemistry, 6(8), pp. 4876–4883.

Price, M. L. P., Ostrovsky, D. and Jorgensen, W. L. (2001) 'Gas-phase and liquid-state properties of esters, nitriles, and nitro compounds with the OPLS-AA force field', *Journal of Computational Chemistry*, 22(13), pp. 1340–1352.

Prisle, N. L. *et al.* (2008) 'Surfactant partitioning in cloud droplet activation: A study of C8, C10, C12 and C14 normal fatty acid sodium salts', *Tellus, Series B: Chemical and Physical Meteorology*, 60 B(3), pp. 416–431.

Pruppacher, H. R., Klett, J. D. and Wang, P. K. (1998) 'Microphysics of Clouds and Precipitation', *Aerosol Science and Technology*, 28(4), pp. 381–382.

Rahman, A. (1964) 'Correlations in the motion of atoms in liquid argon', *Physical Review*. American Physical Society, 136(2A), p. A405.

Ramanathan, V. *et al.* (1989) 'Cloud-radiative forcing and climate: Results from the earth radiation budget experiment', *Science*, 243(4887), pp. 57–63.

Ravishankara, A. R. (1997) 'Heterogeneous and multiphase chemistry in the troposphere', *Science*, 276(5315), pp. 1058–1065.

Reay, D. *et al.* (2007) *Intergovernmental Panel on Climate Change. Fourth Assessment Report. Geneva, Switzerland: Inter-gov- ernmental Panel on Climate Change. Cambridge; UK: Cambridge University Press; 2007.*

Reinhardt, A. *et al.* (2012) 'Local order parameters for use in driving homogeneous ice nucleation with all-atom models of water', *Journal of Chemical Physics*, 137(19), pp. 1–10.

Renbaum-Wolff, L. *et al.* (2013) 'Viscosity of a-pinene secondary organic material and implications for particle growth and reactivity', *Proceedings of the National Academy of Sciences of the United States of America*, 110(20), pp. 8014–8019.

Renou, R. *et al.* (2014) 'Concentration dependence of the dielectric permittivity, structure, and dynamics of aqueous NaCl solutions: Comparison between the drude oscillator and electronic continuum models', *Journal of Physical Chemistry B*, 118(14), pp. 3931–3940.

Richardson, C. B. and Snyder, T. D. (1994) 'A Study of Heterogeneous Nucleation in Aqueous Solutions', *Langmuir*, 10(7), pp. 2462–2465.

Rickayzen, G. (1983) 'Molecular Theory of Capillarity', *Physics Bulletin*. IOP Publishing, 34(10), pp. 437–438.

Rosta, E., Buchete, N. V. and Hummer, G. (2009) 'Thermostat Artifacts in Replica Exchange Molecular Dynamics Simulations', *Journal of Chemical Theory and Computation*, 5(5), pp. 1393–1399.

Roth, C. M., Goss, K. U. and Schwarzenbach, R. P. (2005) 'Sorption of a diverse set of organic vapors to urban aerosols', *Environmental Science and Technology*, 39(17), pp. 6638–6643.

Ruehl, C. R. *et al.* (2012) 'Strong evidence of surface tension reduction in microscopic aqueous droplets', *Geophysical Research Letters*, 39(23).

Ruehl, C. R., Davies, J. F. and Wilson, K. R. (2016) 'An interfacial mechanism for cloud

droplet formation on organic aerosols', *Science*, 351(6280), pp. 1447–1450.

Russo, J., Romano, F. and Tanaka, H. (2014) 'New metastable form of ice and its role in the homogeneous crystallization of water', *Nature Materials*, 13(7), pp. 733–739.

Ryckaert, J. P., Ciccotti, G. and Berendsen, H. J. C. (1977) 'Numerical integration of the cartesian equations of motion of a system with constraints: molecular dynamics of n-alkanes', *Journal of Computational Physics*, 23(3), pp. 327–341.

Salameh, A. and Daskalakis, V. (2017) 'Atmospheric Ice Nucleation by Glassy Organic Compounds: A Review', *Chemistry of Compounds Journal Atmospheric*, 1(1), pp. 13–23.

Salameh, A., Vorka, F. and Daskalakis, V. (2016) 'Correlation between Surface Tension and the Bulk Dynamics in Salty Atmospheric Aquatic Droplets', *Journal of Physical Chemistry C*, 120(21), pp. 11508–11518.

Sanz, E. *et al.* (2013) 'Homogeneous ice nucleation at moderate supercooling from molecular simulation', *Journal of the American Chemical Society*. American Chemical Society, 135(40), pp. 15008–15017.

Sareen, N. *et al.* (2013) 'Surfactants from the gas phase may promote cloud droplet formation', *Proceedings of the National Academy of Sciences of the United States of America*, 110(8), pp. 2723–2728.

Sassen, K. and Dodd, G. C. (1988) 'Homogeneous nucleation rate for highly supercooled cirrus cloud droplets', *Journal of the Atmospheric Sciences*, 45(8), pp. 1357–1369.

Saukko, E. *et al.* (2012) 'Humidity-dependent phase state of SOA particles from biogenic and anthropogenic precursors', *Atmospheric Chemistry and Physics*, 12(16), pp. 7517–7529.

Schill, G. P., De Haan, D. O. and Tolbert, M. A. (2014) 'Heterogeneous ice nucleation on simulated secondary organic aerosol', *Environmental Science and Technology*, 48(3), pp. 1675–1682.

Schill, G. P. and Tolbert, M. A. (2013) 'Heterogeneous ice nucleation on phase-separated organic-sulfate particles: Effect of liquid vs. glassy coatings', *Atmospheric Chemistry and Physics*, 13(9), pp. 4681–4695.

Schlick, T. (2010) *Molecular Modeling and Simulation: An Interdisciplinary Guide*, *Interdisciplinary Applied Mathematics*.

Seinfeld, J. H. and Pandis, S. N. (2016) *Atmospheric Chemistry and Physics: From Air Pollution to Climate Change, 3rd Edition | Wiley*. John Wiley & Sons, Inc.

Shiraiwa, M. *et al.* (2011) 'Gas uptake and chemical aging of semisolid organic aerosol particles', *Proceedings of the National Academy of Sciences*, 108(27), pp. 11003–11008.

Shiraiwa, M. *et al.* (2013) 'Size distribution dynamics reveal particle-phase chemistry in organic aerosol formation', *Proceedings of the National Academy of Sciences of the United States of America*, 110(29), pp. 11746–11750.

Shiraiwa, M., Pfrang, C. and Pöschl, U. (2010) 'Kinetic multi-layer model of aerosol surface and bulk chemistry (KM-SUB): The influence of interfacial transport and bulk

diffusion on the oxidation of oleic acid by ozone', *Atmospheric Chemistry and Physics*, 10(8), pp. 3673–3691.

Shiraiwa, M., Pöschl, U. and Knopf, D. A. (2012) 'Multiphase chemical kinetics of NO 3 radicals reacting with organic aerosol components from biomass burning', *Environmental Science and Technology*. American Chemical Society, 46(12), pp. 6630–6636.

Shirts, M. R. *et al.* (2003) 'Extremely precise free energy calculations of amino acid side chain analogs: Comparison of common molecular mechanics force fields for proteins', *Journal of Chemical Physics*, 119(11), pp. 5740–5761.

Shivakumar, D. *et al.* (2010) 'Prediction of absolute solvation free energies using molecular dynamics free energy perturbation and the opls force field', *Journal of Chemical Theory and Computation*, 6(5), pp. 1509–1519.

Shivakumar, D. *et al.* (2012) 'Improving the prediction of absolute solvation free energies using the next generation opls force field', *Journal of Chemical Theory and Computation*, 8(8), pp. 2553–2558.

Shulman, M. L. *et al.* (1996) 'Dissolution behavior and surface tension effects of organic compounds in nucleating cloud droplets', *Geophysical Research Letters*, 23(3), pp. 277–280.

Sillmann, J. *et al.* (2017) 'Understanding, modeling and predicting weather and climate extremes: Challenges and opportunities', *Weather and Climate Extremes*. Elsevier B.V., 18, pp. 65–74.

Simonson, T. (1996) 'Accurate calculation of the dielectric constant of water from simulations of a microscopic droplet in vacuum', *Chemical Physics Letters*, 250(5–6), pp. 450–454.

Slade, J. H. and Knopf, D. A. (2014) 'Multiphase OH oxidation kinetics of organic aerosol: The role of particle phase state and relative humidity', *Geophysical Research Letters*, 41(14), pp. 5297–5306.

Sokhan, V. P. *et al.* (2015) 'Signature properties of water: Their molecular electronic origins', *Proceedings of the National Academy of Sciences of the United States of America*, 112(20), pp. 6341–6346.

Sorjamaa, R., Raatikainen, T. and Laaksonen, A. (2004) 'The role of surfactants in Köhler theory reconsidered', *Atmospheric Chemistry and Physics Discussions*, 4(3), pp. 2781–2804.

Sosso, G. C., Chen, J., *et al.* (2016) 'Crystal Nucleation in Liquids: Open Questions and Future Challenges in Molecular Dynamics Simulations', *Chemical Reviews*, 116(12), pp. 7078–7116.

Sosso, G. C., Tribello, G. A., *et al.* (2016) 'Ice formation on kaolinite: Insights from molecular dynamics simulations', *Journal of Chemical Physics*, 145(21), p. 211927.

Van Der Spoel, D., Van Maaren, P. J. and Berendsen, H. J. C. (1998) 'A systematic study of water models for molecular simulation: Derivation of water models optimized for use with a reaction field', *Journal of Chemical Physics*, 108(24), pp. 10220–10230.

Stan, C. A. *et al.* (2009) 'A microfluidic apparatus for the study of ice nucleation in supercooled water drops', *Lab on a Chip*, 9(16), pp. 2293–2305.

Steinhardt, P. J., Nelson, D. R. and Ronchetti, M. (1983) 'Bond-orientational order in liquids and glasses', *Physical Review B*, 28(2), pp. 784–805.

Stephens, G. L. (2005) 'Cloud feedbacks in the climate system: A critical review', *Journal of Climate*, 18(2), pp. 237–273.

Stillinger, F. H. and Rahman, A. (1974) 'Improved simulation of liquid water by molecular dynamics', *The Journal of Chemical Physics*, 60(4), pp. 1528–1532.

Sun, J. and Ariya, P. A. (2006) 'Atmospheric organic and bio-aerosols as cloud condensation nuclei (CCN): A review', *Atmospheric Environment*. Pergamon, 40(5), pp. 795–820.

Sun, L. *et al.* (2012) 'Molecular dynamics simulations of the surface tension and structure of salt solutions and clusters', *Journal of Physical Chemistry B*. American Chemical Society, 116(10), pp. 3198–3204.

Sun, Q. *et al.* (2016) 'Molecular Simulations of Hydrogen Bond Cluster Size and Reorientation Dynamics in Liquid and Glassy Azole Systems', *Journal of Physical Chemistry B*, 120(39), pp. 10411–10419.

Swope, W. C. *et al.* (1982) 'A computer simulation method for the calculation of equilibrium constants for the formation of physical clusters of molecules: Application to small water clusters', *The Journal of Chemical Physics*, 76(1), pp. 637–649.

Tan, Y. *et al.* (2010) 'SOA from methylglyoxal in clouds and wet aerosols: Measurement and prediction of key products', *Atmospheric Environment*. Elsevier Ltd, 44(39), pp. 5218–5226.

Thijssen, H. A. C., Vorstman, M. A. G. and Roels, J. A. (1968) 'Heterogeneous primary nucleation of ice in water and aqueous solutions', *Journal of Crystal Growth*, 3–4(C), pp. 355–359.

Tironi, I. G. *et al.* (1995) 'A generalized reaction field method for molecular dynamics simulations', *The Journal of Chemical Physics*, 102(13), pp. 5451–5459.

Tomasi, C. *et al.* (2017) *Atmospheric Aerosols: Life Cycles and Effects on Air Quality and Climate*.

Tomasi, C. and Lupi, A. (2016) 'Primary and Secondary Sources of Atmospheric Aerosol', in *Atmospheric Aerosols*. Weinheim, Germany: Wiley-VCH Verlag GmbH & Co. KGaA, pp. 1–86.

Tong, C. *et al.* (2006) 'Secondary organic aerosol formation by heterogeneous reactions of aldehydes and ketones: A quantum mechanical study', *Environmental Science and Technology*, 40(7), pp. 2333–2338.

Tong, H. J. *et al.* (2011) 'Measurements of the timescales for the mass transfer of water in glassy aerosol at low relative humidity and ambient temperature', *Atmospheric Chemistry and Physics*, 11(10), pp. 4739–4754.

Topper, R. Q. *et al.* (2011) 'Simulated annealing and density functional theory

calculations of structural and energetic properties of the ammonium chloride clusters (NH 4Cl) n, (NH 4+)(NH 4Cl) n, and (Cl -)(NH 4Cl) n, n = 1-13', *Journal of Physical Chemistry A*. American Chemical Society, 115(38), pp. 10423–10432.

Torres-Sánchez, A., Vanegas, J. M. and Arroyo, M. (2015) 'Examining the mechanical equilibrium of microscopic stresses in molecular simulations', *Physical Review Letters*, 114(25).

Tröstl, J. *et al.* (2016) 'The role of low-volatility organic compounds in initial particle growth in the atmosphere', *Nature*, 533(7604), pp. 527–531.

Turnbull, D. and Vonnegut, B. (1952) 'Nucleation Catalysis.', *Industrial & Engineering Chemistry*, 44(6), pp. 1292–1298.

Vali, G. *et al.* (2015) 'Technical Note: A proposal for ice nucleation terminology', *Atmospheric Chemistry and Physics*, 15(18), pp. 10263–10270.

Vanegas, J. M., Torres-Sánchez, A. and Arroyo, M. (2014) 'Importance of force decomposition for local stress calculations in biomembrane molecular simulations', *Journal of Chemical Theory and Computation*, 10(2), pp. 691–702.

Vega, C. and Abascal, J. L. F. (2011) 'Simulating water with rigid non-polarizable models: A general perspective', *Physical Chemistry Chemical Physics*, pp. 19663–19688.

Vega, C. and De Miguel, E. (2007) 'Surface tension of the most popular models of water by using the test-area simulation method', *Journal of Chemical Physics*, 126(15), pp. 1–10.

Verlet, L. (1967) 'Computer "experiments" on classical fluids. I. Thermodynamical properties of Lennard-Jones molecules', *Physical Review*, 159(1), pp. 98–103.

Vignati, E. *et al.* (2010) 'Global scale emission and distribution of sea-spray aerosol: Sea-salt and organic enrichment', *Atmospheric Environment*. Pergamon, 44(5), pp. 670–677.

Villa, A. and Mark, A. E. (2002) 'Calculation of the free energy of solvation for neutral analogs of amino acid side chains', *Journal of Computational Chemistry*, 23(5), pp. 548–553.

Virtanen, A. *et al.* (2010) 'An amorphous solid state of biogenic secondary organic aerosol particles', *Nature*, 467(7317), pp. 824–827.

Volmer, M.; Weber, A. (1926) 'Nucleus Formation in Supersaturated Systems', *Z. Phys. Chem (Leipzig)*, 119, pp. 277–301.

Wagner, R. *et al.* (2012) 'Ice cloud processing of ultra-viscous/glassy aerosol particles leads to enhanced ice nucleation ability', *Atmospheric Chemistry and Physics*, 12(18), pp. 8589–8610.

Wagner, R. *et al.* (2017) 'Heterogeneous ice nucleation of α-pinene SOA particles before and after ice cloud processing', *Journal of Geophysical Research*, 122(9), pp. 4924–4943.

Wagner, R. *et al.* (2018) 'Heterogeneous Ice Nucleation Ability of NaCl and Sea Salt Aerosol Particles at Cirrus Temperatures', *Journal of Geophysical Research: Atmospheres*, 123(5), pp. 2841–2860.

Wang, B., Laskin, A., *et al.* (2012) 'Heterogeneous ice nucleation and water uptake by

field-collected atmospheric particles below 273 K', *Journal of Geophysical Research Atmospheres*, 117(17), pp. 1–15.

Wang, B., Lambe, A. T., *et al.* (2012) 'The deposition ice nucleation and immersion freezing potential of amorphous secondary organic aerosol: Pathways for ice and mixed-phase cloud formation', *Journal of Geophysical Research Atmospheres*, 117(16), pp. 1–12.

Wang, B. *et al.* (2015) 'Reactivity of liquid and semisolid secondary organic carbon with chloride and nitrate in atmospheric aerosols', *Journal of Physical Chemistry A*, 119(19), pp. 4498–4508.

Wang, X. *et al.* (2018) 'Molecular dynamics simulation of the surface tension of aqueous sodium chloride: From dilute to highly supersaturated solutions and molten salt', *Atmospheric Chemistry and Physics*, 18(23).

Wei, Y. Z., Chiang, P. and Sridhar, S. (1992) 'Ion size effects on the dynamic and static dielectric properties of aqueous alkali solutions', *The Journal of Chemical Physics*, 96(6), pp. 4569–4573.

Weinberg, M. C., Poisl, W. H. and Granasy, L. (2002) 'Crystal growth and classical nucleation theory', *Comptes Rendus Chimie*, 5(11), pp. 765–771.

Werner, J. *et al.* (2014) 'Succinic acid in aqueous solution: Connecting microscopic surface composition and macroscopic surface tension', *Physical Chemistry Chemical Physics*, 16(39), pp. 21486–21495.

Whale, T. F. (2018) *Ice Nucleation in Mixed-Phase Clouds*, *Mixed-Phase Clouds: Observations and Modeling*. Elsevier Inc.

Wheeler, M. J. and Bertram, A. K. (2012) 'Deposition nucleation on mineral dust particles: A case against classical nucleation theory with the assumption of a single contact angle', *Atmospheric Chemistry and Physics*, 12(2), pp. 1189–1201.

Wilson, T. W. *et al.* (2012) 'Glassy aerosols with a range of compositions nucleate ice heterogeneously at cirrus temperatures', *Atmospheric Chemistry and Physics*, 12(18), pp. 8611–8632.

Wilson, T. W. (2012) *Ice nucleation under cirrus cloud conditions*.

Wilson, T. W. *et al.* (2015) 'A marine biogenic source of atmospheric ice-nucleating particles', *Nature*, 525(7568), pp. 234–238.

Yakobi-Hancock, J. D. *et al.* (2014) 'CCN activity of size-selected aerosol at a Pacific coastal location', *Atmospheric Chemistry and Physics*, 14(22), pp. 12307–12317.

Yakobi-Hancock, J. D., Ladino, L. A. and Abbatt, J. P. D. (2014) 'Review of Recent Developments and Shortcomings in the Characterization of Potential Atmospheric Ice Nuclei: Focus on the Tropics', *Revista de Ciencias*, 17(3), pp. 15–34.

Zakharov, V. V., Brodskaya, E. N. and Laaksonen, A. (1997) 'Surface tension of water droplets: A molecular dynamics study of model and size dependencies', *Journal of Chemical Physics*, 107(24), pp. 10675–10683.

Zeb, B. *et al.* (2018) 'On the morphology and composition of particulate matter in an

urban environment', *Aerosol and Air Quality Research*. AAGR Aerosol and Air Quality Research, 18(6), pp. 1431–1447.

Zhai, Y. *et al.* (2018) 'A review on airborne microorganisms in particulate matters: Composition, characteristics and influence factors', *Environment International*. Elsevier Ltd, pp. 74–90.

Zhang, Q. *et al.* (2007) 'Ubiquity and dominance of oxygenated species in organic aerosols in anthropogenically-influenced Northern Hemisphere midlatitudes', *Geophysical Research Letters*, 34(13), pp. 1–6.

Zhang, R. *et al.* (2012) 'Nucleation and growth of nanoparticles in the atmosphere', *Chemical Reviews*, pp. 1957–2011.

Zieger, P. *et al.* (2017) 'Revising the hygroscopicity of inorganic sea salt particles', *Nature Communications*. Nature Publishing Group, 8, p. 15883.

Ziemann, P. J. and Atkinson, R. (2012) 'Kinetics, products, and mechanisms of secondary organic aerosol formation', *Chemical Society Reviews*, 41(19), pp. 6582–6605.

Zobrist, B., Marcolli, C., Pedernera, D. A., *et al.* (2008) 'Do atmospheric aerosols form glasses?', *Atmospheric Chemistry and Physics*, 8(17), pp. 5221–5244.

Zobrist, B., Marcolli, C., Peter, T., *et al.* (2008) 'Heterogeneous ice nucleation in aqueous solutions: The role of water activity', *Journal of Physical Chemistry A*, 112(17), pp. 3965–3975.

Zobrist, B., Weers, U. and Koop, T. (2003) 'Ice nucleation in aqueous solutions of poly[ethylene glycol] with different molar mass', *Journal of Chemical Physics*. American Institute of Physics, 118(22), pp. 10254–10261.